Fluctuating Wind Power Penetration as Limited by Frequency Standard

Changling Luo

B. Eng. Concordia University, Montreal, Canada

A thesis submitted to the Faculty of Graduate Studies and Research in partial fulfillment of the requirements for the degree of Master of Engineering

Department of Electrical Engineering

McGill University

Montreal, Quebec, Canada

April, 2005

© Changling Luo, 2005

Library and
Archives Canada

Published Heritage
Branch

395 Wellington Street
Ottawa ON K1A 0N4
Canada

Bibliothèque et
Archives Canada

Direction du
Patrimoine de l'édition

395, rue Wellington
Ottawa ON K1A 0N4
Canada

Your file Votre référence
ISBN: 978-0-494-22654-4
Our file Notre référence
ISBN: 978-0-494-22654-4

NOTICE:
The author has granted a non-exclusive license allowing Library and Archives Canada to reproduce, publish, archive, preserve, conserve, communicate to the public by telecommunication or on the Internet, loan, distribute and sell theses worldwide, for commercial or non-commercial purposes, in microform, paper, electronic and/or any other formats.

The author retains copyright ownership and moral rights in this thesis. Neither the thesis nor substantial extracts from it may be printed or otherwise reproduced without the author's permission.

AVIS:
L'auteur a accordé une licence non exclusive permettant à la Bibliothèque et Archives Canada de reproduire, publier, archiver, sauvegarder, conserver, transmettre au public par télécommunication ou par l'Internet, prêter, distribuer et vendre des thèses partout dans le monde, à des fins commerciales ou autres, sur support microforme, papier, électronique et/ou autres formats.

L'auteur conserve la propriété du droit d'auteur et des droits moraux qui protège cette thèse. Ni la thèse ni des extraits substantiels de celle-ci ne doivent être imprimés ou autrement reproduits sans son autorisation.

In compliance with the Canadian Privacy Act some supporting forms may have been removed from this thesis.

While these forms may be included in the document page count, their removal does not represent any loss of content from the thesis.

Conformément à la loi canadienne sur la protection de la vie privée, quelques formulaires secondaires ont été enlevés de cette thèse.

Bien que ces formulaires aient inclus dans la pagination, il n'y aura aucun contenu manquant.

Canada

Dedication

Dedicated to my respected parents,

my lovely sister and brother in-law,

and my kind aunts & uncles

Claims to Originality

To the best of the author's knowledge, the following claims are original:

1. Application of the Transfer Functions of a thermal power plant to estimate frequency deviation from the 60 Hz standard.

2. An analytical method to estimate the wind power penetration of a utility grid comprising multiple power plants.

3. An analytical method of evaluating the factor of attenuation of wind power by the inertia of wind turbine generator.

Abstract

Fluctuating wind power is due to wind turbulence and is the part which should be filtered out leaving behind the more predictable mean wind power which can be traded in the hourly energy market. The power fluctuations cause the frequency of electric utility to deviate from the 60Hz standard. This thesis is concerned with estimating the maximum fluctuating wind power before the 1% deviation from the 60 Hz standard (required by some utilities) is exceeded. To keep the thesis manageable, the scope is narrowed to thermal power plants with governor speed control but no Automatic Governor Control (AGC). This thesis shows that each governor speed control system provides energy storage buffer to attenuate the wind power fluctuations and arrives at the estimate that the fluctuating wind power penetration is conservatively around 5% of the generation capacity of the utility grid. The methodologies used to reach this estimate are: (i) Transfer Function analysis of power plants; (ii) digital simulations using HYPERSIM. Through the research, an innovative method of predicting the frequency deviation in an electric grid with multiple power plants has been developed and validated by simulation.

The thesis also shows that fluctuating wind power penetration can be higher when there are filtering also in the wind farms. Wind turbines, with small inertias, driving constant speed squirrel cage induction generators are found to provide poor filtering. On the other hand, the fluctuating wind power penetration limit is increased to 18% in the case of wind turbines, with large inertias, driving variable-speed doubly-fed induction generators (DFIG) with decoupled P-Q control to implement optimal wind power acquisition.

Résumé

Les fluctuations du niveau de production d'énergie éolienne sont causées par les turbulences du vent. C'est en contrant ces fluctuations que l'énergie éolienne pourra devenir une source d'énergie plus prévisible. Plus spécifiquement, les fluctuations du niveau de production entraînent des variations de la fréquence du réseau auquel les éoliennes sont raccordées. Ce mémoire adresse ce phénomène en tentant d'estimer le niveau de fluctuation requis afin que la variation de la fréquence atteigne la limite admissible de 1% de la fréquence nominale de 60 hertz—un critère d'exploitation répandu dans les grands réseaux électriques.

Afin de limiter l'envergure du problème, ce mémoire ne considère que des réseaux constitués d'unités de production thermiques équipés de régulateurs de vitesse (régulation primaire) mais ne possédant pas de mécanismes de régulation secondaire, mieux connus sous l'appellation anglo-saxonne « automatic generation control. » Ce mémoire démontre que chacune des unités de production thermiques, via son mécanisme de régulation primaire, atténuent les fluctuations de puissance de la production éolienne de manière satisfaisante jusqu'à un niveau d'intégration de capacité éolienne correspondant à 5% de la capacité de production thermique existante. Nous utilisons deux méthodes afin de réaliser cette estimation : premièrement, via une analyse des fonctions de transfert des unités de production thermiques et, deuxièmement, par des simulations sous la plate-forme HYPERSIM. La méthode d'estimation de variations de la fréquence d'un réseau est innovatrice et est validée par les simulations.

De plus, ce mémoire démontre que les fluctuations de la production éolienne peuvent aussi être amoindries par le design même des groupes turbine alternateur. Les turbines avec une faible inertie et accouplées à des alternateurs à rotor en court-circuit ne peuvent contribuer que très peu à l'amortissement des fluctuations. Cependant, lorsque les turbines possèdent une inertie plus importante et qu'ils sont accouplés à des alternateurs à rotor bobinés asservis par un contrôle découplé de type P-Q, la borne supérieure du niveau d'intégration éolienne passe à 18% de la capacité thermique existante.

Acknowledgements

Grateful thanks from my heart go to Professor B.T. Ooi for his guidance, supervision, encouragement and helpful discussions all through my entire graduate studies.

I wish to thank Dr. L.-A. Dessaint, l'Ecole de Technologie Superieure, for access to HYPERSIM.

I wish to thank Mr. Baike Shen, whose software on decoupled P-Q control of the doubly-fed induction generator has enabled me to shorten the duration of my research in chapter 5. I wish to thank Dr. Hadi Banakar for drawing my attention to the steady-state stability boundaries of doubly-fed induction generators in chapter 5. I wish to thank Mr. Francois Bouffard for his help to translate my abstract into French.

My thanks go to author's colleagues for their friendship, help and kindness in the Power Group of the Department of Electrical and Computer Engineering, McGill University. They are: Mr. FengQuan Zhou, Mr. Wei Li, Mr. Pei Li, Mr. Francois Bouffard, Mr. Chad Abbey, Mr. Josė Restrepo, Mr. Alaa Abdul Samad, Mr. Sameh El Khatib, Mr. Hasan Ebrahim A. Rahman, Dr. Khalil El Arroudi, Mr. Arabind Nanda, Mr. Kelvin Lee, Mr. Iman Khosravi and Mr. Loic Owatta.

My thanks go belatedly to the late Dr. LianWei Jiao of Tsinghua University, China, who was post doctoral fellow in McGill University in 2003-04. Dr. Jiao began the research on the steady-state stability boundaries of doubly-fed induction generators which was completed by Dr. Banakar when he returned to China. He passed away in January 2005. My condolence goes to his widow and son.

List of Contents

Fluctuating Wind Power Penetration as Limited by Frequency Standard

Changling Luo
B. Eng. Concordia University, Montreal, Canada

A thesis submitted to the Faculty of Graduate Studies and Research in partial fulfillment of the requirements for the degree of Master of Engineering

Department of Electrical Engineering
McGill University
Montreal, Quebec, Canada

April, 2005

© Changling Luo, 2005

List of Figures

Chapter 6

List of Tables

List of Acronyms

Automatic Governor Control:	AGC
Doubly-Fed Induction Generator:	DFIG
Fast Fourier transforms:	FFT
Low/Intermediate/High Pressure	LP/IP/HP
Insulated Gate Bipolar Transistor	IGBT
Phase Lock Loop:	PLL
Pulse Width Modulation:	PWM
Sinusoid Pulse Width Modulation	SPWM
Static Var Compensators:	SVC
Standard Deviation:	STD
Voltage-Source Converter:	VSC
Wind Turbine Generator:	WTG

List of Symbols

C_p	Power coefficient
f_W	Frequency of wind fluctuation
f_{base}	Base frequency = 60 Hz
F_a	Attenuation factor
H	Inertia
mhuh	Flow of high-pressure stage
M_W	Magnitude of wind fluctuation
P_e	Electrical power of generator
$\Delta P_e(t)$	Perturbation of electrical power of generator
$P_{\mathrm{mod}-ref}$	Reference of real power of wind generator
P_{w-ave}	Constant part of real power output of wind generator
P_W	Wind power
P_L	Real power consumption of load
P_m	Mechanical power of generator
P_{ref}	Real power reference
$\Delta P_{\sum wind}$	Total wind power penetration
$\Delta P_m(t)$	Perturbation of mechanical power of generator

ΔP_{accel}	Accelerate energy on the rotor of generator
PF_{rated}	Power factor = 0.85
$Psih$	Steam output of boiler
Q_{ref}	Reactive power reference
R	Blade radius
S_{base}	Base power = 192 MVA
T_h, T_i, T_l	Mechanical torque of high, intermediate, and low-pressure turbine
T_e / T_m	Electrical/Mechanical torque
$V_{base-generator}$	Base voltage of generator = 18 KV
$V_{base-Network}$	Base voltage of transmission line = 230 KV
V_W	Wind Speed
ω_r	Power system frequency
ω_m	Mechanical speed of machines
ω_{ref}	Reference of frequency (60 Hz)
ω_0	Reference of frequency in per unit (1 per unit)
$\Delta \omega_r$	Perturbation of rotor speed of generator
x	Valve opening of steam turbine
λ	Tip ratio
ρ	Air density

CHAPTER 1

INTRODUCTION

1.1 Overview

Electricity, which is the life-blood of modern civilization, is generated mostly by non-renewable and polluting crude oil and coal. Their greenhouse gas (GHG) emissions are bringing us to the brink of environmental disasters. Signatories of the Kyoto Protocol, who are committed to reducing greenhouse gas emissions, are turning to clean and renewable power sources both to sustain the pace of growth of the Gross Domestic Product (GDP) and to retire power plants which are the sources of GHG emissions.

What are classified today as renewable energy sources are few: hydro, tidal, solar and wind. Tidal and hydro are limited to the locations favored by geographical terrain whereat gravity and water allow potential energy to be converted to electrical energy. In the developed world, most hydro potentials have already been harnessed. Many environmental pressure groups oppose the development of the remainder because flora and fauna are drowned by the extensive reservoirs behind the dams.

Research and development of solar and photovoltaic energy sources continue to be supported by governments and some private enterprises, but progress is slow because of factors related to efficiency of conversion and cost. The most promising renewable energy source is wind. The price of wind power is estimated to be 8 cents per kilowatt-hour compared to 6 cents charged by Hydro-Quebec.

In fact, wind energy industry has taken off. The global installation of wind power in

2004 is estimated as 47 GW in 2004 [1-1] and is predicted to grow to 1245 GW in the year 2020 [1-2]. The confident growth of the wind industry is in part the result of better understanding of wind characteristics. Underlying the seemingly random fluctuations of the wind velocity is a mean component which is predictable at least an hour ahead of time. This predictability enables wind energy to be traded in the hourly energy market. Riding on top of this mean is the turbulent component, the component which is the subject of this thesis. The factors, which have brought down the price of wind energy, are: the advances by civil engineers who erect the tall slender towers which do not buckle under wind forces; the advances of aerodynamic engineers who design the turbine blades; the advances of mechanical engineers in charge of turbine blade pitch and wind direction control.

The advances of electrical engineers are the progressive development squirrel cage induction generators, doubly-fed induction generators, permanent magnet generators on the power conversion side. A parallel advance is in power electronic technology, in particular decoupled P-Q control. The P-control is essential for delivering constant power as promised in the hour-long trading contract, in the face of power fluctuations arising from the turbulent component of the wind. The reactive power or Q-control is essential for ac voltage support in remotely located wind farms.

Energy from wind farms must reach consumers. The most economic delivery system is the existing electric utility grid. But the electric utility grid has stringent standards regarding frequency deviation and voltage magnitudes. Presently, meeting the standard has not been a problem because the wind power penetration of Denmark, which has the highest level of wind power penetration, is still only 7%. The huge investments in developing economic wind turbine systems will come to naught if the regulatory standards limit wind penetration to a low percentage. For this reason, it is important to research on the factors which set the limit to penetration and how to raise the limit.

Scope of Research

In this thesis, the research on wind penetration limit in the utility grid is restricted to the frequency deviation from the 60 Hz standard caused by the fast power fluctuations associated with wind turbulence. The steady-state frequency deviation limit (59.4Hz to 60.6Hz) or 1% of 60 Hz, used in this thesis, is taken from page 16 of 30 pages of document d'appel d'offrers A/O 2003-02, issued on 12 May, 2003 by Hydro-Quebec Distribution to wind power providers.

In the electric utility grid, the fast power fluctuations of the wind are perceived as fluctuations of the counter-torques of the electric generators. The shaft systems of the turbine-generator units, which are driven by the steam turbines of thermal plants, for example, accelerate and decelerate. The wavering rotor speeds, carrying the magnetic fluxes of the field excitation systems, cause the frequency to deviate from the 60 Hz. Power plants, which carry governor speed control, have feedback loops which increase or decrease the prime mover power to null the frequency deviation.

This thesis does not treat the very low frequency wind power fluctuations which fall in frequency range of the Automatic Governor Control (AGC). (According to the thesis supervisor, this topic will be the subject of a future thesis.) Power plant(s) operating, singly or in a group, under an AGC continuously adjust their power reference settings in negative feedback response to null frequency deviations from the 60 Hz. Until the advent of wind power, the function of the AGC is to compensate for the difference between the actual and forecasted demands of the loads. When wind farms become part of the utility system the firm component of wind power is subtracted from the forecasted demands of the loads. The very low frequency wind power fluctuations become part of the actual demand which the AGC has to compensate for. The sampling rate of AGC is usually 1 sample per 2 seconds.

Apart for the difference that the AGC is slow and the governor speed control is fast, it is significant to note how the wind power fluctuations are handled to keep the frequency fluctuations small. For example, in governor speed control of thermal plants, the governor valve reduces steam output in the crest of wind power and the saving is expended in the dip. Thus the wind power fluctuation is accommodated by "virtual storage". In contrast, the power references of the power plants under AGC control are changed continuously so that prolonged unidirectional difference between actual and forecasted wind power can be handled.

In order to narrow the scope of the thesis, the coverage is limited to utility systems with thermal plants only. At the end of the study, it is found that the methodology developed is general enough to be applicable to hydro-systems and systems with mixed thermal and hydro plants because it is a matter of modeling the system dynamics as a transfer function $G(s)$.

Methodologies

The research tools, used in this thesis, consist of: (i) analysis using the transfer functions of power plants; (ii) digital simulations.

Transfer Function Approach

Although wind velocity data files for individual wind turbines are available, data from wind farms are still in the process of being collected and analyzed [1-3]. In the absence of suitable wind farm data, this thesis has taken a deterministic approach. In fact, without probabilistic consideration to distract, the deterministic analysis clarifies how perturbation wind power $\Delta P_{wind}(t)$, fluctuating at frequency f_W, affects $\Delta\omega_r(t)$, the frequency deviation from 60Hz of the utility grid. In the frequency domain ($s=j2\pi f_W$), each power plant is regarded as a transfer function $G(s)$ and the frequency deviation problem is simply posed as: $\Delta\omega_r(s)=G(s)\Delta P_{wind}(s)$. At such time as probability-vs-frequency spectrum becomes available, it is a matter of computing the statistical standard deviation of $\Delta\omega_r$, in response to the statistical standard deviation of the fluctuating power component ΔP_{wind}. The transfer function approach is validated by digital simulations.

Digital Simulation Approach

For digital simulations, the authors have access to Hydro-Quebec's HYPERSIM, whose collection of power plant components are based on detail models recommended by IEEE Committee Reports. The components are: the generator [4], the field excitation system [5], the power system stabilizer [6], the boiler [7], the high pressure, intermediate pressure, and low pressure turbines [8], as well as the governor [7] and the shaft inertias [8]. The icons of these components are connected together to form a power plant. Icons of transmission lines connect power plants together to form a utility grid.

Simplifying Assumptions

As the spectrum of wind power fluctuation overlaps the 0.5 to 2 Hz operating range of the power system stabilizer (PSS), the PSS has been excluded from the present study and its inclusion is deferred to later thesis. As subsynchronous resonance (SSR) frequencies will be outside the frequency range of wind power, another simplification made is to assume that the inertias of the high pressure, intermediate pressure, and low pressure turbines are mounted rigidly to the generator rotor.

1.2 Research Objective

The UN Climate Change Conference in Buenos Aires on November 1998 reached the conclusion that within the next 20 to 25 years, wind power could easily provide up to 10 per cent of global electricity consumption [1-9]. However, from the engineering viewpoint, the following technical questions arise: What is the maximum penetration of wind power can be achieved without jeopardizing the existing power systems? Is there an analytical way to calculate the maximum penetration of wind?

Fig 1.1 illustrates the 3 parts of the wind power generation system as it interacts with the electric utility power system. Each part is discussed to show how the above questions are addressed in the quest for the answers.

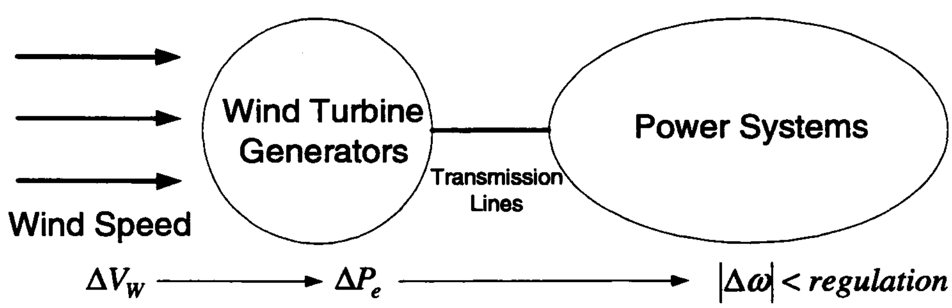

Fig 1.1. Research flow chart

The first part relates to the wind speed V_W, which is the power source. Wind speed data files are available and the metric for quantifying the stochastic process is the mean value and the standard deviation of wind speed. In the absence of wind data files, mathematical software such as MATLAB has programs to generate time series function which can be used for wind speed in the assumption that wind has Weibull or Rayleigh distributions [1-10].

The second part is at each individual wind turbine, which is coupled to the electric generator. The input is the wind speed V_W and the intermediate output is wind power P_W of the turbine. The large diameter blades of MW-size wind turbines carry large moments of inertia (J or H) and kinetic energy ($0.5J\omega_m^2$) where ω_m is the turbine shaft speed. The kinetic energy offers a filtering stage to attenuate the fluctuations. The final output of the second part is the electrical power $P_e = -(P_W - d(0.5J\omega_m^2)/dt)$.

The third part in Fig. 1.1 is the electric utility power system which conveys wind power to the load. The power fluctuations of individual wind turbine-generators undergo a further stage of spatial filtering because a wind farm typically has scores of wind turbine-generators spaced at distances apart so the same wave front passes over them at different time instants so that there can be cancellation of temporal crests by dips. Although wind velocity data files for individual wind turbines are available, data from wind farms are still in the process of being collected and analyzed [1-3]. In the absence of suitable wind farm data, this thesis has taken a deterministic approach. The power fluctuation of a wind farm due to wind turbulence is characterized, one frequency f_W at a time, by $\Delta P_W = M_W \sin(2\omega f_W t)$. This power fluctuation will affect the frequency deviation

$\Delta\omega(t)$. The filtering available in the power plants are: (i) the kinetic energy in the moments of inertia of the turbine stages and the synchronous generator; (ii) the "virtual storage" as steam is saved in one half cycle and over-expended in the later half cycle.

1.3 Organization of Thesis

The steps taken to show the how the impact of wind power fluctuations affect the frequency deviation from 60 Hz are described in the many chapters of the thesis.

The simulation software to represent the wind power fluctuations of wind farms is developed in Chapter 2. Then the thermal power plant model is reviewed in chapter 3. Chapter 4 brings the wind power fluctuations of wind farm to the thermal plants and by simulations and transfer function analysis evaluates the extent of frequency deviation from the 60 Hz. Chapter 5 returns to the source of the power fluctuations, which is to the individual wind turbine-generators of the wind farm. The intent here is to explore to what extent the power fluctuations can be attenuated before wind power enters the electric utility grid. The objective is to show that frequency deviation can be minimized by filtering at the wind farm end and at the thermal power plant end. Chapter 6 presents the conclusion.

Chapter 2 takes the first step in modeling the wind power fluctuations from the wind farms for simulations by HYPERSIM, the simulation software used in the thesis. The thesis presents for the first time, the S-Modulator, which outputs at the point of connection of the wind farm to the power grid, the complex power $S(t)=P(t)+jQ(t)$. The real power $P(t)$ and reactive power $Q(t)$ can be any function of time t. In the deterministic approach of this thesis, $P(t)=P_{ave}+M_W sin(2\omega f_W t)$. Throughout the research of this thesis, the magnitude of bus voltage at the point of connection is regulated by a feedback loop which nulls the voltage error by injection of the reactive current $Q(t)$. The point of connection becomes a P-V bus.

Chapter 3 is concerned with modeling the thermal power plant. The component sub-systems are: the generator [1-4], the field excitation system [1-5], the power system stabilizer [1-6], the boiler [1-7], the high pressure, intermediate pressure, and low pressure turbines [8], the governor [1-7] and the shaft inertias [1-8]. These models are available in HYPERSIM as icons which are connected together to form a plant. HYPERSIM's models are based on detail models recommended by IEEE Committee Reports. The IEEE Committee Reports present them in block diagrams and they are reproduced in this thesis from [1-11] in Appendix A, B and C.

Chapter 4 connects the S-modulators modeling wind farms together with power plants. The frequency deviations from 60 Hz are studied by simulations and then by analysis based on transfer functions. As frequency deviation is reduced by filtering power fluctuations through energy storage, a side study examines the roles played by: (i) the kinetic energy storage in the moments of inertia of the HP, IP and LP turbines and the generator rotor; (ii) the "virtual storage" of steam. The analytical study has yielded a quantitative method of predicting the frequency deviation from 60 Hz in a utility grid made up of multiple power plants.

Chapter 5 is a study of how the frequency deviation from 60 Hz can be reduced further if the fluctuating wind power can be filtered at the wind farm end. This is because each wind turbine has a large moment of inertia for kinetic energy storage. This storage, combined with the doubly-fed induction generator (DFIG) which is amenable to decoupled P-Q control, enables filtering to be implemented.

The author is indebted to fellow master student, Mr. Baike Shen, for the use of his software implementation of a decoupled P-Q controlled DFIG. The thesis supervisor is insistent that the author should use Mr. Shen's software and not to "reinvent the wheel" by re-developing this software. According to him, the success of one team member should be capitalized to advance the research goals of the team further. In this case, the research goal is to evaluate the strategies of DFIG operation for maximizing wind power acquisition and minimizing frequency deviation. The three strategies examined are:

(i) Power reference kept constant strategy: P_{ref}(=constant)-vs-ω_m (where ω_m is the speed of the DFIG).

(ii) Linear slope strategy: $P_{ref}(=k\omega_m)$-vs-ω_m.

(iii) Maximum wind power acquisition strategy: $P_{ref}(=k\omega_m^3)$-vs-ω_m

Chapter 6 evaluates the combined filtering from the thermal power plant of chapter 2 and from the wind turbine inertia with decoupled P-Q controlled DFIG of chapter 5. As the spatial filtering is not included, the estimate lies on the conservative side.

Chapter 7 presents the conclusions and makes suggestions on future research work.

1.4 Softwares: HYPERSIM, EMTP-RV and MATLAB

For computation intensive simulations in chapter 4, HYPERSIM has been used. HYPERSIM is a powerful software and hardware facility developed by Hydro Quebec. It has 12 parallel processors to simulate large power systems in real-time [1-12]. Because the system under study is small, neither parallel computation nor real-time is required for the research. HYPERSIM has been used for 2 reasons: (1) it has a good library of default models of sub-systems of the power grid; (2) the thesis supervisor has plans to use HYPERSIM for large systems studies and the work of the thesis is a preparatory stage

Because the available HYPERSIM facility does not have a software model of the wound rotor induction machine around which to build a decoupled P-Q controlled doubly-fed induction generator (DFIG), the research of chapter 5 has been simulated using EMTP-RV (the well-known ElectroMagnetic Transient Program of Professor Dommel, Revised Version). The software package developed by Mr. Baike Shen has been written in EMTP-RV.

MATLAB is used in non-simulation work.

CHAPTER 2

WIND FARM MODELED BY S-MODULATOR

2.1 Objective of Model

It is necessary to model the output power of wind farms. The software HYPERSIM does not have icons modeling wind farms. In the research of this thesis, wind farms are modeled by S-modulators.

This chapter describes the construction of an S-modulator which injects arbitrary time-varying real and reactive 3-phase power $S=P(t)+jQ(t)$ into a voltage bus of the power grid in HYPERSIM. The magnitude, the frequency and the phase angle of the voltage at bus may be changing in time, as they do when large fluctuating complex powers are injected into the power system and they are simulated by HYPERSIM. But the S-modulator keeps delivering the complex power set by the time varying references $P_{ref}(t)$ and $Q_{ref}(t)$. The time varying references, $P_{ref}(t)$ and $Q_{ref}(t)$, compact the fluctuating complex powers of arrays of wind-turbine generators of a wind farms as the equivalent complex power outputs at the point of connection to the utility grid. As this thesis is primarily a deterministic study, the real power reference takes the form $P_{ref}(t)= -[P_{w-ave}+M_W sin(2\pi f_W t)]$ in chapter 3. When data files of wind farms become available, they can be loaded as $P_{ref}(t)$ and $Q_{ref}(t)$.

The S-modulator makes use of the icons which are available in HYPERSIM: the Phase Lock Loop (PLL), the a-b-c to o-d-q transformation block, the inverse o-d-q to a-b-c transformation block, 3-phase Controlled Current Sources, adders and multipliers.

The S-modulator makes use of the following ideas:

(1) Using the PLL to track the bus frequency and voltage to establish the d-q frame; the a-b-c frame bus voltages are transformed to the o-d-q frame voltages. The d-q frame voltages ($V_{d,}$, V_q) are (0, V_q) because a PLL is applied to establish the d-q axes.

(2) In the d-q frame, $P=v_di_d+v_qi_q$ and $Q=-v_di_q+v_qi_d$. Since $V_d=0$, decoupling of P from Q is possible. Therefore the injected currents to control $P_{ref}(t)$ and $Q_{ref}(t)$ are: $i_{q\text{-}ref}(t)=P_{ref}(t)/V_q$, $i_{d\text{-}ref}(t)=Q_{ref}(t)/V_q$.

(3) The d-q currents $i_{q\text{-}ref}(t)$, $i_{d\text{-}ref}(t)$ undergo an inverse transformation to a-b-c current references ($i_{a\text{-}ref}$, $i_{b\text{-}ref}$, $i_{c\text{-}ref}$).

(4) Feedback regulation of complex power.

2.2 Construction of S-Modulator

2.2.1 P-Q Type

As illustrated in Fig. 2.1, the a-b-c voltages of the bus are transformed to the 0-d-q reference frame. Internally, there are 2-steps to the transformation. The Phase Lock Loop (PLL) acquires the frequency and the phase angle of the a-b-c bus voltages. When the phase of the a-phase is made to coincide with the α-phase in the α-β frame, the α-β frame voltages has the form $[cos(\theta),sin(\theta)]$ where $\theta=\omega_t t$. The second step of transformation from α-β frame to the d-q frame voltages brings the voltage to $(0,\ V_q)$. Since $V_d=0$, it allows decoupled P-Q control. The real power $P=V_di_d+V_qi_q$ becomes $P=V_qi_q$. Thus the power $P_f(t)$ is achieved by injecting $i_{q\text{-}ref}(t)=P_f(t)/V_q$. The reactive power

$Q=V_q i_d - V_d i_q$ becomes $Q=V_q i_d$ and by injecting $i_{d\text{-}ref}(t)=Q(t)/V_q$, the reactive power Q is obtained. The reference currents ($i_{d\text{-}ref}(t)$, $i_{q\text{-}ref}(t)$) are transformed back to the α-β frame using the same [$cos(\omega_f t), sin(\omega_f t)$] information from the PLL. After the α-β to a-b-c transformation, the three phase currents ($i_{a\text{-}ref}$, $i_{b\text{-}ref}$, $i_{c\text{-}ref}$) are injected by 3-phase controlled current source icons available in HYPERSIM.

Fig. 2.1 shows that close regulation to the references $P_{ref}(t)$, $Q_{ref}(t)$ is obtained by measuring the complex power $P_m(t)$, $Q_m(t)$ and passing the errors between them through a proportional-integral block before becoming P, Q.

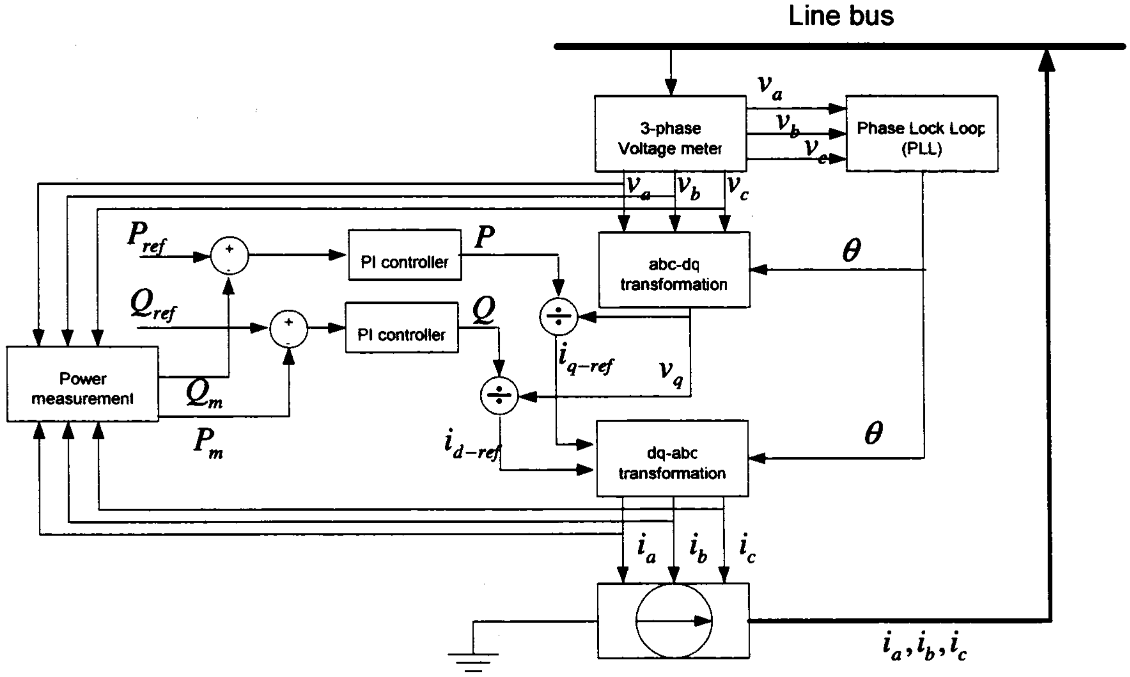

Fig. 2.1. Diagram of S-Modulator in P-Q type

2.2.2 P-V Type

There are occasions when reactive power Q needs to be injected by the S-modulator so as to regulate the magnitude of the voltages of the bus. As shown in Fig. 2.2, the magnitude of the bus voltage V_t is measured and compared with the voltage reference V_{ref}. The error, after passing through a proportion-integral transfer function block, is applied to Q in negative feedback. In nulling the error, the ac voltage is regulated.

In the research in chapter 3, the P-V type has been applied throughout because in the opinion of the research supervisor, the thesis should be focused on the deviation of ω_r by fluctuating real power. The effect of fluctuating reactive power, while important and interesting, will be a subject of future research.

The following observations taken from the simulation experiments in chapter 3 are worth noting:

(1) The size of Q is large when integral feedback is used to null the error.

(2) The size of Q is significantly reduced when a small voltage error is tolerated by using proportional feedback only.

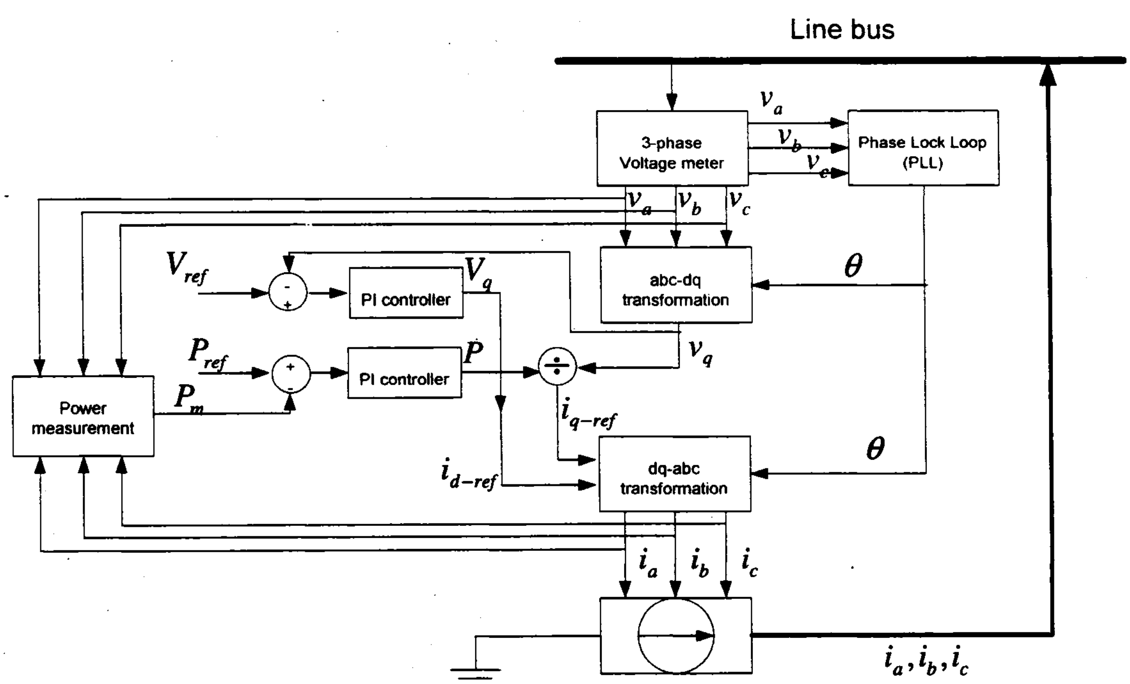

Fig. 2.2. Diagram of S-Modulator in P-V type

2.3 Applications of S-Modulator

(1) Real power outputs of Wind Farms.

The time varying function in the real power reference $P_{ref}(t)$ allows wind farms to be modeled in HYPERSIM. Presently wind data of wind farms in the frequency range of wind turbulence are not available. When they become available in data files, it is matter of transferring them to $P_{ref}(t)$.

For this thesis, a deterministic study is pursued before considering stochastic wind power. In chapter 3, the test setting is: $P_{ref}(t)= -[P_{w\text{-}ave}+M_W sin(2\pi f_W)]$ where M_W is the peak sinusoidal power component at frequency f_W riding on the average power $P_{w\text{-}ave}$. The interest is in finding from simulations how the outputs of thermal power plants respond to wind power fluctuation at a single frequency f_W. The study of the output/input response over a spectrum of wind power frequencies f_W is a systematic approach by which the filtering characteristics of power plants are evaluated before proceeding to stochastic studies in future theses.

(2) Voltage Support System

When the bus voltage of the wind farm voltages is regulated, power fluctuations propagate in the power grid as current fluctuations through the transmission lines. Because of voltages drops across line impedances, the buses and nodes inside the power grid experience voltage fluctuations. As much as frequency margins must be met (which is the concern of this thesis), voltage margins must also be met. In order to meet the regulations on voltage magnitude, voltage support systems in the forms a combination of Switched Capacitors and Static Var Compensators (SVC) or Switched Capacitors and

STATCOMs will be required.

As this thesis does not treat voltage support, the problem is side-stepped by connecting S-modulators at buses with voltage fluctuations. The S-modulator injects reactive power Q to regulate the bus voltage.

2.4 Conclusion

This chapter has presented the S-Modulator, which has proven to be a very useful simulation tool in the research carried out in chapter 3.

CHAPTER 3

SUB-SYSTEM MODELS OF THERMAL PLANT

3.1 General Introduction

Having described the S-modulator in chapter 2, this chapter presents the models of the sub-systems of power plants available in HYPERSIM. The many sections in this chapter present the sub-systems in block diagram form [3-1]. As chapter 4 will proceed with analysis by Transfer Functions, this chapter is only concerned with:

(i) Deriving the Transfer Functions, using small perturbation linearization wherever nonlinear equations are encountered;

(ii) Presenting the characteristics of the sub-systems in the form of Bode Diagrams (using the parameters listed in Appendix B).

In this thesis, it is assumed that power system is made up of thermal plants only. The reasons for this decision are:

(i) Thermal plants are more complex than hydro plants and once the more complex plant is shown to amenable to analysis, it follows that the simpler plant will present no problem;

(ii) In leveling wind power fluctuations, power plants must be capable of temporarily storing wind power peaks to fill in valleys so that nuclear plants, which are operated to deliver constant power, are considered to be unsuited for filtering;

(iii) A mix of thermal and hydro plants will add complication without bringing understanding to the issues.

The thermal power plant of this thesis is made of the sub-systems in Fig. 3.1. The boiler at the left-hand end feeds high pressure steam (P_{sih}) to the turbines. It is assumed P_{sih} is constant. The turbine torque T_m drives the synchronous generator against the counter torque T_e of the synchronous generator at the right-hand end. Of particular interest in this thesis is the "Shaft Swing Equation" by which the combined inertias of the turbine and the generator rotor are accelerated and decelerated by the resultant torque ($T_m + T_e$). This is because the frequency of the generator frequency ω_f is proportional to the rotor speed ω_m.

Fig. 3.1 also shows the 2 main control blocks: the speed governor and the field excitation system. The speed governor has 2 inputs, the speed reference ω_{ref} and the power reference P_{ref}. The speed governor determines the opening or the closing of the steam valve (X) from the feedback signal of the rotor speed ω_m.

The excitation control block monitors E_t, the terminal voltage of the generator. Regulation to the voltage reference V_{ref}, is by using the voltage error, in negative feedback, to increase or decrease the field exciter voltage E_{fd}.

In situations where the power system has unstable or lightly damped oscillations, a power system stabilizer (PSS) is added to stabilize or increase the damping. The oscillations are typically between 0.1 and 2.0 Hz [3-2] which are in the range of the fluctuating wind frequencies. As the overlap in frequency ranges are likely to cause complicated interaction, on the advice of the research supervisor, the PSS is not included in the scope of this thesis and will be the subject of a later thesis.

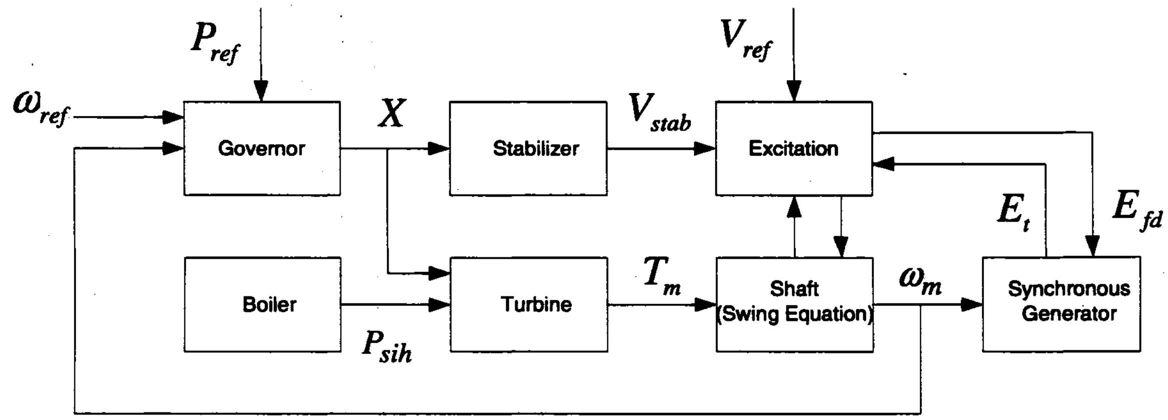

Fig. 3.1. Model of thermal plant

3.2 Linearization and Transfer Functions of Thermal Plant

The mathematical models of the sub-systems of thermal plant contain nonlinear elements. In order to proceed to the Transfer Function analysis, small-signal perturbation linearization is applied to derive the Transfer Functions.

3.2.1 Governor

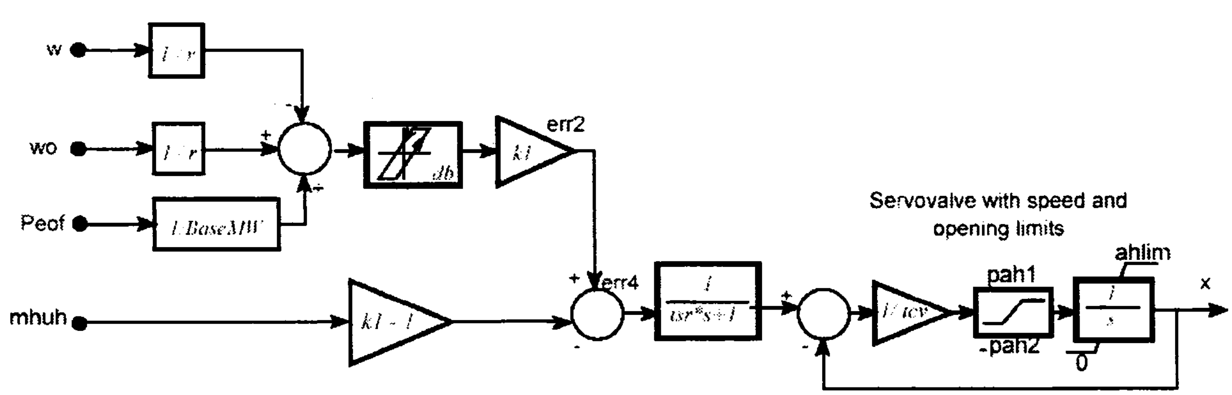

Fig. 3.2. Model of speed governor

As a speed regulator, the governor's main task is to regulate the generator speed ω_m

which is proportional to the frequency ω_r. The frequency ω_r (w in Fig. 3.2) is compared with the reference ω_{ref} (ω_o in Fig. 3.2) and the error $\Delta\omega_r = \omega_{ref} - \omega_r$ is divided by the droop r. The output of the governor is the position of valve X. The fluctuation of $\Delta\omega_r$ makes the steam valve open and close.

The governor droop r is defined as $r = \Delta\omega_r / \Delta X$, i.e. the speed change over the valve position change. Typically, the droop is 0.05. This means that 5 percent of rotor speed change leads 100 percent valve position change (fully open to fully close). Ignoring the hysteresis and limit blocks in Fig. 3.2, the linearized transfer function of the governor defined as:

$$G_{gov}(s) = \frac{\Delta X(s)}{\Delta\omega_r(s)} \qquad (3\text{-}1)$$

Fig. 3.3 shows the Bode diagram shown for r=0.02, 0.03 and 0.04.

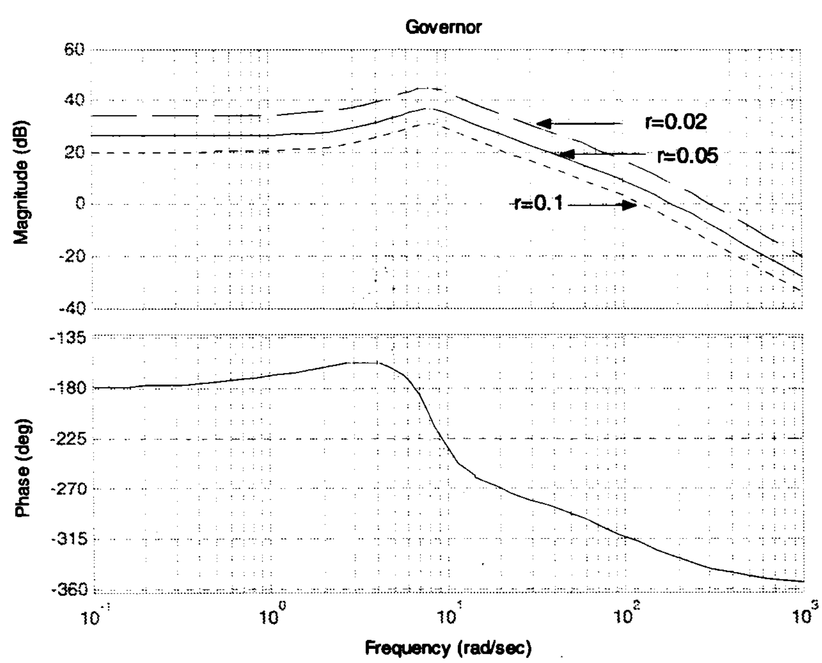

Fig. 3.3. Bode diagram of governor transfer function

In the frequency domain, the governor has the characteristics of as a Low Pass Filter (LPF) with a peak value around 1.27 Hz. The magnitude drops down significantly at high frequencies. When the droop is changed, the magnitude response moves up and down but the phase response is not affected.

3.2.2 Excitation System

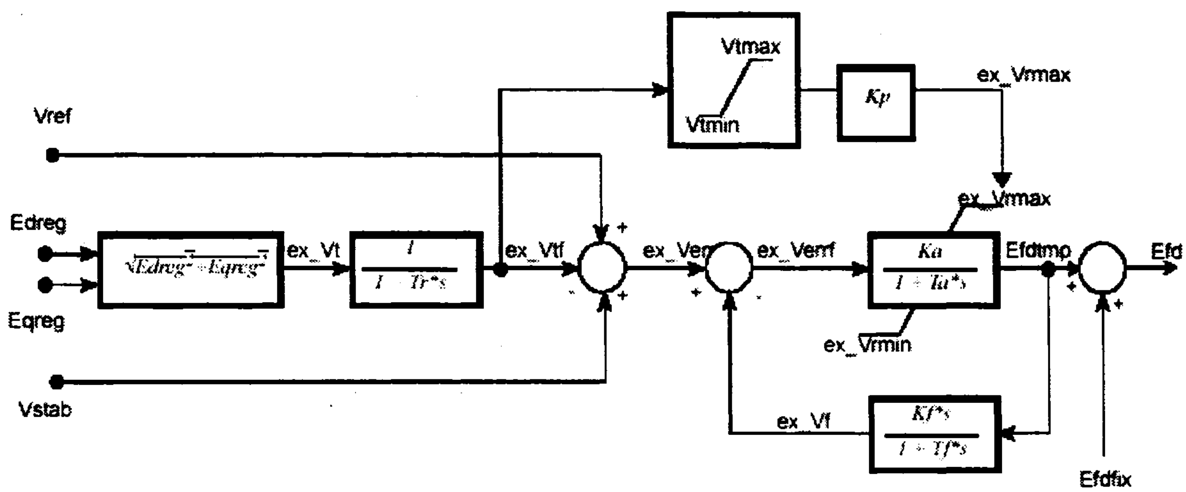

Fig. 3.4. Model of excitation system

The excitation system regulates the terminal voltage V_t of the generator by increasing or decreasing the dc field current. In Fig. 3.4, the voltage reference is V_{ref}. The 3-phase terminal voltage measurements have been transformed into the d-q frame voltages as E_{dreg}, E_{qreg} and its magnitude $[(E_{dreg})^2+(E_{qreg})^2]^{0.5}$. After passing through a filter of time constant T_r, V_t is compared with the reference V_{ref}. The output of the Excitation System is the voltage E_{fd}. An important parameter is the gain K_a. The transfer function of the exciter is:

$$G_{exc}(s) = \frac{\Delta E_{fd}(s)}{\Delta V_t(s)} \qquad (3\text{-}2)$$

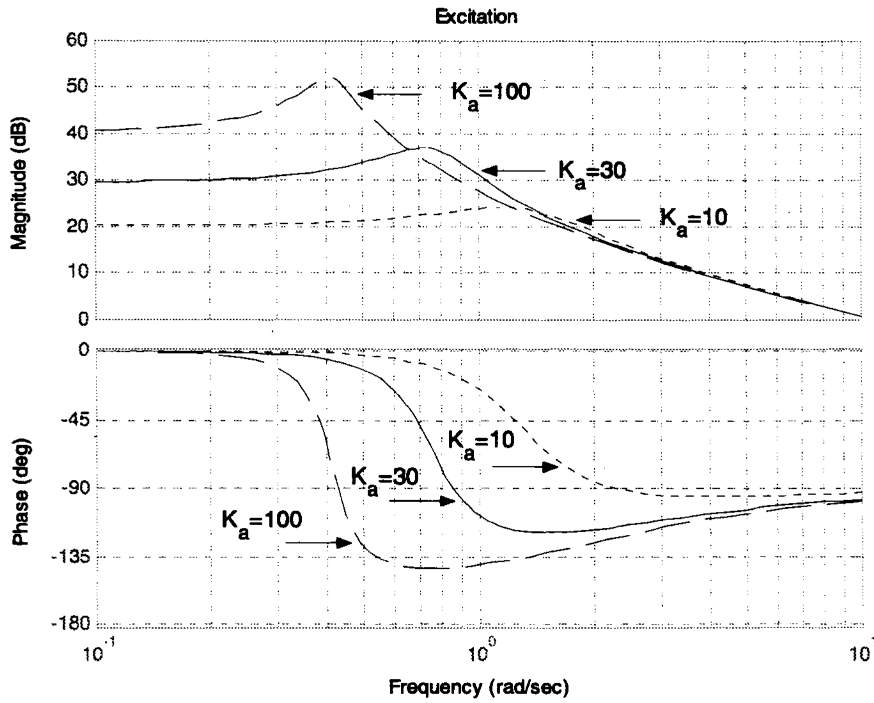

Fig. 3.5. Bode diagram of excitation system transfer function

The excitation system has Low Pass Filter characteristics. Both the magnitude and the phase responses change with the excitation gain K_a.

3.2.3 Boiler

The model of the boiler is shown in Fig. 3.6. The time constants of the component blocks indicate that the boiler has a very long time response. Thus the output *psih* is treated as a constant 1.0 pu. This means that it supplies 1 per unit power to the steam turbine.

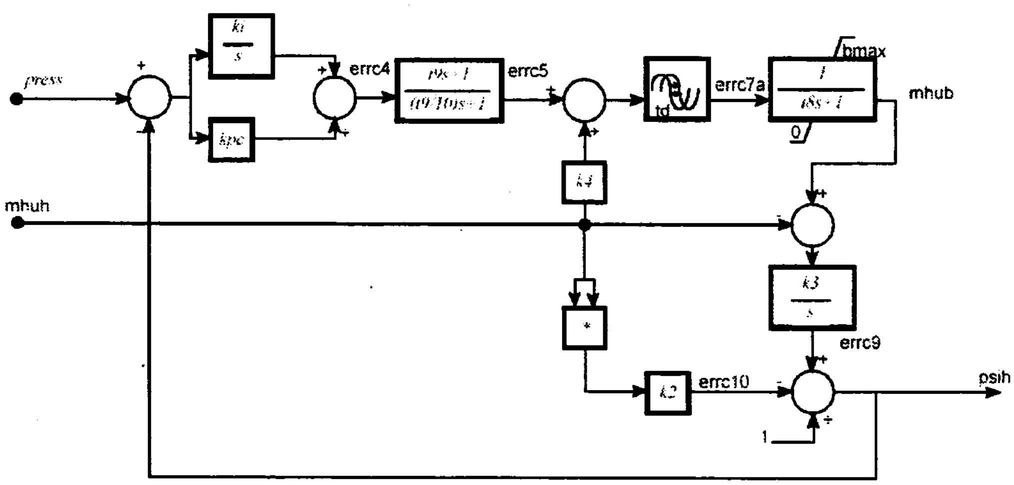

Fig. 3.6. Model of boiler

3.2.4 Turbine

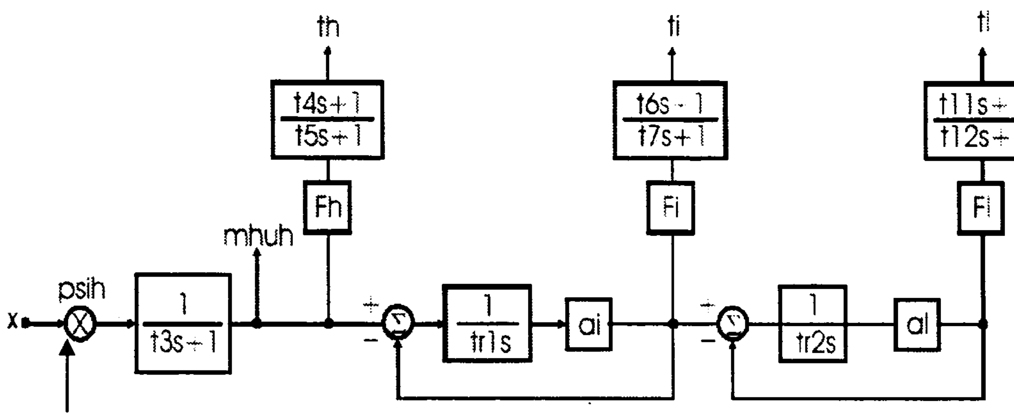

Fig. 3.7. Model of Turbine

The steam turbine of Fig. 3.7 has 3 stages: the high pressure turbine (HP), the intermediate pressure turbine (IP) and the low pressure turbine (LP). Each stage outputs torques: *th* (T_h), *ti* (T_i), and *tl* (T_l). The power into the turbine is controlled by the valve position *X* (from the governor) which is multiplied to *psih* (from the boiler). The input is

X and the output is the mechanical torque $T_m = T_h + T_i + T_l$ driving shaft against the generator counter torque T_e. The transfer function of the turbine is:

$$G_{turb}(s) = \frac{\Delta T_m(s)}{\Delta X(s)} = \frac{\Delta T_l(s) + \Delta T_i(s) + \Delta T_h(s)}{\Delta X(s)} \tag{3-3}$$

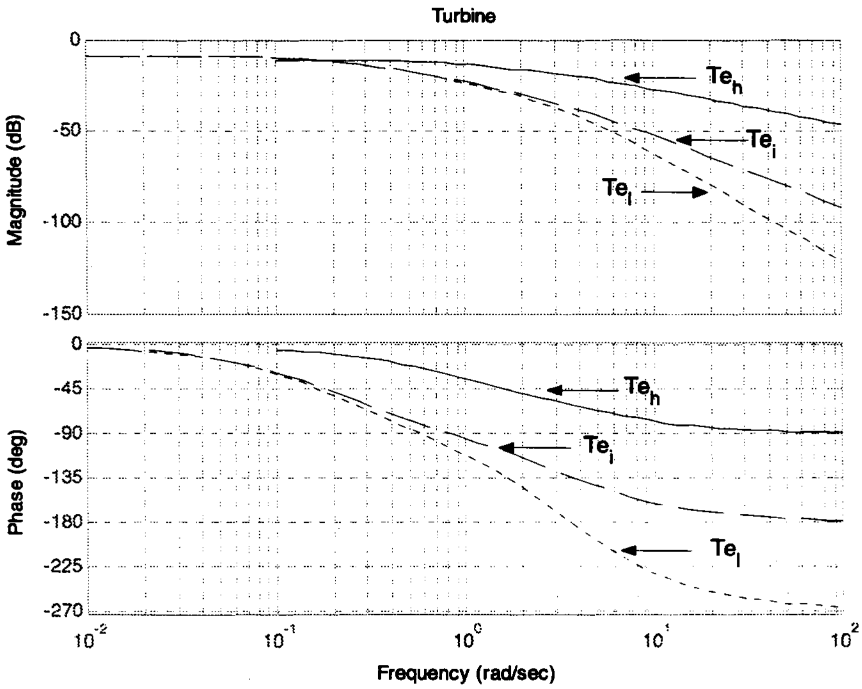

Fig. 3.8. Bode diagram of turbine transfer function

The turbine has the characteristics of a Low Pass Filter. The 3 different stages of the turbine have different phases and magnitude gains. The overall response of the turbine is the sum of three parts.

In this thesis, the torsional spring constants of the turbine shaft between turbine inertias are not modeled. The shaft is considered to be inelastic so that there is no torsional resonance. The mechanical power from the turbine is $P_m = \omega_r(T_h + T_{mi} + T_i)$.

3.2.5 Shaft (Swing equation)

The most important equation in this thesis is Newton's Law of Motion (in rotational frame) regarding the acceleration of the moments of inertia J belonging to the shaft by the combined turbine torque T_m against the generator counter torque T_e.

$$J(d\omega_r/dt)=T_m - T_e$$

Multiplying both sides by the synchronous speed ω_{r0} and applying per unitization, using the MVA of the plant, one has

$$2H(d\omega_r/dt)=P_m - P_e \qquad (3\text{-}4)$$

where ω_r should strictly be rewritten as ω_r/ω_{r0}. The moment of inertia J (whose dimension is given in kg-m^2) has been transformed to H (whose dimension is given in second). The inertia constant H includes those of the rotors of the generator, the high pressure turbine, the intermediate pressure turbine and the low pressure turbine. All the rotors rotate at the same speed per unitized speed ω_r.

As the per unitized speed ω_r is the same as the per unitized frequency, the deviation of grid frequency $\Delta\omega_r$ is caused by the accelerating power $P_{accel} = P_m - P_e$. Defining the transfer function of the shaft dynamics as $G_{shaft}(s)$ as:

$$G_{shaft}(s) = \frac{\Delta\omega_r(s)}{\Delta P_{accel}(s)} \qquad (3\text{-}5)$$

Its Bode diagram is shown in Fig 3.9.

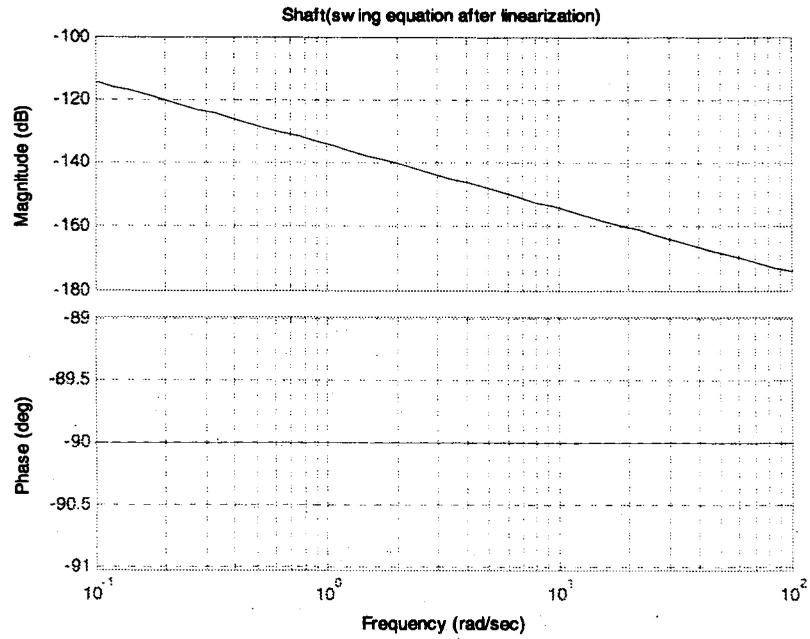

Fig. 3.9. Bode diagram of shaft transfer function $G_{shaft}(s)$

3.3 Transfer Function of Thermal Plant

Having defined the transfer functions and viewed their Bode diagrams of the sub-systems of the thermal plant of Fig. 3.1, this section integrates the many parts together into a form which can be used in the study how fluctuations in wind power ΔP_{wind} affects the grid frequency deviation $\Delta\omega_r$.

In the first place, it is assumed that in the absence of wind turbulence, ω_r=1 pu and $P_{acce0l}=P_{m0}-P_{e0}=0$. P_{e0} is the power taken by the load of the grid, with the steady state component of wind power P_{wind0} subtracted from it, i.e. $P_{e0}=P_{Load}-P_{wind0}$. To meet this load commitment the power reference of the plant is set to $P_{ref}=P_{m0}=P_{e0}$. The fluctuating component of wind power is defined as P_{wind}. The total wind power is $P_{wind}= P_{wind0}+\Delta P_{wind}$. Since P_{Load} is assumed to remain constant, the entry of fluctuating wind power ΔP_{wind} has the effect of relieving the generation power so that

$$P_e = P_{Load} - P_{wind0} - \Delta P_{wind}$$

or $\Delta P_e = -\Delta P_{wind}$. Therefore, the study is focused on how the grid frequency deviation $\Delta\omega_r$ is affected by ΔP_e.

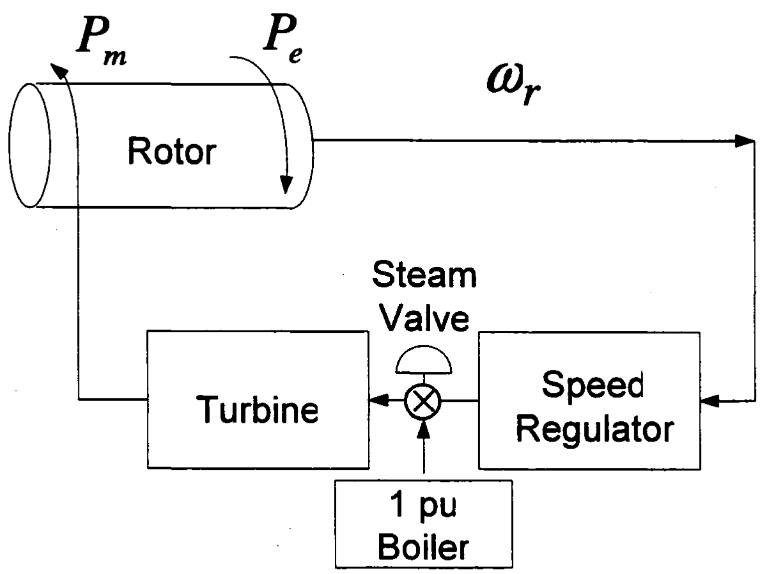

Fig. 3.10. Diagram of prime moyer and energy supply of thermal plant

Fig. 3.10 highlights the speed regulation of the power plant. The shaft dynamics (swing equation) determines the rotor speed ω_r from the acceleration power $P_{accel}=P_m-P_e$. The rotor speed ω_r is the feedback information which the speed regulator uses to determine X, the opening of the steam valve, to increase or decrease the power plant power P_m. The overall transfer function $G_3(s)=\Delta\omega_r(s)/\Delta P_e(s)$ is made up $G_1(s)$ and $G_2(s)$ shown in Fig. 3.11 and described in greater detail in the sub-sections below.

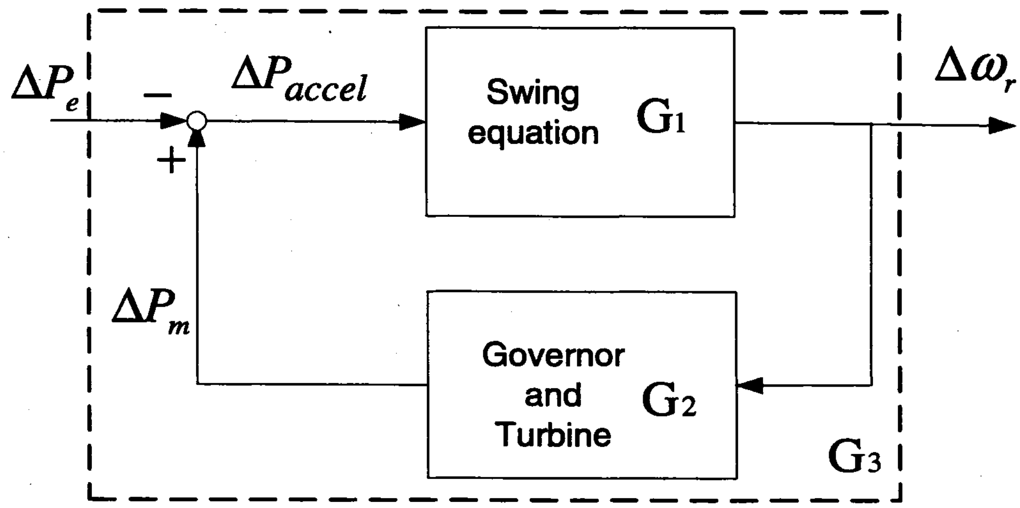

Fig. 3.11. Transfer Function $G_3(s)= \Delta\omega_r(s)/\Delta P_e(s)$

(1) Shaft Transfer Function of $G_1(s)$

$G_1(s)$ is the same as $G_{shaft}(s)$ of (3-5). This transfer function relates grid frequency deviation $\Delta\omega_r(s)$ (rotor speed) to the perturbation accelerating power $\Delta P_{accel}(s) = \Delta P_m(s) - \Delta P_e(s)$ and is taken from $2\omega_0 H(d\omega_r/dt)=T_m-T_e=T_{accel}$.

$$G_1(s) = \frac{\Delta\omega_r(s)}{\Delta P_{accel}(s)} \qquad (3\text{-}6)$$

(2) Turbine and Governor Transfer Function $G_2(s)$

$G_2(s)$ is the transfer function of the steam turbine system and the governor system. Based on $\Delta\omega_r(s)$, the governor opens the steam valve to admit the turbine power $\Delta P_m(s)$. The governor droop r is an important parameter inside $G_2(s)$ which is defined as:

$$G_2(s) = \frac{\Delta P_m(s)}{\Delta\omega_r(s)} \qquad (3\text{-}7)$$

(3) Transfer Function $G_3(s)$

$G_3(s)$ is the transfer function of the overall closed loop feedback of Fig. 3.11.

$$G_3(s) = \frac{\Delta\omega_r(s)}{\Delta P_e(s)} = \frac{G_1(s)}{G_1(s)G_2(s)-1} \tag{3-8}$$

It is obtained by substituting $\Delta P_{accel}(s)$ in $G_1(s)$ in (3-6) and applying $G_2(s)$ and (3-7) to eliminate $\Delta P_m(s)$.

Fig. 3.12 (a), (b) and (c) respectively present the Bode diagrams of $|G_1(s)|$, $|G_2(s)|$ and $|G_3(s)|$ for permanent droop r=0.05 (linear vertical scale). Their phase angles have not been plotted. $G_1(j2\pi f_W)$ has a $1/jf_W$ function dependency, which explains, in part, for the attenuation of $|G_3(s)|$ at high frequencies. The phase lag of 90° in $G_1(j2\pi f_W)$ (not shown) contributes to the presence of the resonant peak in $|G_3(s)|$ in Fig. 3.12 (c).

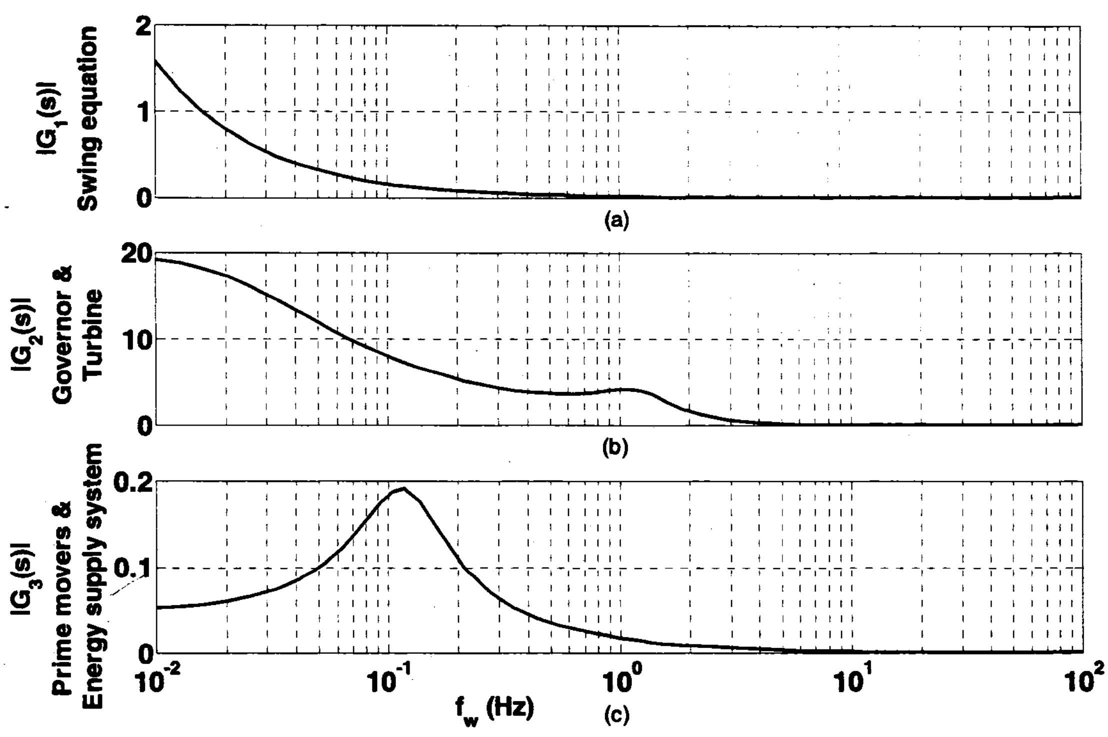

Fig. 3.12. (a) $|G_1(s)|$, (b) $|G_2(s)|$ and (c) $|G_3(s)|$

3.3.1 Effect of Droop on Power Plant Transfer Function

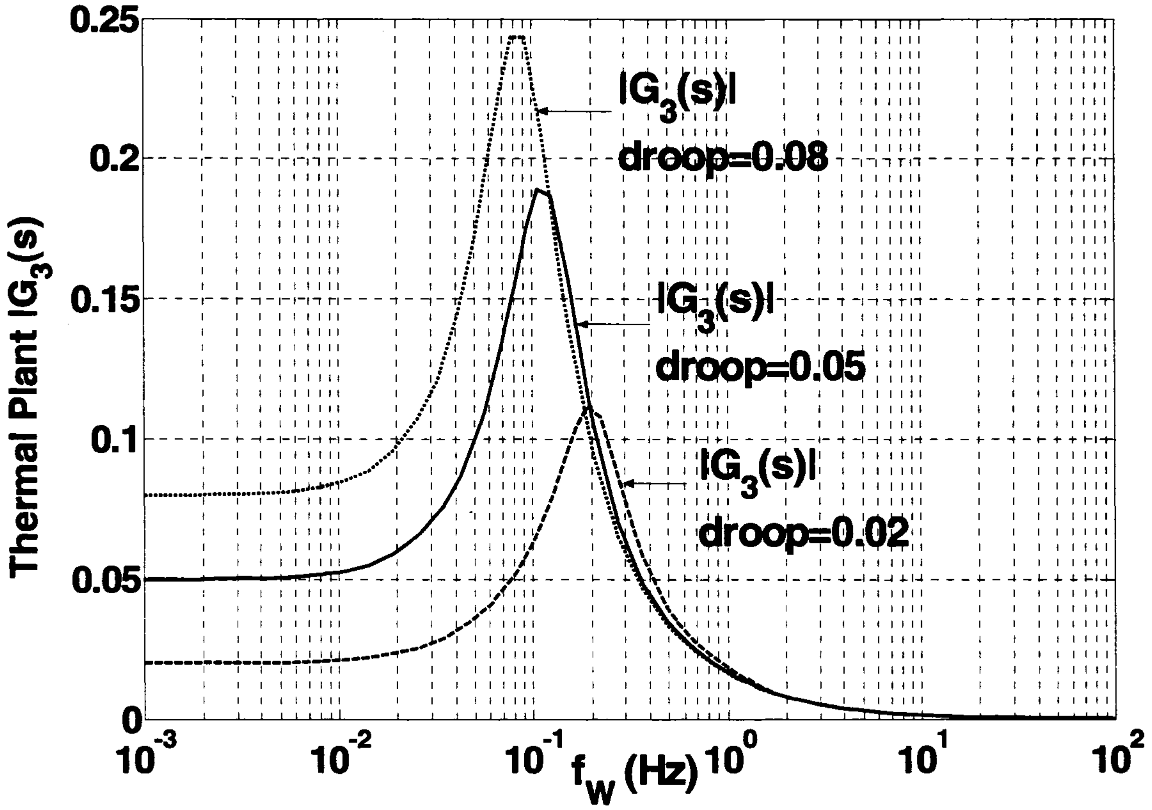

Fig. 3.13. Effect of regulation droop on $G_3(s)$

Fig. 3.13 is a study of the effect of the size of the droop r on $|G_3(s)|$. When the droop is increased, the resonant peak of $|G_3(s)|$ is raised and the corresponding resonant frequency is shifted to the low frequency region.

As $\Delta\omega_r(s)=G_3(s)\Delta P_e(s)$, for low frequency deviation, $|G_3(s)|$ should be kept small. There is little chance of being allowed to vary the droop from the traditional value of 0.05 because plant operators are concerned about the other practical constraints which must be respected.

3.4 Conclusions

This chapter has developed the transfer function $G_3(s)=\Delta\omega_r(s)/\Delta P_e(s)$ which is suited for the study of grid frequency deviation due to wind power fluctuation. Chapter 4 will present good agreement between the measurements from simulation tests and the predictions from the transfer function, which validates the assumptions made in this chapter regarding the linearized models.

CHAPTER 4

POWER FLUCTUATIONS IN THERMAL POWER PLANTS

4.1. Introduction

The objective of the thesis is to relate quantitatively the frequency deviation from the 60 Hz standard of power plants due to the power fluctuations caused by wind turbulence. This chapter applies the transfer functions of the sub-system components of thermal power plants described in chapter 3 to make the quantitative evaluations. The transfer function approach is accompanied by digital simulations by HYPERSIM, which besides providing cross-checks to accuracy and correctness offers graphical waveform displays. Following the visual clue of identical frequency deviations from separate power plants, it has been possible to develop a far reaching method of predicting the frequency deviation of a multi-plant power network.

This chapter begins by first considering the interaction of a single thermal plant and a single wind farm. The single wind farm is represented by the S-modulator described in chapter 2. In keeping with the deterministic approach, the fluctuation wind power due to turbulence is represented by $M_W sin(2\pi f_W t)$ at wind frequency f_W. The first order of business is to use the simulations of HYPERSIM to establish that the transfer function predictions can be relied on. The second objective is to understand the relative importance of the *kinetic energy storage* of the turbine-generator shaft system and the "*virtual storage*", of the governor system in providing filtering to the power fluctuation.

This chapter then proceeds to a 3-plant, 9-bus system joined by relatively short transmission lines. Although small, the study has yielded useful information as to how the transfer function method developed in this chapter can be extended to large multi-plant systems.

4.2. Single wind farm interacting with single thermal plant

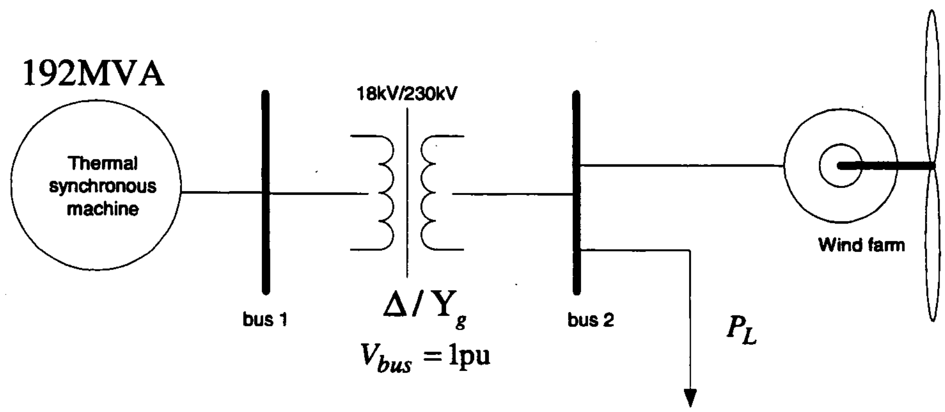

Fig. 4.1. Single wind farm interacting with single thermal plant

Fig. 4.1 shows a single wind farm connected across the output transformer of a single 192 MVA (163.2 MW) thermal plant. Located at bus2, the power of the load is P_L. The parameters of the thermal plant are listed in Appendix B. The wind farm is modeled by S-Modulator of Chapter 2. The S-modulator injects 3-phase complex power $S_W=P_W+jQ_W$ into a voltage bus. The real power is $P_W=P_{ave\text{-}W}+ M_W sin(2\pi f_W t)$. Using negative feedback, the reactive power Q_W is modulated to regulate the ac voltage of the bus. It is assumed throughout this paper that the power plant power output, the average wind power $P_{ave\text{-}W}$ and the load power P_L are balanced and the focus of interest is on how perturbation wind power $\Delta P_{\Sigma wind}=M_W sin(2\pi f_W t)$ affects $\Delta\omega_r(t)$, the frequency deviation from the 60 Hz reference.

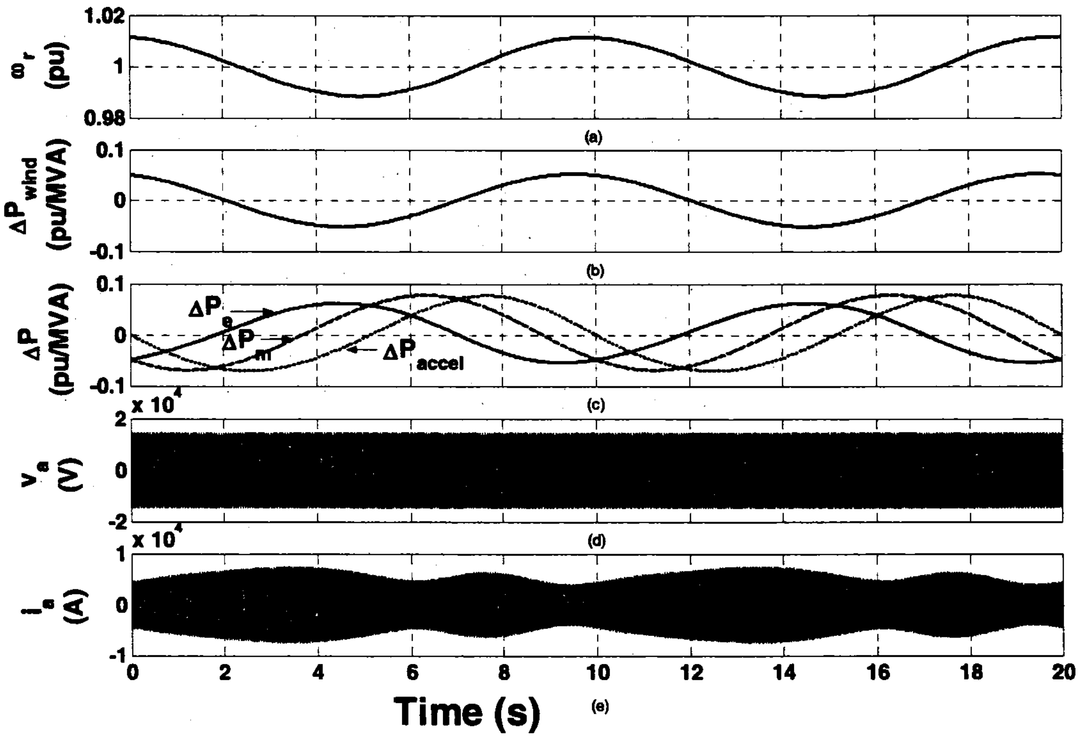

Fig. 4.2. Case study--$\Delta P_{\Sigma wind}$=10sin(2πfwt) MW, f_W=0.1 Hz; (a) grid frequency ω_r pu; (b) perturbation wind power ΔP_{wind} MW. (c) ΔP_{accel}, ΔP_m and ΔP_e; (d) phase voltage; (e) phase current of transmission line.

Fig. 4.2 presents the simulation results for wind power injections $\Delta P_{\Sigma wind}=M_W sin(2\pi f_W t)$ for M_W = 10 MW and f_W = 0.1 Hz. The quantities in the graphs of Fig. 4.2 are: (a) the grid frequency $\omega_r(t)$, (b) the wind power fluctuation $M_W sin(2\pi f_W t)$, (c) $\Delta P_e(t)$, $\Delta P_m(t)$ and $\Delta P_{accel}(t)$ which are perturbations of the powers defined in Fig. 3.11, (d) a line-to-ground voltage at the point of connection and (e) a line current. For the time scale used, the 60 Hz voltage and current appear as smudges in Fig. 4.2 (d) and (e). The voltage envelope shows that the ac voltage is regulated by the negative feedback using Q-control to inject reactive power. The envelope of the line currents shows distortion of the 60 Hz by the wind power fluctuating at frequency f_W =0.1 Hz.

From such simulation results, measurement of $|\Delta\omega_r|$ are gathered and plotted in Fig. 4.3 against M_W for different wind power fluctuating frequencies f_W. The gradients of the straight lines increase from f_W=0.05 Hz to 0.1 Hz and then decrease to a low value at f_W=1 Hz, suggesting that there is a resonant peak in between 0.1 Hz and 1 Hz.

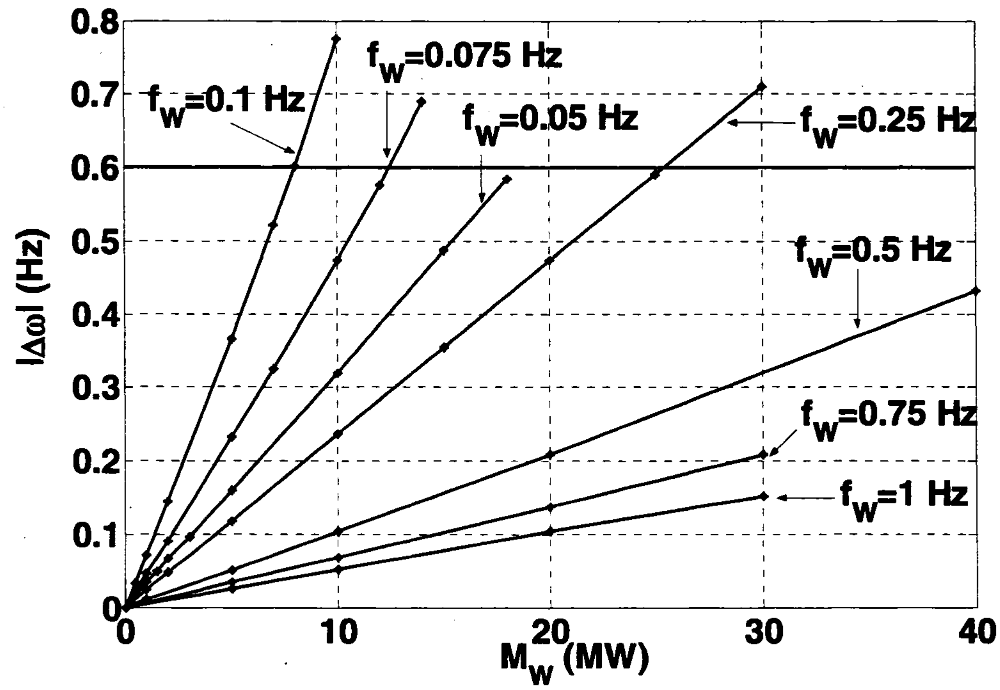

Fig. 4.3. $|\Delta\omega_r|$-vs-M_W at different wind power fluctuating frequency f_W

If the frequency deviation $\Delta\omega_r$ is to be kept acceptably small, there must be significant temporary storages by which the fluctuating wind power $M_W sin(2\pi f_W t)$ is absorbed in one half cycle and then released in the second half cycle. Since the wind power relieves the generator power of the plant, ΔP_e in Fig. 4.2 (c) is equal and opposite to the perturbation wind power $\Delta P_{\Sigma wind}=M_W sin(2\pi f_W t)$ in Fig. 4.2 (b). The thermal plant is "aware" of the wind power as $-\Delta P_e(t)$. Fig. 4.2 (c) shows how turbine power $\Delta P_m(t)$ and the accelerating power $\Delta P_{accel}(t)$ maintain instantaneous power balance with $-\Delta P_e(t)$.

The power components of the storages are: (i) $\Delta P_{accel}(t)$, the power which accelerates or decelerates the shaft inertia H (kinetic energy); and (ii) $\Delta P_m(t)$, the turbine power of the "virtual storage", where steam energy is saved for one half a cycle and returned in the other half cycle. As Fig. 4.2 (c) shows, there are phase differences in $\Delta P_e(t)$, $\Delta P_m(t)$ and $\Delta P_{accel}(t)$, indicating that these storages are not by arithmetic sum. Fig. 4.4 (a), (b), (c) and (d) show the phasor diagrams of ΔP_e, ΔP_m and ΔP_{accel}, for f_W=0.05Hz, f_W=0.07Hz, f_W=0.1Hz, and f_W=2.5Hz respectively. As a reference for comparison, $|\Delta P_e|$ is kept at 1.0 pu. One notes that the lengths of ΔP_{accel} and ΔP_m (defined in Fig. 3.11,) reveal the relative amounts of ΔP_e that have gone to kinetic storage and "virtual storage". One sees from Fig. 4.4 (a) that "virtual storage" dominates at low values of f_W. There is little kinetic energy in H for low speed fluctuations. For high f_W, kinetic storage takes over, as Fig. 4.4 (d) illustrates. Because of the $1/f_W$ function dependency, $\Delta\omega_r$ is small for high frequencies and the steam valve is almost closed.

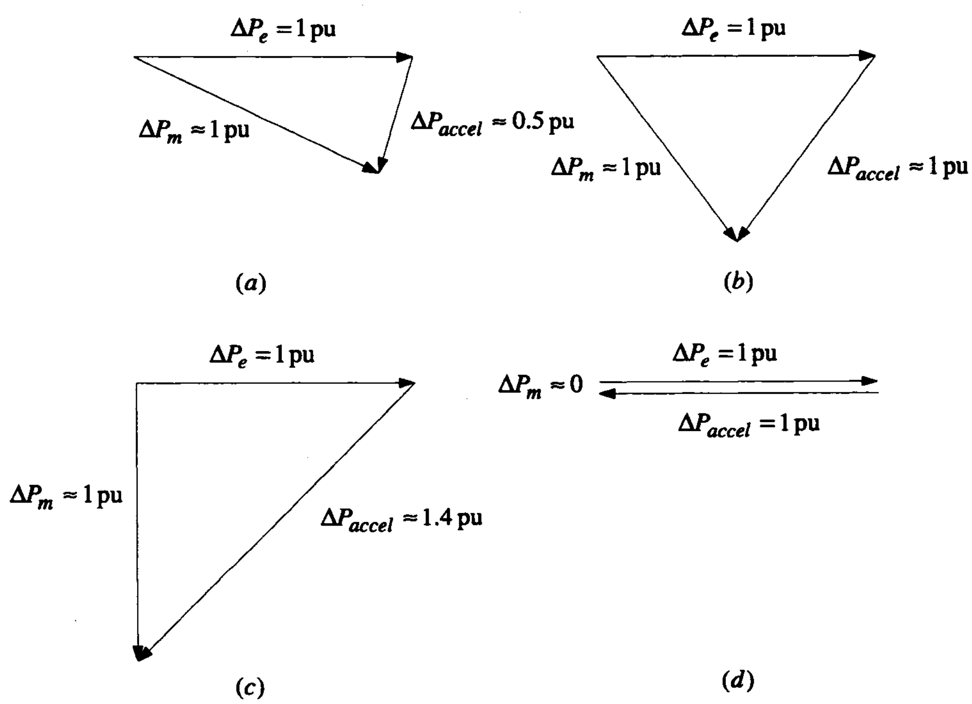

Fig. 4.4. Phasor diagrams of ΔP_{accel}, ΔP_m and ΔP_e of thermal plant. (a) f_W=0.05 Hz. (b) f_W=0.07 Hz. (c) f_W=0.1 Hz. (d) f_W=2.5 Hz

Limit of Wind Power $M_W sin(2\pi f_W t)$

The curves of Fig. 3.12 are for governor droop r=0.05. Since $|\Delta\omega_r(s)|$= $|G_3(s)|\,|\Delta P_{\Sigma wind}(s)|$, the resonant peak of Fig. 3.12 (c) sets the upper limit of grid frequency deviation $\Delta\omega_r$. For 1.0% deviation from 60 Hz (59.4 to 60.6 Hz), M_W can be as high as 5.25% of the 163.2 MW rating. Although Fig. 3.12 (c) comes from deterministic analysis, it gives an idea of the capability of a thermal generation plant to respond to stochastic wind power when the fluctuations are decomposed in the frequency domain.

4.3. Interaction of Multiple Wind Farms with Multiple Thermal Plants

The objective of this section is to use simulation experiments on a small power system to discover how the power fluctuations from multiple wind farms are "filtered" by the storages of multiple thermal plants. After understanding the underlying principles of operation, a method of estimating the frequency deviation quantitatively is developed.

Fig. 4.5 shows a 9-bus system [4-1] with 3 identical generation plants ($j=1,2,3$). Each plant is modeled by the same 192 MVA (163.2 MW) thermal generation plant in section 4.1. Their loads on the 230 kV buses (bus_j $j=1,2,3$) are P_{Lj}, $j=1,2,3$. As the transfer function $G_3(s)$ embodies the characteristics which are important in this thesis, differences in the plants are embedded into $G_{3j}(s)$ $j=1,2,3$, by setting their permanent droops to r_1=0.05, r_2=0.02 and r_3=0.08. In order to illustrate how they are affected by the droops, Fig. 3.13 shows $|G_{3j}(s)|$, $j=1,2,3$.

The 3 thermal generation plants are interconnected by 230 kV transmission lines which are represented by distributed parameter models, a feature available in the software. Their lengths (L_{47}=80Km, L_{48}=100Km, L_{57}=60Km, L_{68}=30Km, L_{35}=60Km and L_{36}=40Km) have been chosen to be unequal to ensure that the conclusions reached are for the general case.

The wind farms are located at bus_j, $j=4,5,6$ and their local loads are P_{Lj}, $j=4,5,6$. Their steady-state average power output are: $P_{w\text{-}avek}$, $k=1,2,3$.

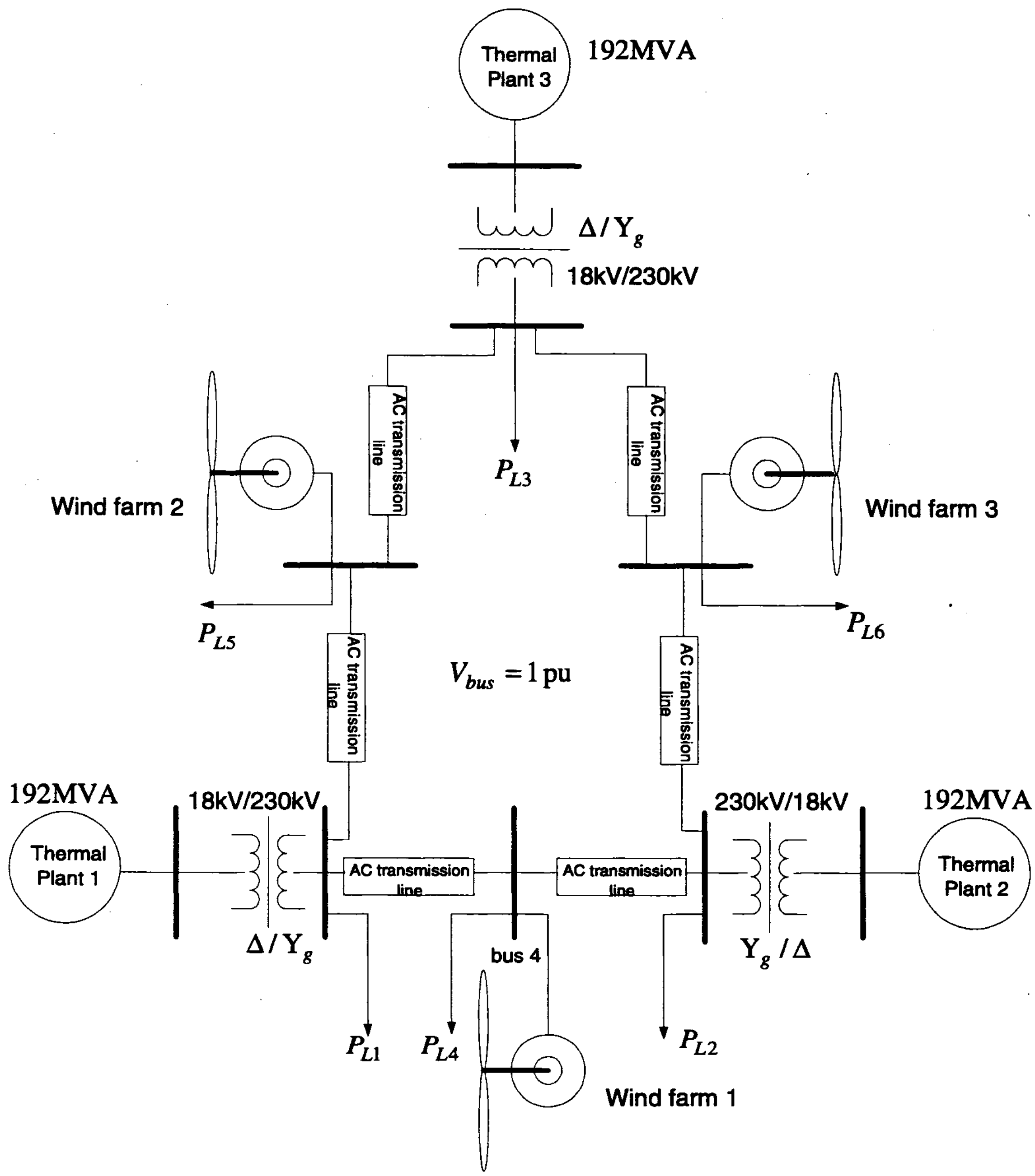

Fig. 4.5. Nine-bus system---three thermal plants and three wind farms.

4.3.1 Simulation Results of Multiple Wind Farms

After the average plant output power, from the 3 thermal plants ($j=1,2,3$) and from the 3 wind farms ($k=1,2,3$), strike steady-state power balance with the loads P_{Lj}, $j=1,2...6$, the wind power fluctuations are injected as: $M_{Wk}sin(2\pi f_W t)$, $k=1,2,3$ with different magnitudes M_{Wk} and frequencies f_W. Fig. 4.6 show simulation results for the case: $\Delta P_{wind1}=15sin(2\pi0.05t)$ MW, $\Delta P_{wind2}=10sin(2\pi0.1t)$ MW and $\Delta P_{wind3}=5sin(2\pi0.25t)$ MW., corresponding to frequencies at 0.05 Hz, 0.1 Hz and 0.25 Hz. They sum together as $\Delta P_{\Sigma wind}=15sin(2\pi0.05t)+10sin(2\pi0.1t)+5sin(2\pi0.25t)$.

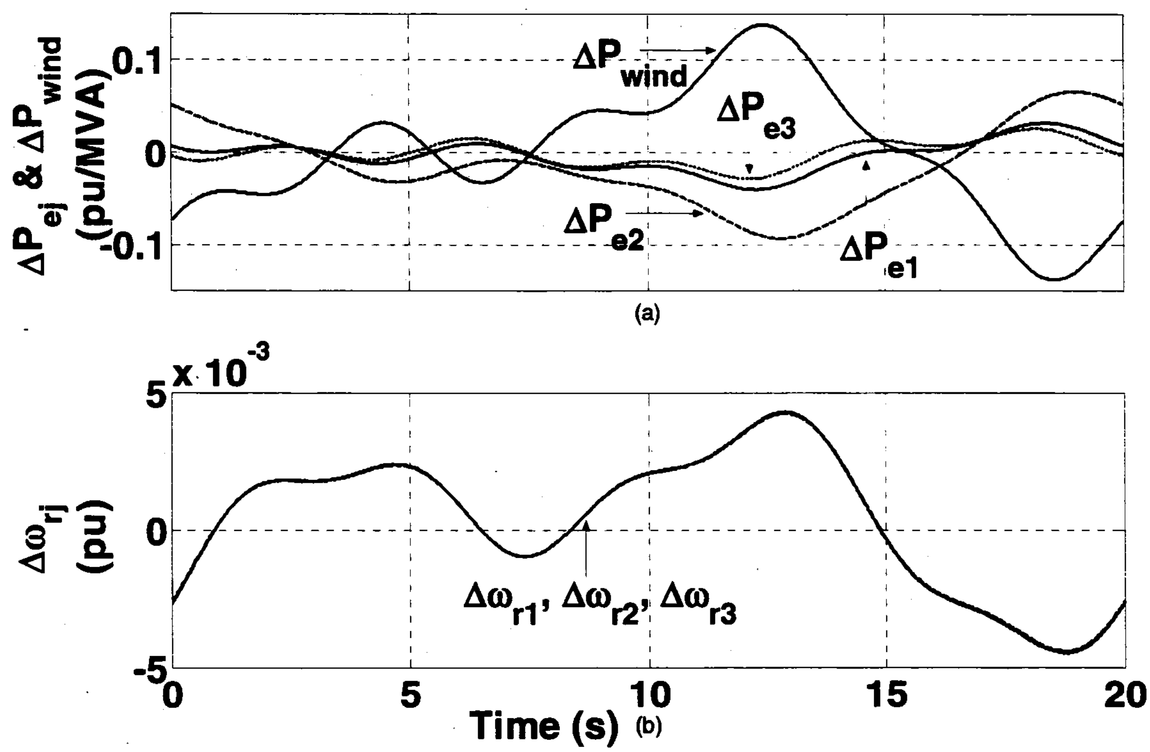

Fig. 4.6. Case study--Nine-bus system. (a) $\Delta P_{\Sigma wind}$ of wind power and ΔP_{ej} of thermal plants. (b) $\Delta\omega_{rj}$ of thermal plants.

Fig. 4.6 (a) show the perturbation generator power ΔP_{ej}, $j=1,2,3$ at each of the power plants and $\Delta P_{\Sigma wind}$ the total wind power fluctuations. As will be explained later in the text, the perturbation generator power ΔP_{ej} is equal and opposite to the weighted sum of the perturbation powers from the wind farms, i.e.

$\Delta P_{ej}= -[g_{j1}sin(2\pi 0.05t+\phi_{j1})+g_{j2}sin(2\pi 0.1t+\phi_{j1})+g_{j3}sin(2\pi 0.25t+\phi_{j1})]$, where g_{jk} and ϕ_{jk} are the magnitudes and the phase angles of $G_{3j}(j2\pi f_{Wk})$.

The frequency deviations $\Delta\omega_{rj}(t)$ in Fig. 4.6 (b) at each of the 3 power plants ($j=1, 2, 3$) are identical and, therefore, their plots appear as superimposed on top of each other. This emphasizes the fact the frequency is common throughout the grid. In fact, Fig. 4.6 (b) is also the frequency deviation at the terminals of the wind farms. (The discussion in Section 4.4.4, which questions the adequacy of the existing frequency regulation standards in promoting high penetration, draws on the implications of this observation.) Norbert Wiener [4-4] noted that this "phenomenon of the attraction of frequencies" is generally found in living and non-living systems. He attributed it to positive feedback, by which the frequencies of oscillators, although initially differing, eventually converge. This attraction of frequencies is the key to the estimation method described in the next paragraphs.

In the example of Fig. 4.6, there are three frequencies of the fluctuating wind power, f_{W1}=0.05, f_{W2}=0.1 and f_{W3}=0.25. The fluctuating wind powers $M_{Wk}sin(2\pi f_{Wk}t)$, $k=1,2,3$ are aggregated as the total perturbation wind power $\Delta P_{\Sigma wind}$. Assuming that transmission line losses can be neglected, the aggregated wind power $\Delta P_{\Sigma wind}$ is absorbed by ΔP_{ej}, $j=1,2,3$ of the thermal plants. In Fig. 4.6 (a), ΔP_{ej}, $j=1,2,3$ add up to $-\Delta P_{\Sigma wind}$. The proportion of "absorption" depends on the magnitudes g_{jk} and the phase angles ϕ_{jk} of $G_{3,j}(j2\pi f_{Wk})$ for each plant j and each fluctuating frequency f_{Wk}.

4.3.2 Lessons from Simulation Experiments

The conclusions from extensive simulation experiments are:

(1) The transmission of perturbation wind powers to the thermal plants is independent of the transmission distances or network topology, a conclusion which has been reached independently in [4-3, 4-4].

(2) The perturbation frequency deviations $\Delta\omega_{rj}(t)$ are identical at every thermal generation plant. In fact, $\Delta\omega_{rj}(t)$ is common throughout the grid and this includes the buses of the wind farms.

(3) For any fluctuating wind power frequency f_W, the perturbation powers $M_{Wk}sin(2\pi f_W t)$ from the wind farms ($k=1,2..K$) are aggregated to form a total perturbation wind power $\Delta P_{\Sigma wind}$.

(4) The generation powers $\Delta P_{ej}(2\pi f_W t)$, $j=1,2,\ldots,J$ of the thermal generation plants "absorb" $\Delta P_{\Sigma wind}$.

(5) Since $\Delta\omega_{rj}(2\pi f_W t)$ is common throughout the grid, the share of "absorption" by thermal plant j is $\Delta P_{ej}(2\pi f_W)=\Delta\omega_{rj}(2\pi f_W)/G_{3j}(2\pi f_W)$, where $\Delta\omega_{rj}(2\pi f_W)$ is an algebraic unknown, which is solved using the method described in section 4.4 below.

4.4 Method of Estimating Fluctuating Wind Power Limit

4.4.1 Analytical Method

The lessons of 4.3.2 enable the perturbation frequency deviation $\Delta\omega_{rj}(t)$ to be estimated from the wind power perturbations. From (5) in section 4.3.2, each power plant takes

$$\Delta P_{ej}(j2\pi f_W) = \frac{\Delta\omega_{rj}(j2\pi f_W)}{G_{3j}(j2\pi f_W)} \text{ for } j = 1,2,\cdots J \qquad (4\text{-}1)$$

The power plants together "absorb" all the perturbation wind power

$$\Delta P_{wind}(f_W) = -\sum_{j=1}^{J} \Delta P_{ej}(2\pi f_W t) \qquad (4\text{-}2)$$

Substituting (4-1) in (4-2), and noting that $\Delta\omega_{rj}(j2\pi f_W)$ is common to all the central generation plants, this frequency deviation is:

$$\Delta\omega_{rj}(j2\pi f_W) = \frac{\Delta P_{wind}(f_W)}{\sum_{j=1}^{J} \frac{1}{G_{3j}(j2\pi f_W)}} \text{ for } j = 1,2,\cdots J \qquad (4\text{-}3)$$

By back substitution, the intake of the j^{th} central generation plant is:

$$\Delta P_{ej} = \frac{\Delta P_{wind}(f_W)}{\sum_{m=1}^{J} \frac{G_{3j}(j2\pi f_W)}{G_{3m}(j2\pi f_W)}} \qquad (4\text{-}4)$$

Based on (4-3), the frequency deviation is computed for the wind power fluctuation $\Delta P_{\Sigma wind}$ for frequency f_{Wk} introduced by the kth wind farm. In this case study, (4-3) is evaluated three times, as there are three wind power frequencies: f_{W1}=0.05, f_{W2}=0.1 and f_{W3}=0.25.

4.4.3 Spot Check by Analytical Computation

In the power system of Fig. 3.13, the parameters of the power plants are set identical except for the droops of the governors which have been set as: $droop_1$=0.05, $droop_2$=0.08 and $droop_3$=0.02. The different droops make the transfer functions $G_{3,1}(s)$, $G_{3,2}(s)$, and $G_{3,3}(s)$ different from each other. For wind frequency chosen as f_W=0.1 Hz, Table 4.1 lists the magnitudes and phase angles of $G_{3,1}(j2\pi f_W)$, $G_{3,2}(j2\pi f_W)$ and $G_{3,3}(j2\pi f_W)$.

Plants (droop)	$G_{3,1}(j2\pi f_W)$ (0.05)	$G_{3,2}(j2\pi f_W)$ (0.08)	$G_{3,3}(j2\pi f_W)$ (0.02)
$\lvert G_{3,j}(s)\rvert$	0.184	0.226	0.063
Phase	-186°	-218°	-149°

Table 4.1. Magnitude and Phase Angles of $G_{3,j}(j2\pi f_W)$ for f_W=0.1 Hz

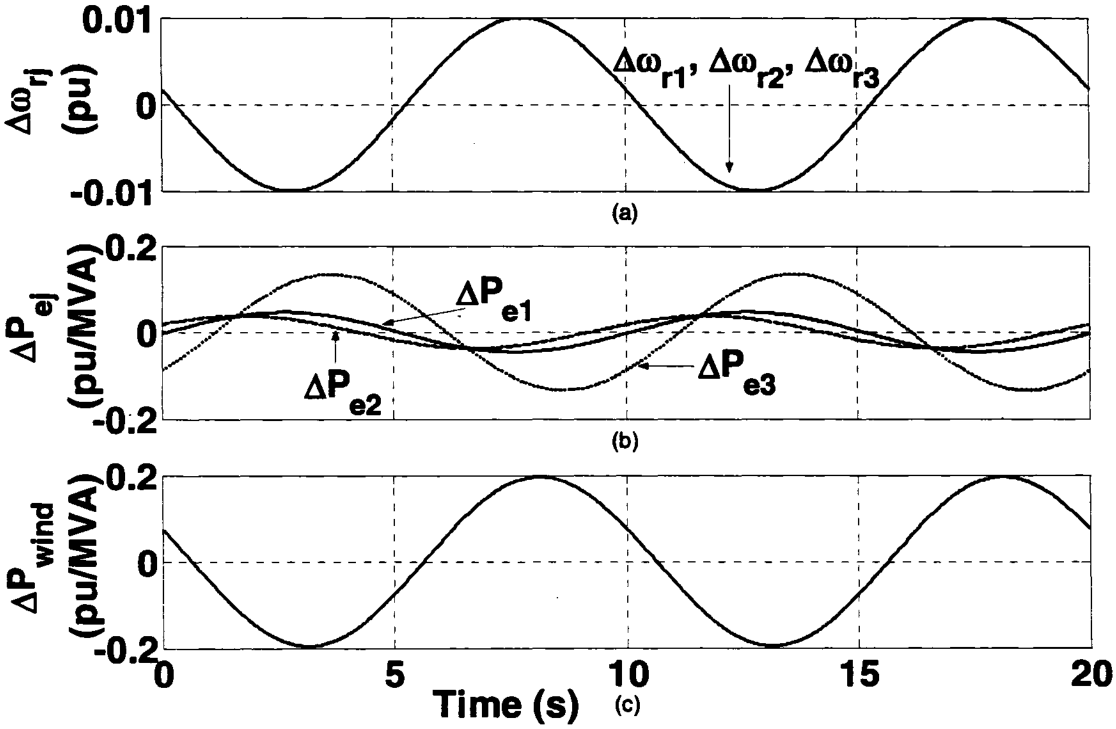

Fig. 4.7. Analytical prediction on wind power variation with f_W=0.1 Hz within Quebec frequency regulation $\Delta\omega_r$=0.6 Hz. (a) $\Delta\omega_{rj}$ of thermal plants. (b) ΔP_{ej} of thermal plants. (c) ΔP_{wind} of wind power.

Assuming the allowed frequency deviation $\Delta\omega_{rj}(t)$ is 1%, which translates to 1.2 Hz peak-to-peak for 60 Hz standard, computations using the Transfer Functions of Table 4.1 show that the total wind perturbation power is:

$$\Delta P_{wind}(f_W) = 37.5\sin(2\pi\cdot 0.1\cdot t + 192.25°)\,\text{MW}$$

For the three central generation plants with a real power rating each of 163.2 MW, the wind power penetration as a percentage of the total real power capacity in the power system is

$$\frac{37.5}{3\times163.2}\times100\% = 7.66\%$$

4.4.4 Cross-Check by Simulations

The correctness of the method of analyzing the impact of wind power fluctuations has been verified by applying simulations to cross check the predictions based on (4-1) to (4-4). In this exercise, it has been found that for the system of Fig. 4.5 and for the transfer functions of Fig. 3.13 (with mixed permanent droops), in respecting grid frequency margin of 1.2 Hz peak-to-peak (1% of 60 Hz) the peak fluctuating power for f_W=0.1 Hz is 37.5 MW, which is 7.66% of the base power, which is taken as 3×163.2 MW.

4.5 Discussions

Filtering in thermal power plants comes from:

(i) Kinetic energy storage in the rotor inertia constant H, characterized by $G_1(s)$ of Fig. 3.12 (a).

(ii) "Virtual storage" by the speed governor system, characterized by $G_2(s)$ of Fig. 3.12 (b). The vector diagrams of Fig. 3.12 show that the powers to the two storages are not as effective as may be desired because they are based on vector addition and not arithmetic addition. As $|G_3(s)|$ should be kept low, its "resonant" peak is undesirable. From Fig. 3.13, decreasing the permanent droop lowers the "resonant" peak and increases the "resonant" frequency.

When acting as power filters, speed governor systems incur increased wear and tear which shorten their operational life. Therefore, one would expect power plants that provide speed regulation services, to charge higher prices in order to recover revenues lost in frequent repairs and/or replacements of governor systems. The wind farm operators do not mind the increased cost since higher wind penetration should bring them higher revenues. Other users of this ancillary service, however, may consider this to be an inequitable arrangement, as they effectively see themselves subsidizing wind farms operation.

There is the option of placing the burden of filtering on the owners of wind farms. In this respect, the present requirement of wind farms having only to comply with a given margin of frequency deviation, at the point of connection of the wind farm to the grid, does not stop them from "polluting" at all. This is because every point in the power grid (and this includes the points of connection of the wind farms to the power grid) shares the same system frequency $\omega_0+\Delta\omega_r$, as Fig. 4.6 (b) of this chapter shows. As explained in Section 4.3, $\Delta\omega_r$ is determined by $\Delta P_{\Sigma wind}$, the summation of fluctuating powers from all the wind farms, so that individual accountability is lost. When wind penetration is low, as it presently is, even the noisy constant speed squirrel cage induction generators satisfy the frequency regulation easily. If a high level of penetration is the goal, individual wind farms should be compelled to filter out the effects of wind turbulences, before their power outputs enter into the power grid. To do this, there is the need of supplementary regulations.

4.6 Conclusions

From the transfer function analysis of thermal generation plants, it is estimated that for an allowable 1% deviation of the 60 Hz, the peak fluctuating power at a single wind frequency is between 5 to 8% of the total power ratings of the thermal plants. The method developed in this paper can be easily extended to larger power grids. Whether the grid consists of thermal, hydro or mixed thermal-hydro plants is immaterial because differences are embedded in the transfer functions $G_{3j}(s)$.

According to the methods summarized in equation (4-3), $G_{3equiv}((j2\pi f_W)$ the equivalent transfer function of multiple power plants is the sum of the contributions of individual power plant connected in parallel across the transmission network.

$$G_{3equiv}(j2\pi f_W) = \sum_{j=1}^{3} \frac{1}{G_{3,j}(j2\pi f_W)}$$

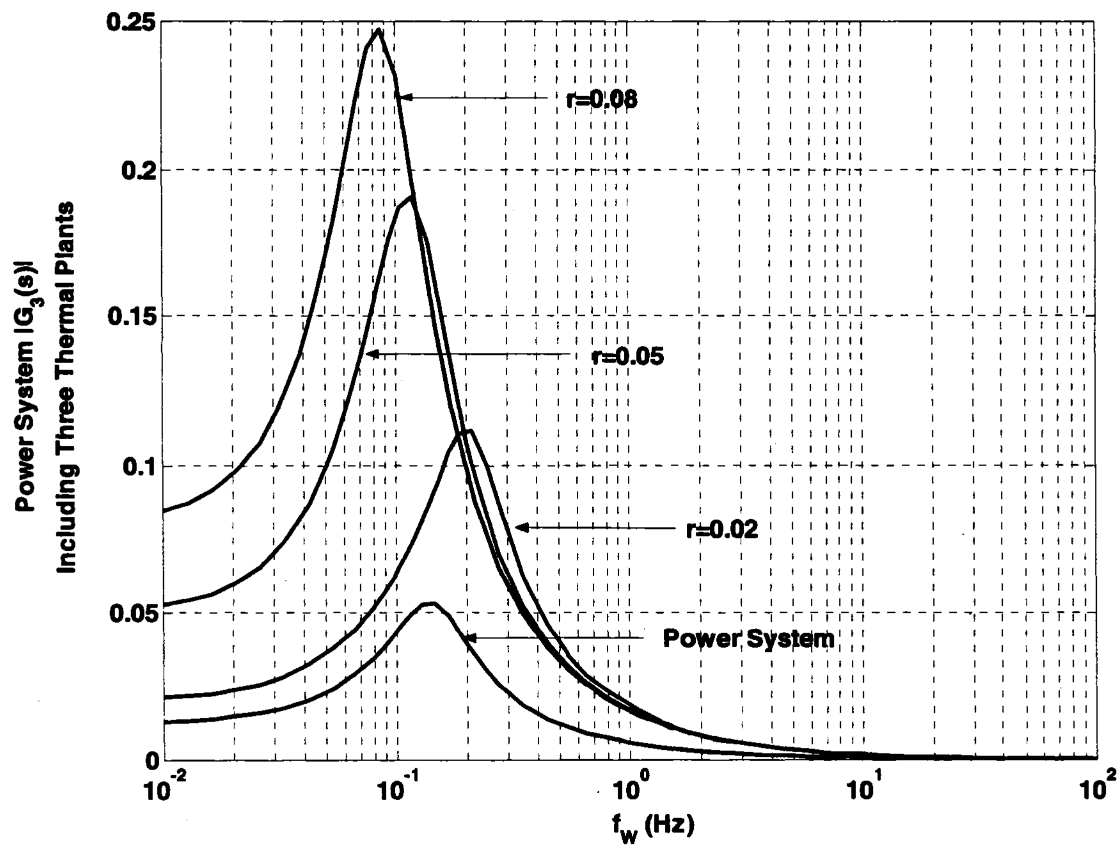

Fig. 4.8. Transfer function of IEEE Nine-bus system (3 thermal plants)

As illustration, fig. 4.8 shows $|G_{3j}(j2\pi f_W)|$ of 3 power plants for permanent droop r=0.08, 0.05 and 0.02. The equivalent transfer function of multiple power plants $|G_{3equiv}(j2\pi f_W)|$ is labeled "Power System".

The maximum wind power fluctuation $\Delta P_S(j2\pi f_W)$ at wind frequency f_W for a given frequency deviation margin $\Delta\omega_{margin}$ (allowed by the regulatory authority) is obtained from $G_{3equiv}((j2\pi f_W)$, the equivalent transfer function of the power system, using the formula:

$$\Delta P_s(s) = \frac{\Delta\omega_{margin}(s)}{G_{3equiv}(s)} = \frac{\text{frequency margin}}{\text{equivalent transfer function of thermal plants}}$$

Thus the whole power system can be simplified to be a transfer function in s-domain. For the single thermal plant, the system order is 10. For the 9-bus system with three thermal plants, the system order is 26. The parameters used in this thesis are listed in decreasing order of s in Appendix C.

The next stage of research is to extend the method to cover the stochasticity of wind power from wind farms. At such time as the probability-vs-frequency power spectrum of wind farms becomes available, it is straightforward to compute the statistical expected fluctuating power from wind farms for a statistical expected 1% frequency deviation from the 60 Hz.

CHAPTER 5

ATTENUATION OF WIND POWER FLUCTUATIONS BY WTG

5.1 Introduction of Wind Turbine Generators

Chapters 4 has shown that for 1% frequency deviation from the 60 Hz, the wind power fluctuation, at a given frequency f_W, can be as high as 5% of the MW rating of the power plants. The speed governor systems accomplish some power filtering using (i) the kinetic energy storage (moments of inertia of generator rotor and HP, MP and LP turbines), (ii) "virtual storage" in the steam chests controlled by the steam valves. Accepting fluctuating wind power filtering duties implies increased wear and tear of the governor hardware and it is desirable that there are other means of filtering. Since the final objective is to maximize the level of wind penetration, it may be necessary to employ a combination of the speed governor systems and the other methods of power filtering.

This chapter examines the filtering that can be done at the source, which is the wind turbine-generator (WTG). As wind turbines increase in ratings, their longer turbine blades, which are mounted in taller towers, have larger moments of inertia H. The large H represents kinetic storage which can also be used for power filtering. This is facilitated by the decoupled P-Q control of the doubly-fed induction generators (DFIG) which are the preferred generators of the recent large wind turbines.

Besides having large moments of inertia H, filtering is facilitated by the freedom to change turbine speed ω_m. When there is excess wind power ΔP_W, H increases its kinetic energy storage by accelerating to high speed and returns it by decelerating to low speed in periods when ΔP_W is in deficit. The kinetic energy storage in the wind turbine inertia is parallel to the storage in the inertias of the steam turbines and the rotor of the generator of the power plant in chapter 4.

Variable pitch of the wind turbine blades is one means of speed control. For a given pitch angle, the operational characteristic of the wind turbine is described by the C_p-vs-λ graph shown in Fig. 5.1. There are C_p-vs-λ graphs corresponding each pitch angle. As an electrical engineering thesis, speed is controlled electrically, i.e. by decoupled P-Q control of the doubly-fed induction generator (DFIG). Consequently, the conclusion regarding filtering is this chapter and in chapter 6 is poorer than if both pitch control and decoupled P-Q control are combined.

This chapter evaluates two strategies of decoupled *P-Q* control of wind turbine-DFIG in the light of filtering:

(1) "Constant-Speed" Wind Turbine Generator (WTG). This section touches on the cheap and robust "constant speed" squirrel cage induction generators. Squirrel cage induction generators are being superseded by DFIGs in the MW range of wind turbines. The purpose is to use it to highlight the fact that wind power filtering by kinetic energy is based on building up storage at high values of ω_m which is then depleted at low values of ω_m. As the "constant speed" squirrel cage induction generators leave little room for changes in ω_m, they offer very little filtering.

(2) Constant P-control. This strategy facilitates wind energy trading. Based on wind prediction for the next hour, a firm commitment is made to supply P_{ref} power in the next hour. Wind turbulence will cause the turbine-generator speed ω_m to fluctuate above and below the statistical expected mean speed. By setting the reference of the decoupled P-Q control as a constant, i.e. $P_{ref}=p_0$, the DFIG maintains a constant power output irrespective of the fluctuations of ω_m caused by wind turbulence. There is perfect filtering, but when the actual wind power is greater or lower than the reference setting P_{ref}, the speed ω_m can drift outside the steady-state stability region and the DFIG loses control.

(3) Linear Slope Strategy. In order to compensate for any error in predicting the statistical expected mean speed (and therefore the wind power), a correction factor in the form of linear slope is added to the aforesaid constant p_0 of Constant P-control. The strategy, $P_{ref} = p_0 + p_1 \omega_m$, restrains the speed from drifting away from the steady-state stability region. The filtering is less than perfect.

(4) Optimal Wind Power Acquisition. For a wind velocity V_W and a turbine pitch, there is a generator speed ω_{mopt}, at which the wind power acquired P_{opt} is maximum. The P_{opt}-vs-ω_{mopt} relationship can be computed and programmed in a Look-Up Table. Corresponding to the turbine pitch and generator speed ω_m, the Look-Up Table outputs P_{opt} which is used as the reference P_{ref} of the decoupled P-Q control. This strategy acquires optimal power as the wind velocity V_W keeps changing. The filtering is poor compared to Constant P-Control but it does not

run into the problems of Constant P-Control.

The evaluations are by simulation tests using the same 18-second wind velocity data file as the input V_W as the common basis for comparison. The objective is to find the extent of filtering made possible by different sizes of moment of inertia expressed as H. As information regarding the size of H are not easily available, the range of H=0.6 s to 12 s has been used, with intermediate values of H=5 s.

5.2 Wind Turbine Fundamentals

This section briefly reviews the functional dependence of wind turbine power P_W with the wind velocity V_W and generator speed ω_m. The generator is geared to the wind turbine shaft rotating at turbine speed ω_T. Their speeds are related by gear ratio=ω_m/ω_T. If the radius of the turbine blade is R, its tip velocity is $\omega_m R/gear\ ratio$.

5.2.1 λ-Tip Speed Ratio

The ratio between the blade tip velocity ($\omega_m R/gear\ ratio$) and the wind velocity V_W is given the term tip speed ratio, defined as

$$tip\ \ ratio : \lambda = \frac{\omega_m \times R}{gear \times V_W} \qquad (5\text{-}1)$$

5.2.2 Performance Coefficient Cp

The performance of a wind-turbine for a given turbine blade pitch is encapsulated in a graph of C_p-vs-λ as shown in Fig. 5.1. These graphs are obtainable from wind turbine manufacturers.

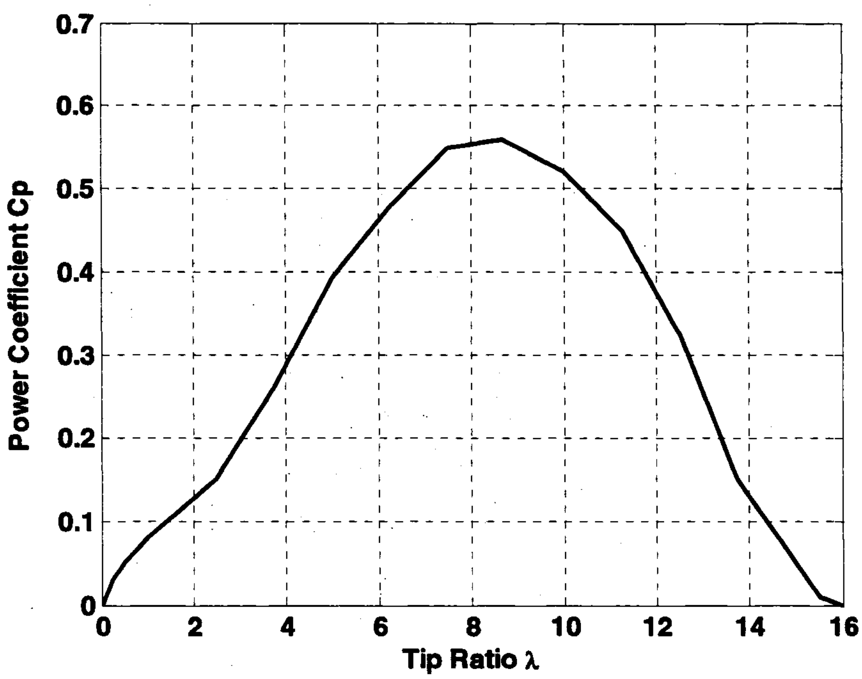

Fig. 5.1. Power coefficient C_p-vs-tip ratio λ

The coefficient C_p is defined as:

$$P_W = 0.5\rho A C_p V_W^3$$

where P_W=wind power captured by turbine

ρ=density of air in kg/m^3 (here 1.225652 kg/m^3)

A=area of blade covered ($\pi \times r^2$) in m^2

From Fig. 5.1, one can construct a P_W-vs-ω_m curve for each wind velocity. Fig. 5.2 shows a family of curves of a 1.5 MW wind turbine. From Fig. 5.2, a family of wind turbine torque T_W-vs-ω_m curves can be generated, since the formula of T_W is:

$$T_m = \frac{P_W}{\omega_m} \qquad (5\text{-}3)$$

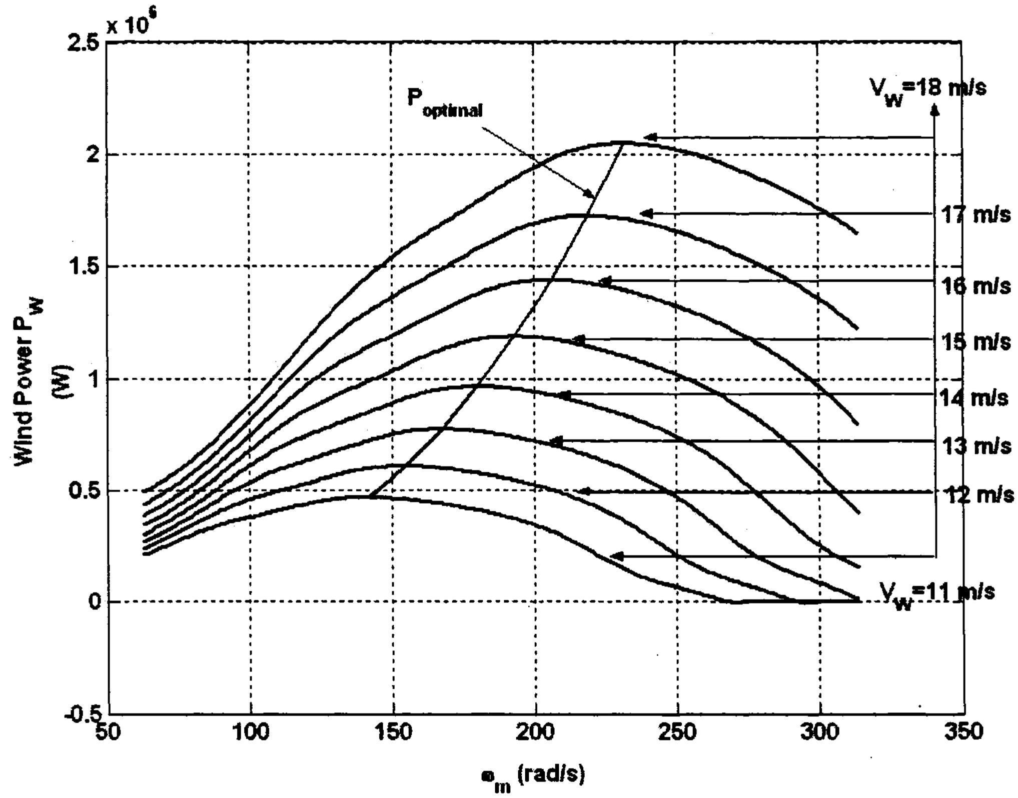

Fig. 5.2. Family of wind power P_W-vs-ω_m curves for different V_W

5.2.3 Optimal Wind Power Acquisition

Corresponding to each wind velocity V_W, there is a peak in Fig. 5.2 which represents the maximum wind power which can be captured by the turbine. The capture requires the generator to operate at ω_{mopt} directly under the peak. Fig. 5.2 shows the $P_{optimal}$-vs-ω_m curve joining all the peaks. The challenge in optimal wind power acquisition is to track this curve automatically. The $P_{optimal}$-vs-ω_m curve constitutes the peak point (C_{pmax}=0.56, λ_{max}=8.5) in Fig. 5.1. In the simulations, which will be pursued in this chapter, C_p is computed to indicate how close is wind power acquisition to the optimal (C_{pmax}=0.56).

5.3 Constant-Speed Wind Turbine Generators—Squirrel Cage Induction Machine

5.3.1 Introduction of Constant-Speed WTG

The constant speed wind turbine generator (WTG) is the first generation of WTG. It is none other than the cheap and robust "constant speed" squirrel cage induction generator. The purpose is to use it to highlight the fact that wind power filtering by kinetic energy is based on building up storage at high values of ω_m which is then depleted at low values of ω_m. The "constant speed" squirrel cage induction generators leave little room for changes in ω_m.

Fig. 5-3 shows the torque-speed (T_e-vs-ω_m) curve of a squirrel cage induction machine. Around the synchronous speed (|slip|<0.05), the speed is kept roughly constant for the full range of generating counter-torque (generating power≈ T_e x ω_m).

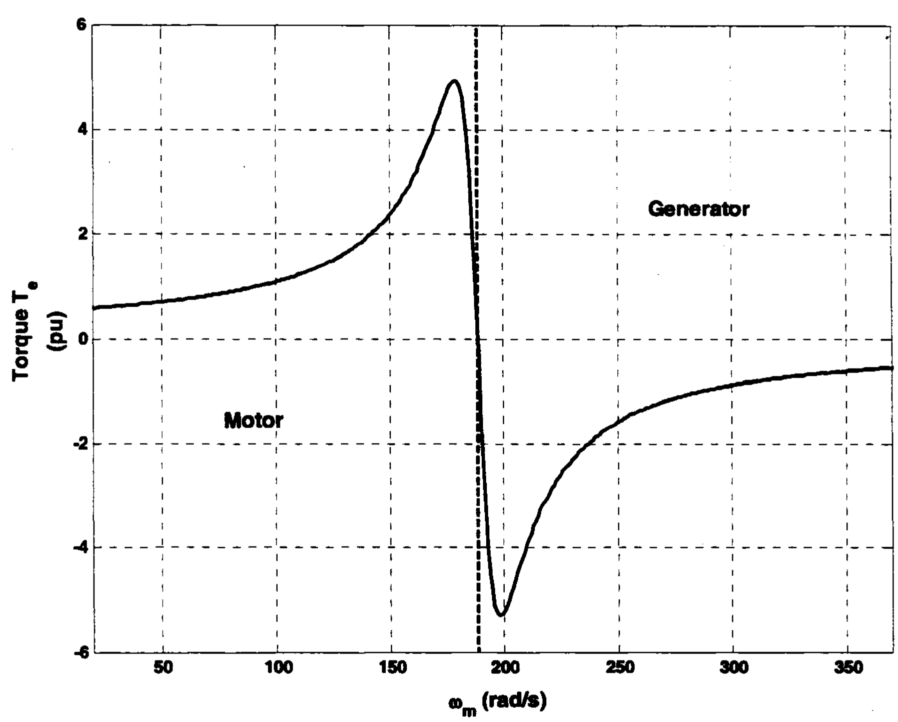

Fig. 5.3. Torque-Speed curve of squirrel cage induction machine

The mechanical equation of motion is:

$$2H\frac{d\omega_m}{dt} = \omega_{m0}(T_W + T_e) \tag{5-4}$$

where H is the combined moment of inertia of the turbine, the gears and the rotor. (Note that in this chapter the sign before T_e is positive in (T_W+T_e) of (5-4) so as to be consistent with Fig. 5.3). As mentioned, there is a family of T_W-vs-ω_m which can be constructed from the P_W-vs-ω_m curves of Fig. 5.2, based on plotting $T_W=(P_W/\omega_m)$ against ω_m. The equilibrium operating points are based on:

$$2H\frac{d\omega_m}{dt} = \omega_{m0}(T_{W0} + T_{e0}) \tag{5-5}$$

As $d\omega_{mo}/dt=0$, the stable operating points, which satisfy $T_{Wo}+T_{eo}=0$, lie in the generator operating region of Fig. 5.3 in the narrow speed range $1.05\geq \omega_m \geq 1.0$ pu with a very large negative gradient $\partial T_e/\partial\omega_m=-D_e$.

Writing $\omega_m=\omega_{mo}+\Delta\omega_m$, $T_W=T_{Wo}+\Delta T_W$ and $T_e=T_{eo}+\Delta T_e$, (5-3) can be decomposed into the equilibrium component of (5-5) and the small perturbation linearized component:

$$2H\frac{d\Delta\omega_m}{dt} = \omega_{m0}(\Delta T_W + \Delta T_e) \tag{5-6}$$

Substituting $\Delta T_e = (\partial T_e/\partial\omega_m)\Delta\omega_m = -D_e\cdot\Delta\omega_m$ in (5-6), it becomes

$$2H\frac{d\Delta\omega_m}{dt} = \omega_{m0}(\Delta T_W - D_e\Delta\omega_m) \tag{5-7}$$

Taking the Laplace's Transform of (5-7) and simplifying, one has

$$\Delta\omega_m(s) = [\omega_{m0}/(2H \cdot s + D_e)] \cdot \Delta T_W(s) \qquad (5\text{-}8)$$

As

$$\Delta T_e(s) = -D_e \Delta\omega_m(s) \qquad (5\text{-}9)$$

it follows that

$$\Delta T_e(s) = -[\omega_{m0} D_e/(2H \cdot s + D_e)] \cdot \Delta T_W(s) \qquad (5\text{-}10)$$

Since the perturbations take place in a narrow speed range (1.01≥ ω_m ≥1.0 pu), the constant speed approximation can be applied so that (5-10) can be approximated as:

$$\Delta P_e(s) \approx -[\omega_{m0} D_e/(2H \cdot s + D_e)] \cdot \Delta P_W(s) \qquad (5\text{-}11)$$

Therefore, the transfer function of the filter is $G(s) = -[\omega_{m0} D_e/(2H \cdot s + D_e)]$. As D_e is very large, G(s)≈-1, unless H is very large. Thus in general, there is little filtering by the squirrel cage induction generators.

5.3.2 Simulation Results of Constant-Speed WTG

Fig. 5.4 to 5.6 present the results of using a squirrel-cage induction machine as the wind-turbine generator. The parameters are shown in Appendix D. In each figure, (a) displays the simulated wind turbine power input P_W and the generator power output P_e; (b) shows the computed value of C_p; (c) shows the fast Fourier transforms (FFT) of P_W and P_e; and (d) shows the speed ω_m.

(1) H=0.6 s

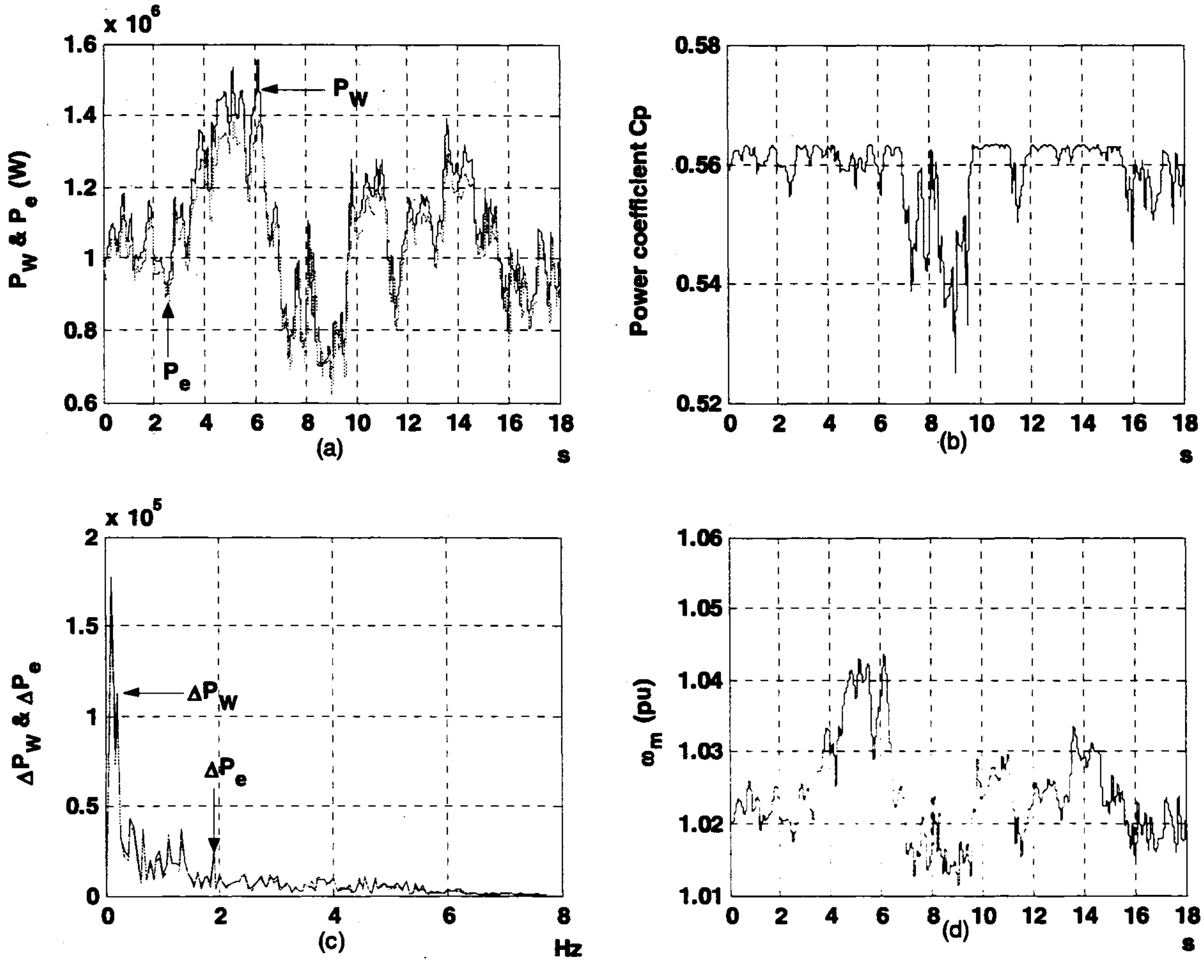

Fig 5.4. Constant-speed WTG with H=0.6 s

(2) H=5 s

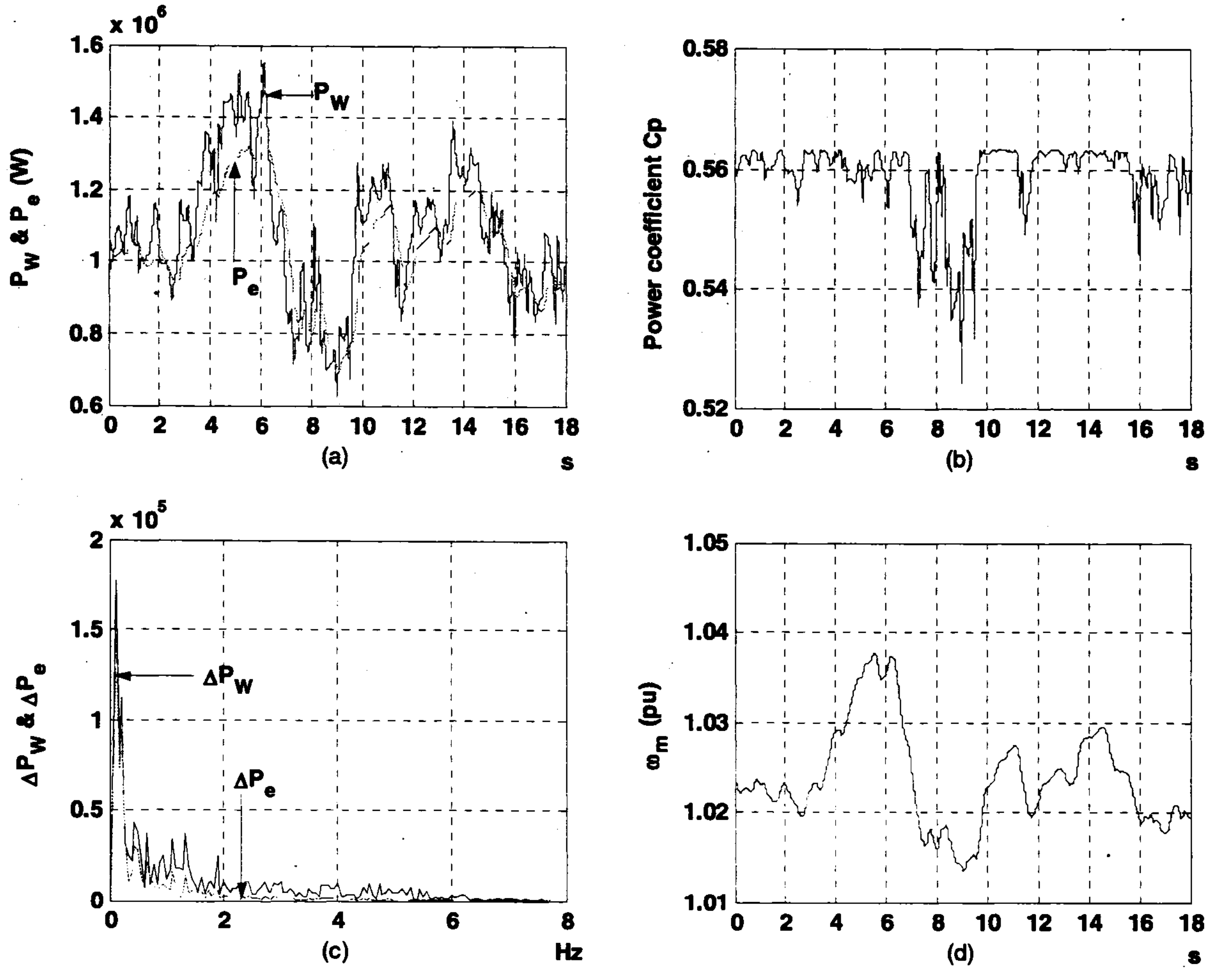

Fig 5.5. Constant-speed WTG with H=5 s

(3) H=12 s

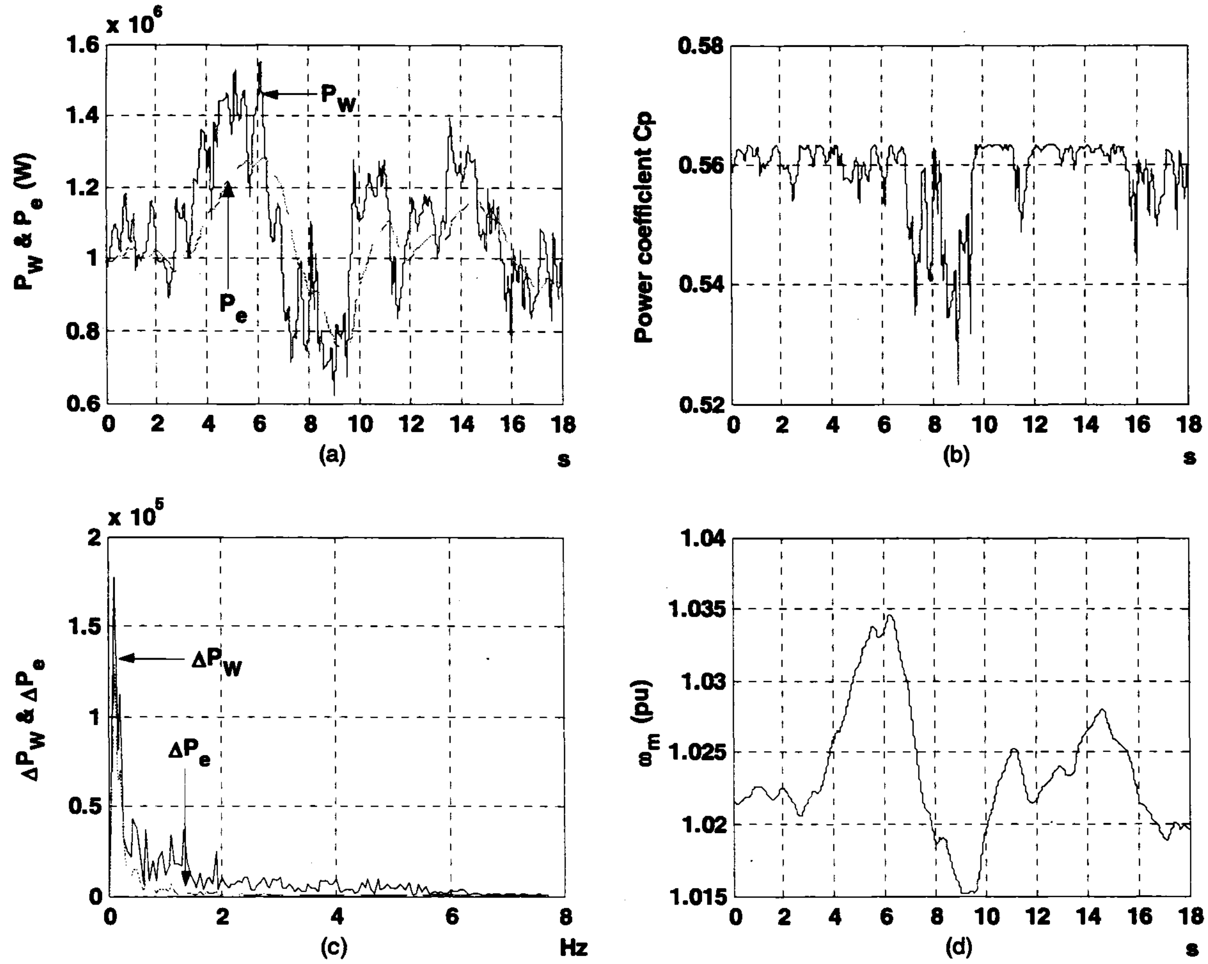

Fig 5.6. Constant-speed WTG with H=12 s

5.3.3 Summary of Constant-Speed WTG

In (a) of Fig. 5-4 to 5-6, unless H is very large, the output, which is the generator power ΔP_e, has experienced very little filtering because the wind power fluctuation ΔP_W has hardly changed.

The high values of C_p in (b) are not typical and come from design. First the mean wind velocity is estimated from the 18 second data file. Then the gear ratio is chosen so that the "constant speed" operating region coincides with the optimal turbine speed for the mean wind velocity. In general, the "constant speed" WTG is not meant for optimal wind power acquisition. One has only to turn to Fig. 5.2 to appreciate that one constant speed vertical line passes at most through one peak.

From the scale of the vertical axes in (d), it is apparent that the steep negative slope in Fig. 5.3 has constrained the speed ω_m to lie within a very narrow range, resulting in "constant-speed" operation.

5.4 Variable-Speed Wind Turbine Generator

5.4.1 Introduction of Doubly-Fed Induction Generator (DFIG)

This section presents a short review of decoupled P-Q control of the doubly-fed induction generator (DFIG) as shown in Fig. 5-7. In this thesis, it is sufficient to view it as a "black box" by which real power $P=P_{ref}$ and reactive power $Q=Q_{ref}$ are injected into the utility grid in response to P_{ref} and Q_{ref} set as the references of the decoupled P-Q control.

The doubly-fed induction generator (DFIG) is no other than the wound-rotor induction machine. By magnitude and phase angle control of the slip frequency voltages injected through the slip rings to the rotor windings, the DFIG can deliver complex power $P_{ref}+jQ_{ref}$ to the 60 Hz grid even though the wind velocity may drive the generator speed over a broad range, typically 0.7 pu$<\omega_m<$1.3 pu.

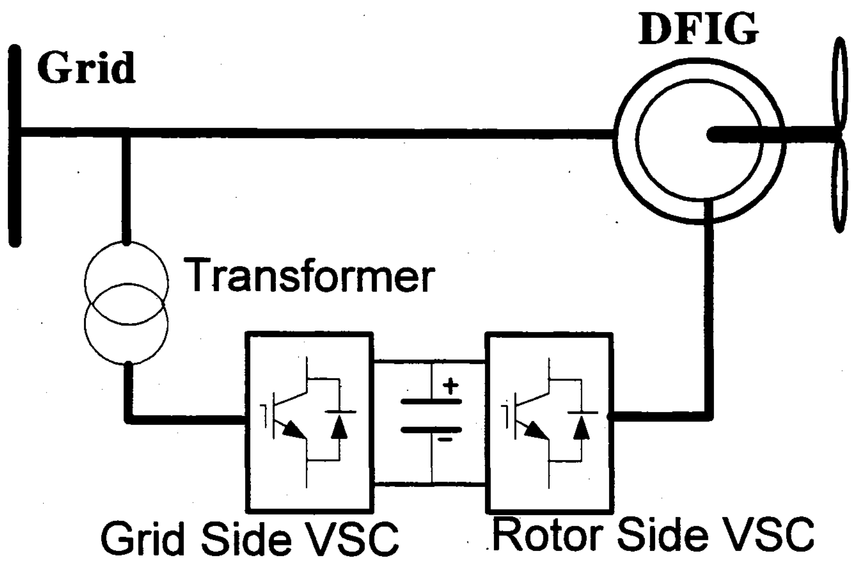

Fig. 5.7. DFIG controlled by back-to-back Voltage-Source Converters [5-1, 5-2, 5-3]

The injection of the slip frequency voltages is accomplished by the rotor-side voltage-source controller (VSC). The voltages of the VSC are produced by pulse-width modulation (PWM) of the dc voltage across the dc capacitor between the rotor-side and the grid-side VSC.

The rotor-side VSC is connected back-to-back to the grid-side VSC at their dc terminals across which is a dc capacitor. The ac terminals of the grid-side are connected by way of 3-phase transformers to the ac grid to which the stator of the DFIG is connected. The parameters of DFIG are shown in Appendix D.

5.4.2 Control Methods

(1) Decoupled P-Q Control

As the author is applying the DFIG decoupled P-Q control software already developed by Mr. Baike Shen [5-2], the research objective is to investigate how the complex power references P_{ref} and Q_{ref} are best used to filter out the turbulent component in the captured wind power.

(2) Reactive Power Control by Q_{ref}

As the wind power output of the wind-turbine DFIG is not controllable by Q_{ref}, Q_{ref} has been passed over in this research for the more important control lever P_{ref}.

(3) Real Power Control by P_{ref}

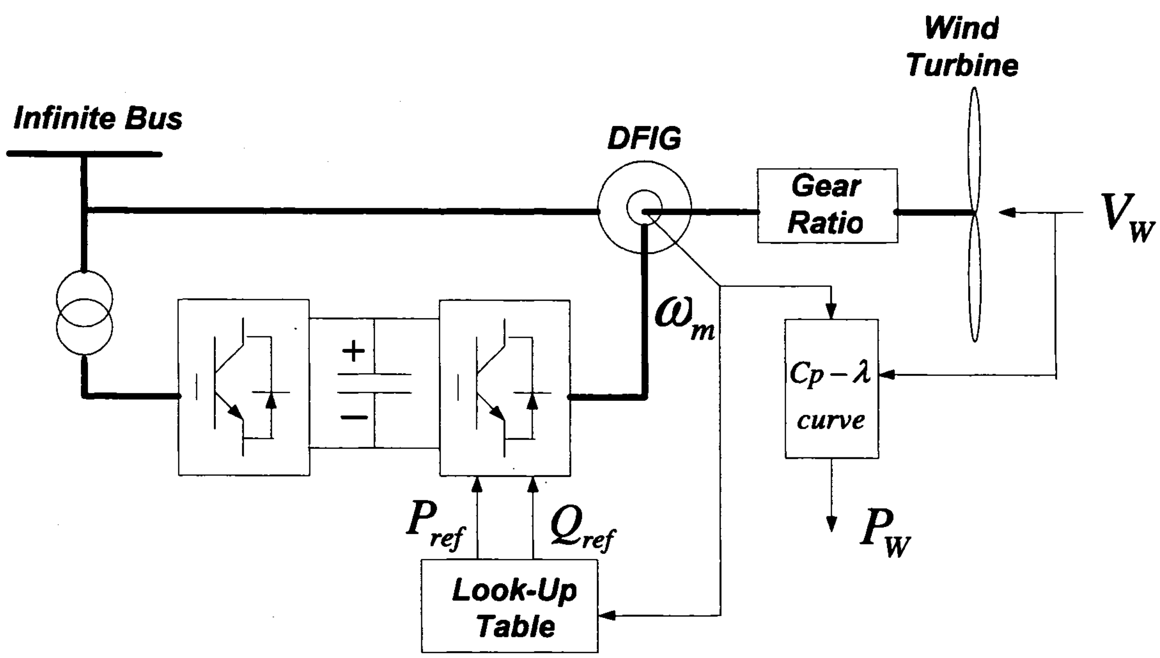

Fig. 5.8. Diagram of simulation experiments on DFIG in EMTP-RV

The block diagram Fig. 5.8 illustrates how the simulation experiments have been performed on the wind-turbine DFIG. The input consists of the wind velocity V_W, taken from the same 18 second wind data file used throughout this chapter. The output consists of P_e, the total output real power (sum of stator and rotor powers) of DFIG. The decoupled P-Q control offers the real power reference P_{ref} as a lever to implement control strategies based on specifying $P_{ref}(\omega_m)$-vs-ω_m dependence. The generator speed ω_m is obtained by measurement. $P_{ref}(\omega_m)$ is stored in a Look-Up Table and the speed ω_m is used as a pointer to output $P_{ref}(\omega_m)$.

The $P_{ref}(\omega_m)$-vs-ω_m strategy must necessarily ensure automatic convergence to the equilibrium speed. For any wind velocity V_W and turbine speed ω_m there is a wind power P_W, from Fig. 5.2. For the same speed ω_m, the torque of the DFIG is $T_e=P_{ref}(\omega_m)/\omega_m$. From (5-4), if the counter-torque $-T_e$ is larger than the wind torque $T_W=P_W(V_W,\omega_m)$, the speed decelerates. Conversely, if the counter-torque $-T_e<T_W$, the speed accelerates. Thus the speed ω_m is driven in the direction until $-T_e\approx T_W$ at which point equilibrium speed is attained.

5.4.3 Analysis of Power Filtering by DFIG

In extending the power filtering analysis to DFIGs, one multiplies (5-4) by ω_m to yield

$$2H\frac{d\omega_m}{dt}=\omega_{m0}\left(T_W\omega_m+T_e\omega_m\right) \qquad (5\text{-}12)$$

which becomes

$$\frac{H}{\omega_{m0}}\frac{d\omega_m^2}{dt}=P_W+P_e \qquad (5\text{-}13)$$

The quantity $H\omega_m^2$ is the kinetic energy of the rotating mechanical system. Assuming that there exists ω_{mo} where $P_{Wo}+P_{eo}=0$ around which small perturbation linearization is applied, i.e. $\omega_m=\omega_{mo}+\Delta\omega_m$, $P_W=P_{Wo}+\Delta P_W$ and $P_e=P_{eo}+\Delta P_e$, one has

$$\frac{d(2H\Delta\omega_m)}{dt}=\Delta P_W+\Delta P_e \tag{5-14}$$

Assuming that the DFIG output power P_e tracks P_{ref},

$$P_e=P_{ref}(\omega_m) \tag{5-15}$$

Substituting

$$\Delta P_e=\left\lfloor \partial P_{ref}(\omega_n)/\partial\omega_m \right\rfloor_{\omega_{m0}}\Delta\omega_m \tag{5-16}$$

in (5-14), one has

$$2H\frac{d\Delta\omega_m}{dt}=\Delta P_W+\left[\frac{\partial P_{ref}(\omega_m)}{\partial\omega_m}\right]_{\omega_{m0}}\Delta\omega_m \tag{5-17}$$

Taking the Laplace's Transform of (5-17), $\Delta\omega_m\rightarrow\Delta\omega_m(s)$, $d(\Delta\omega_m)/dt\rightarrow s\Delta\omega_m(s)$ and $\Delta P_W\rightarrow\Delta P_W(s)$, (5-17) simplifies to

$$\Delta\omega_m(s)=\frac{\Delta P_W(s)}{2H\cdot s-\left\lfloor \partial P_{ref}(\omega_m)/\partial\omega_m \right\rfloor_{\omega_{m0}}} \tag{5-18}$$

Back substituting to (5-16)

$$\Delta P_e(s)=\frac{\left\lfloor \partial P_{ref}(\omega_m)/\partial\omega_m \right\rfloor_{\omega_{m0}}\Delta P_W(s)}{2H\cdot s-\left\lfloor \partial P_{ref}(\omega_m)/\partial\omega_m \right\rfloor_{\omega_{m0}}} \tag{5-19}$$

Up to this point, $P_{ref}(\omega_m)$ has not been specified. In general, $P_{ref}(\omega_m)$ can be a polynomial in ω_m.

$$P_{ref}(\omega_m)=p_0+p_1\omega_m+p_2\omega_m^2+p_3\omega_m^3+p_4\omega_m^4\cdots \tag{5-20}$$

The term within square bracket in (5-16) is evaluated at the equilibrium speed ω_{mo}.

$$\frac{\partial P_{ref}(\omega_m)}{\partial \omega_m} = p_1 + 2p_2\omega_m + 3p_3\omega_m^2 + 4p_4\omega_m^3 \cdots \qquad (5\text{-}21)$$

5.4.4 Constant Power Reference Strategy

The constant power strategy requires (5-20) to be specified as $P_{ref}(\omega_m)=p_O$. From (5-21), one has $[\partial P_{ref}(\omega_m)/\partial\omega_m]=0$. It follows from (5-19), that $\Delta P_e(s)=0$, that is the filtering is perfect, which is proven by the simulations below.

$P_{W\text{-}ave}$, the mean value of P_W has been estimated as 1.0 MW. Setting $P_{ref}=p_O$ =1.0 MW, the simulation in Fig. 5.9 (a) shows that $P_e(\omega_m)$ tracks p_O=1.0 MW and the fluctuations in P_W are filtered out. Fig. 5.9 (b) shows the acceleration of the speed ω_m as $P_W > p_O$ and the deceleration as $P_W < p_O$. The inertia constant is H=5 s. The wind power deviation is taken up by the kinetic energy.

This perfect filtering is fortuitous and depends on being able to predict $P_{W\text{-}ave}$ accurately in setting $P_{ref}=p_O$. The next 2 simulations show the cases of under and over estimation.

(1) $P_{ref} = p_0 = 1.0$ MW $\approx P_{W\text{-}ave}$

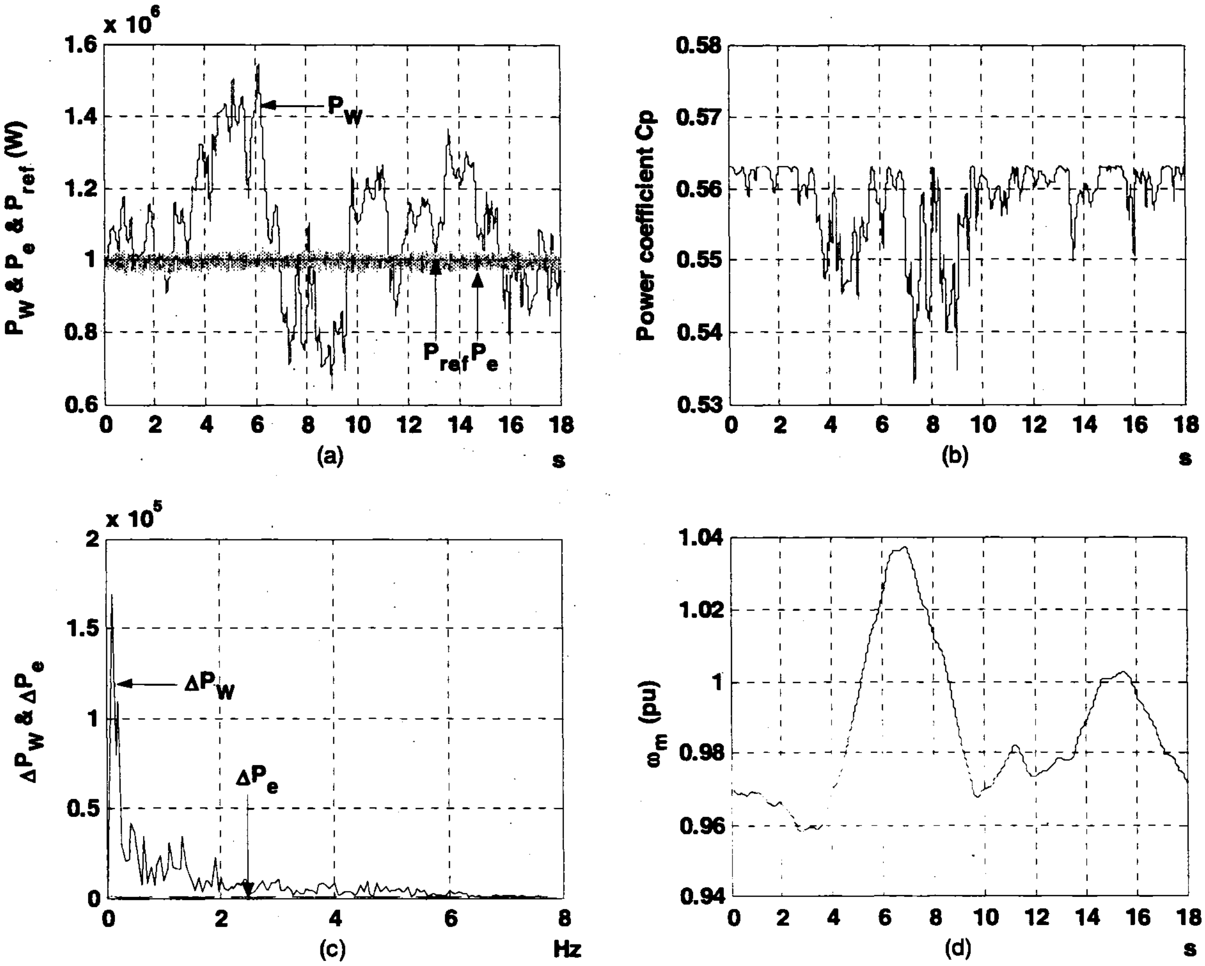

Fig 5.9. DFIG with P_{ref}=1.0 MW

(2) $P_{ref} = p_O = 0.5$ MW $< P_{W\text{-}ave}$

Fig. 5.10 shows the case of setting $P_{ref}=p_O=0.5$ MW. Because $P_W>p_O$, ω_m keeps accelerating as shown in Fig. 5.10 (d). Around 7 seconds, ω_m exceeds 1.27 pu. As shown in Fig. 5.10 (a), P_e ceases to track $P_{ref}=p_O$ and oscillates uncontrollably.

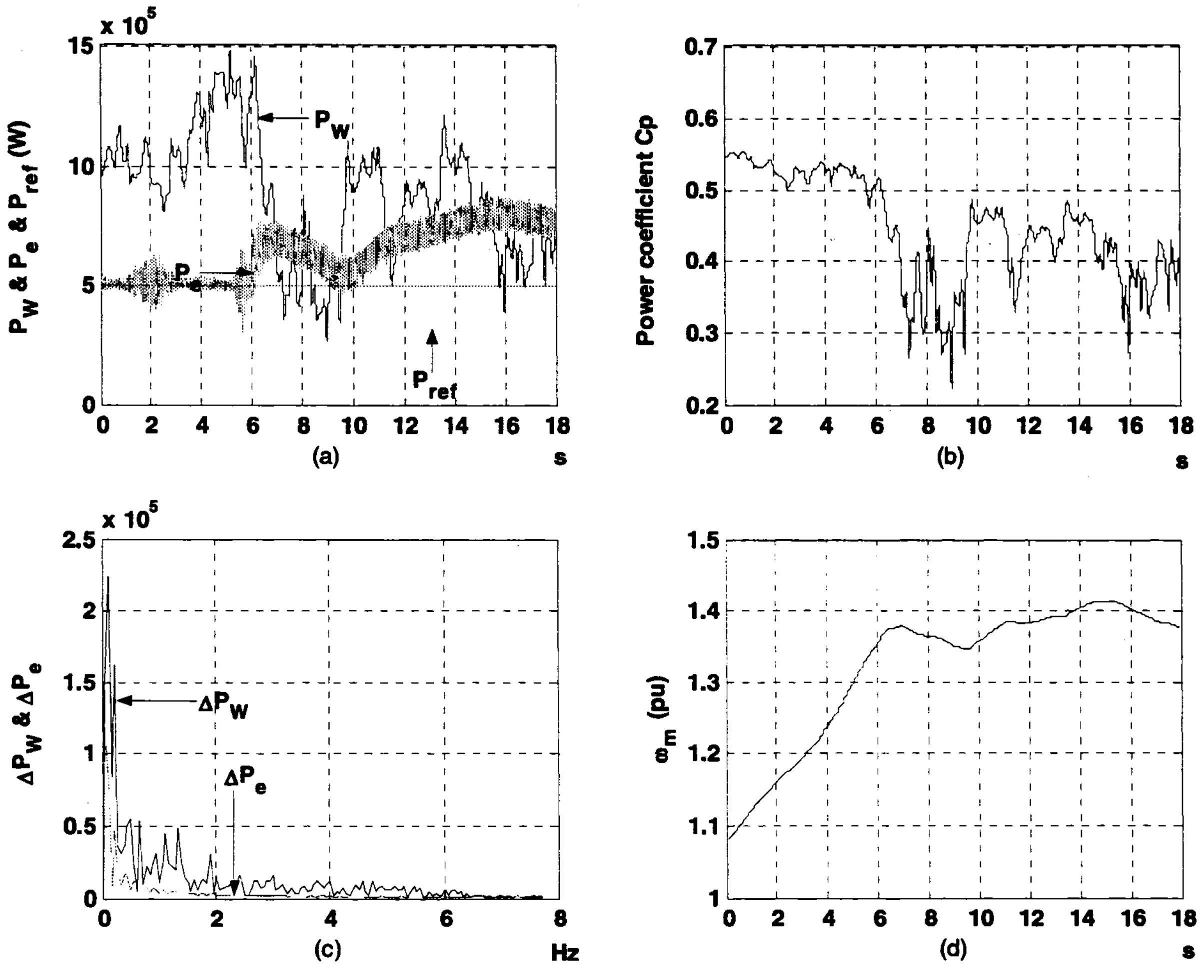

Fig 5.10. DFIG with P_{ref}=0.5 MW

(3) $P_{ref} = p_O = 1.2$ MW > $P_{W\text{-}ave}$

Fig. 5.11 shows the case of setting $P_{ref}=p_O=1.2$ MW. Because $P_W<p_O$, ω_m keeps decelerating as shown in Fig. 5.11 (b). Around 6 seconds, ω_m falls below 0.75 pu. As shown in Fig. 5.11 (a), P_e ceases to track $P_{ref}=p_O$ and oscillates uncontrollably.

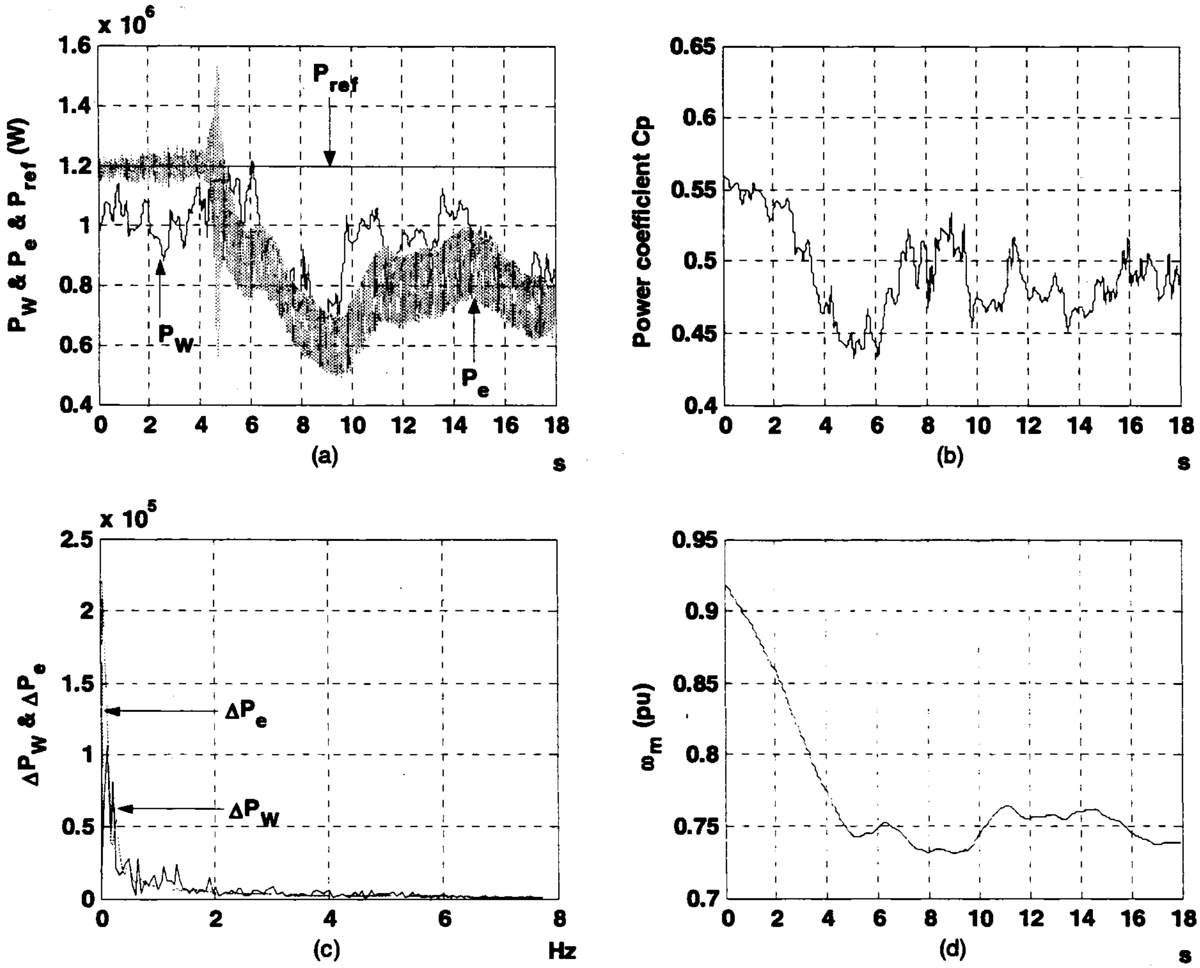

Fig 5.11. DFIG with $P_{ref}=1.2$ MW

5.4.5 Steady-State Instability of DFIG

The reason for the uncontrolled oscillations in Fig. 5.10 and Fig.5.11 is steady-state instability. The presence of steady-state instability has only been recently discovered in

McGill University by Dr. Lianwei Jiao, Dr. Hadi Banakar and Professor B.T. Ooi. The author reproduces with their permission Fig. 5.12, which is taken from their manuscript submitted for acceptance as an IEEE transaction paper [5-4].

The heavy thick lines mark the steady-state stability boundaries of a doubly-fed induction machine whose parameters are the same as the 1.0 MW DFIG used in the simulations in this chapter. The criterion of steady-state stability is based on all the eigenvalues of the [A] matrix lying on the left hand side of the complex s-plane. The [A] matrix is obtained by small perturbation linearization of the γ-δ frame dynamic equations of the induction machine. The DFIG operating region is the negative (generation) lower half of Fig. 5.12. Stable operation lies between $\omega_m \approx 0.1$ pu and $\omega_m \approx 1.25$ pu. The two boundaries at low speed and at high speed correspond to operating the DFIG at 0.8 pf leading and lagging.

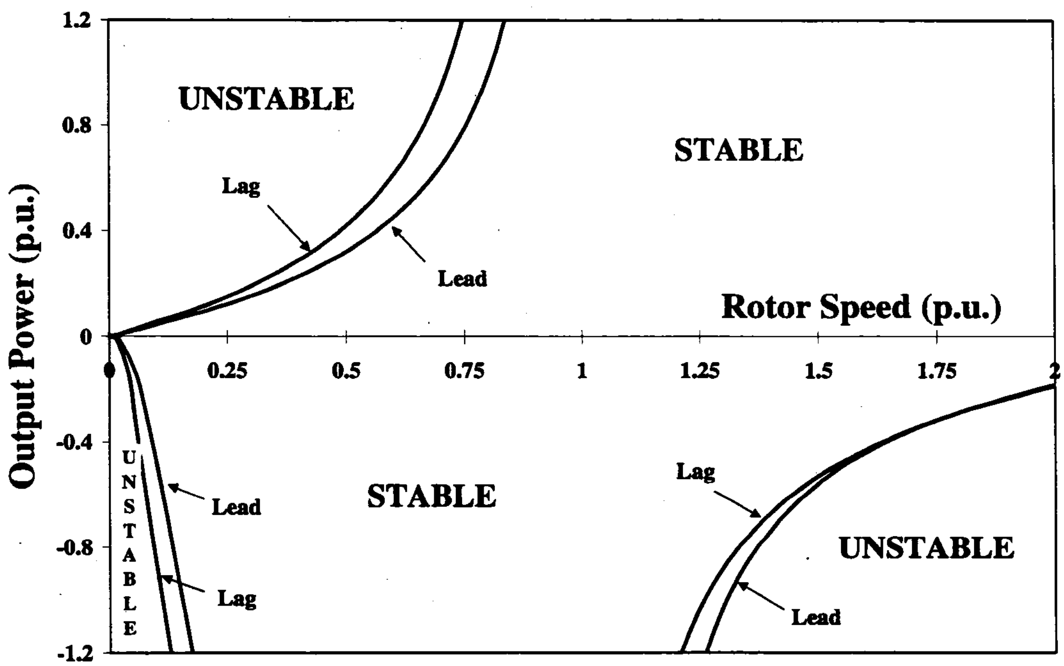

Fig. 5.12. Limits of Operation of Doubly-Fed Induction Machine

In Fig. 5.10 and Fig.5.11, one sees the cases of acceleration and deceleration from the stable operating region to unstable operating regions.

5.4.6 Linear Slope Strategy

The weakness of the Constant Power Strategy is that $P_{ref}(\omega_m)=p_0$ is not sufficient to restrain the fluctuating wind power from driving the system into the unstable regions. The Linear Slope Strategy, $P_{ref}(\omega_m)=p_0+p_1\omega_m$ uses a speed dependent term to restrain the speed excursions. As the wind power accelerates and decelerates ω_m, $P_{ref}(\omega_m)=p_0+p_1\omega_m=(p_0+p_1\omega_{m0})+p_1(\omega_m-\omega_{m0})$ should be a better estimate of the mean value P_W than $P_{ref}(\omega_m)=p_0$.

Based on (5-18), (5-19)

$$\frac{\Delta\omega_m(s)}{\Delta P_W(s)}=\frac{1}{2H\omega_{m0}\cdot s+p_1\omega_{m0}} \tag{5-22}$$

$$\frac{\Delta P_e(s)}{\Delta P_W(s)}=\frac{-p_1\omega_{m0}}{2H\omega_{m0}\cdot s+p_1\omega_{m0}} \tag{5-23}$$

When p_1 is large, there is less tendency for the speed to stray beyond the unstable operating region .On the other hand, the power fluctuation of P_e is more severe.

In Fig. 5.13 (a), the DFIG is stabilized even when p_0 is not chosen properly. In Fig. 5.13 (b), the speed ω_m fluctuation is kept within the stable region of Fig. 5.12.

Linear Slope Strategy: P_{ref}=1.2+0.01(ω_m-ω_{m0}) MW

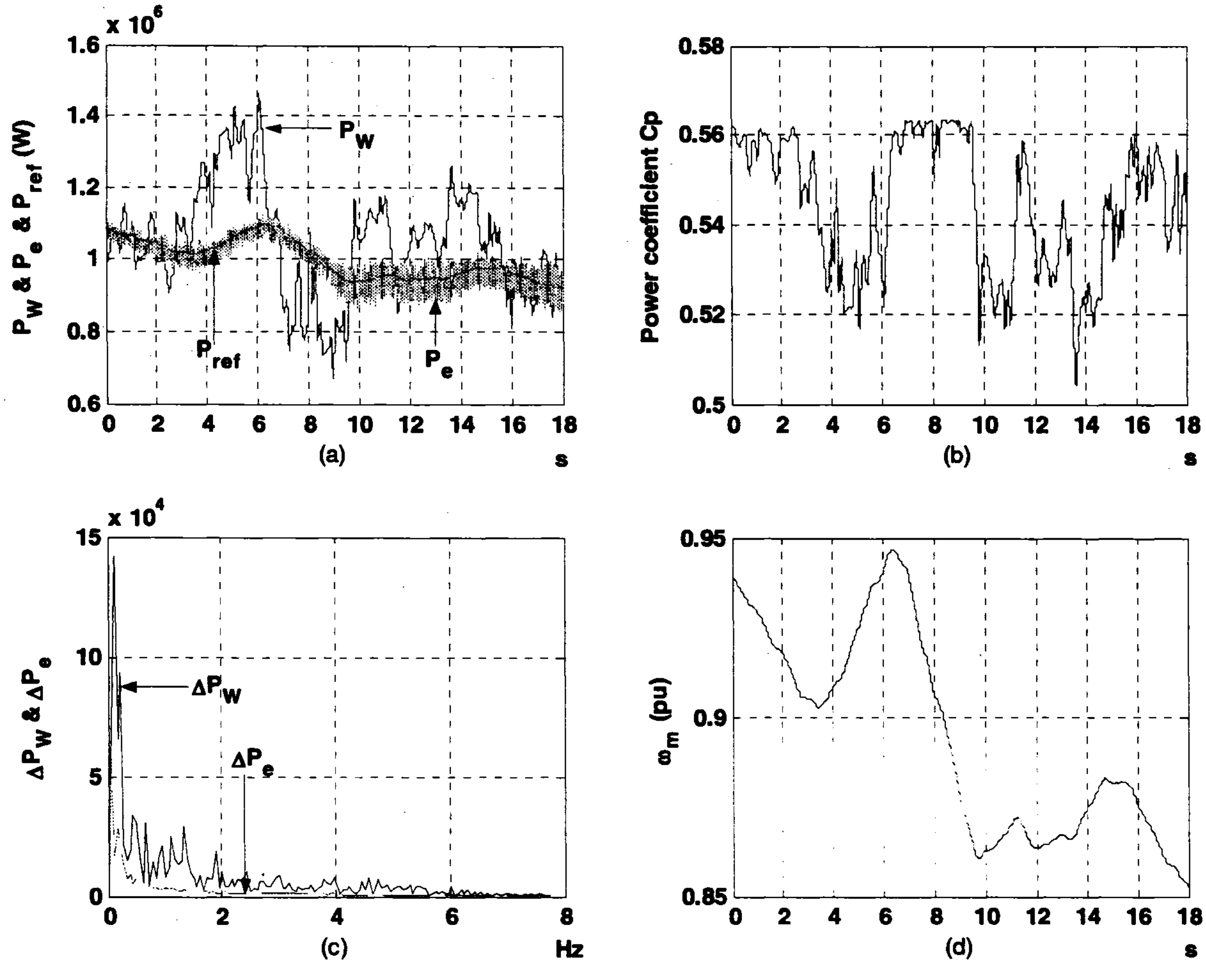

Fig. 5.13. Linear slope strategy when P_{ref}=1.2+0.01(ω_m-ω_{m0}) MW

5.4.7 Optimal Wind Power Aquisition Strategy

Optimal wind power acquisition means operating at the maximum C_{pmax} in the ordinate of Fig. 5.1 corresponding to λ_{max} in the abscissa. Substituting C_{pmax} in (5-2), one has

$$P_W = 0.5\rho A C_{p\max} V_W^3 \qquad (5\text{-}24)$$

From (5-1)

$$V_W = \frac{\omega_m \cdot R}{(gear\ ratio) \cdot \lambda_{\max}} \qquad (5\text{-}25)$$

Substituting (5-25) in (5-24)

$$P_W = p_3 \omega_m^3 \qquad (5\text{-}26)$$

where p_3 is the coefficient of ω_m^3 after the substitution. The cubic curve is the $P_{optimal}$ curve illustrated in Fig. 5-2.

In decoupled P-Q control of the wind turbine driven DFIG, the reference set to the real power control is

$$P_{ref} = p_3 \omega_m^3 \qquad (5\text{-}27)$$

Based on (5-19)

$$\frac{\Delta P_e(s)}{\Delta P_W(s)} = \frac{3p_3\omega_m^2}{2H\omega_{m0} \cdot s - 3p_3\omega_m^2} \qquad (5\text{-}28)$$

The results of simulation tests, for Optimal Wind Power Acquisition Strategy, are shown in Fig. 5.14 for H=0.6 s, in Fig. 5.15 for H=5 s and Fig. 5.16 for H=12 s. Based on the computed values of C_p in (b), one sees that when H is small so that P_e can track P_W optimal power acquisition is approached. Filtering depends on H or the $2H\omega_{mo}s$ term on (5-28) as the graphs in (a) show very clearly.

(1) H=0.6 s

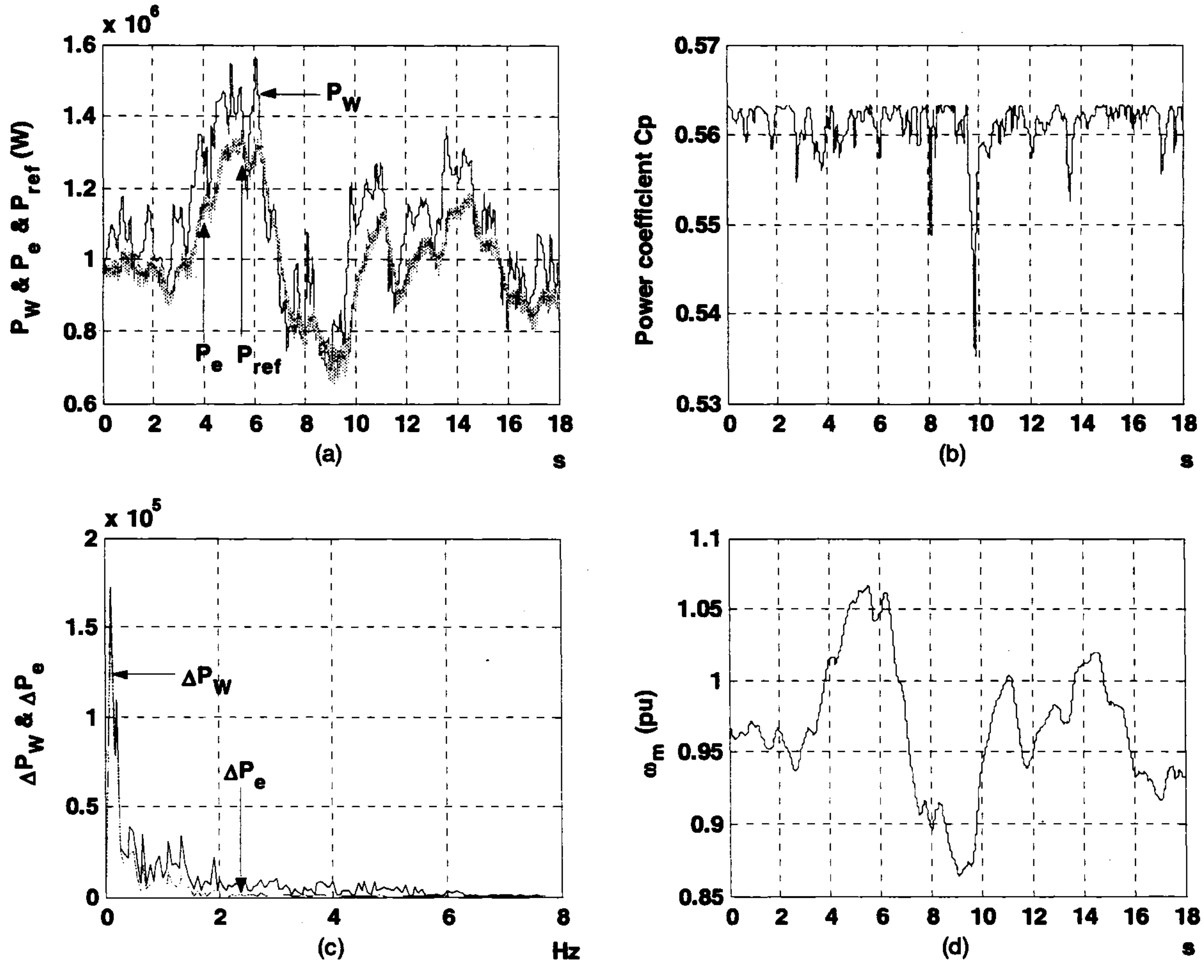

Fig. 5.14. DFIG with optimal control when H=0.6 s

(2) H=5 s

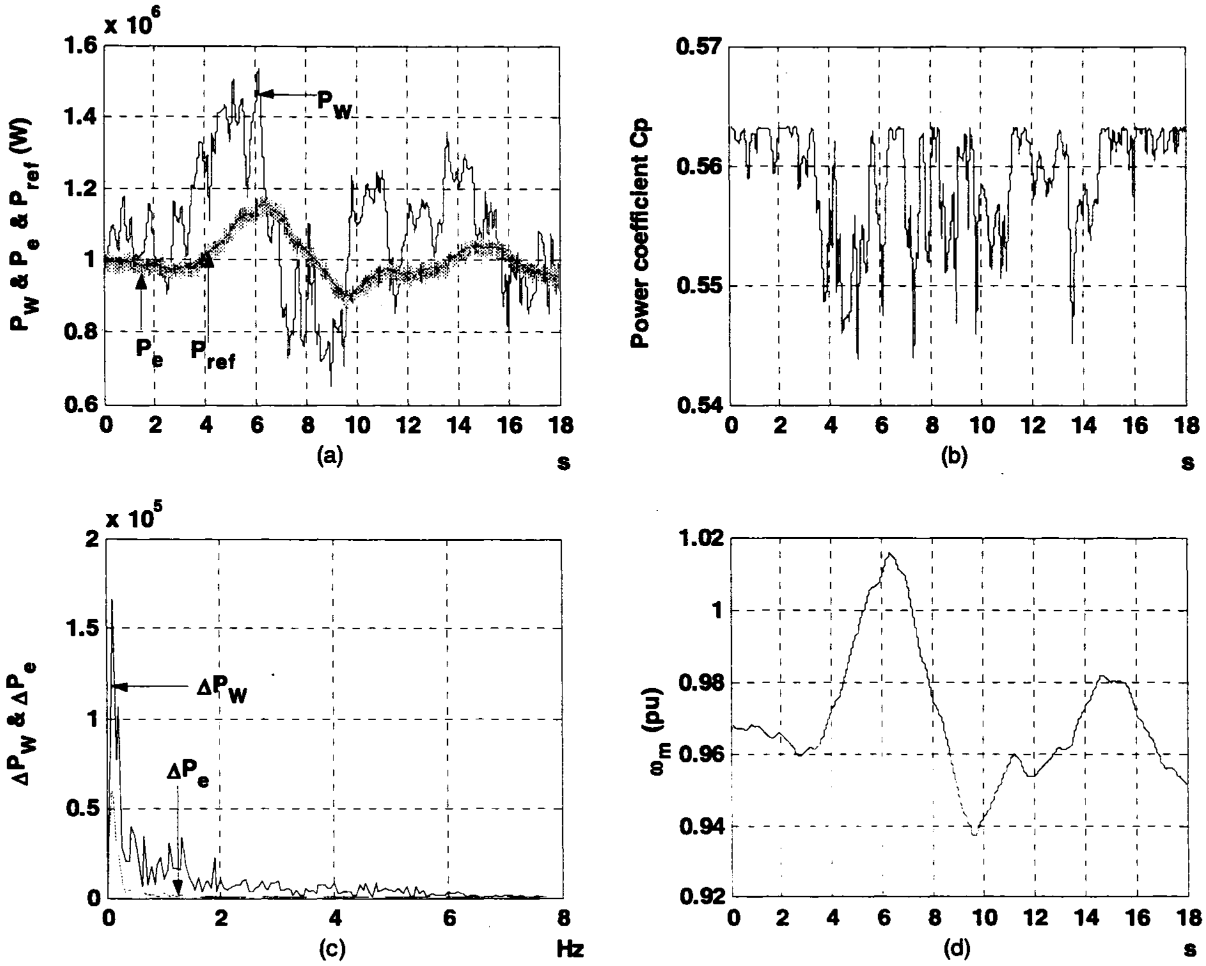

Fig. 5.15. DFIG with optimal control when H=5 s

(3) H=12 s

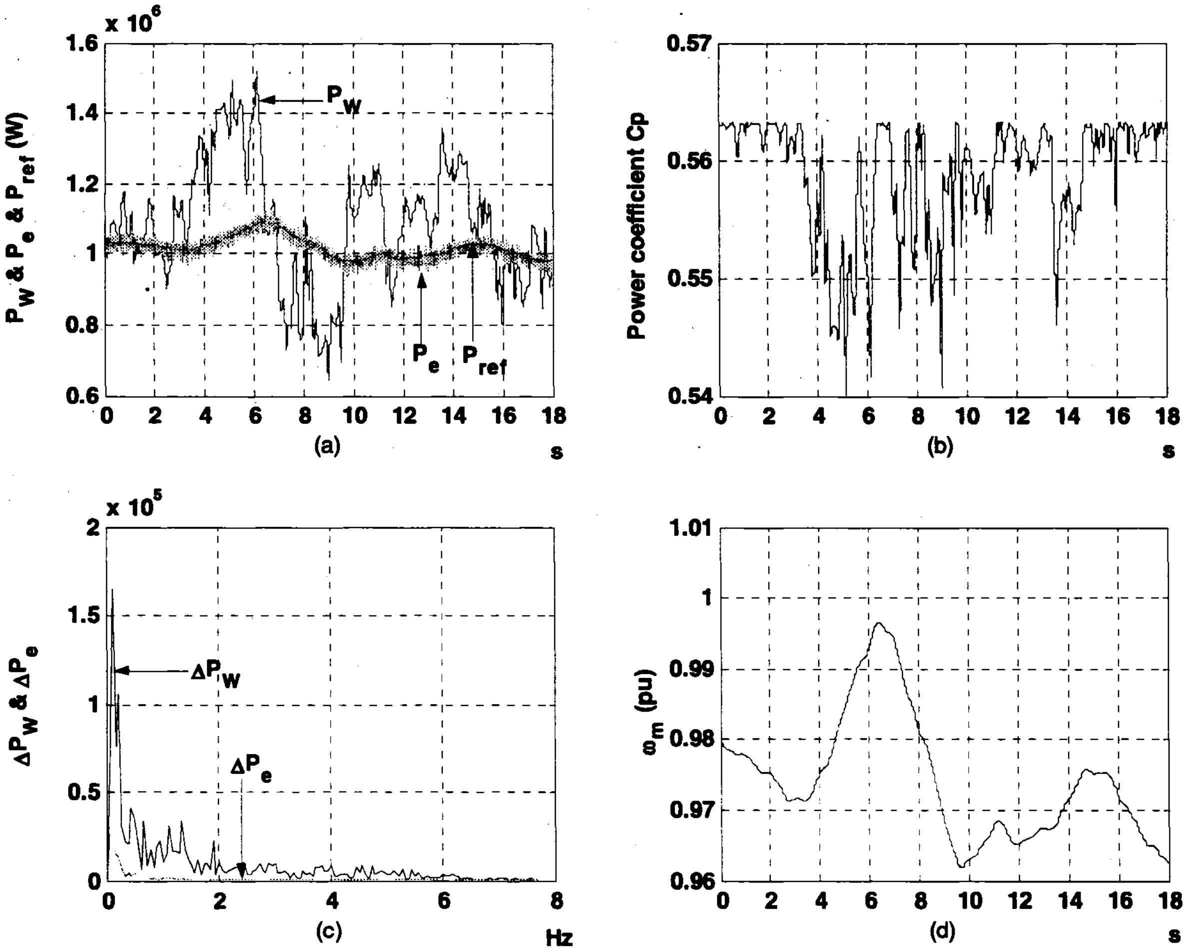

Fig. 5.16. DFIG with optimal control when H=12 s

The simulations show that when large inertias are available, reasonable filtering accompanies reasonable optimal wind power acquisition. From the computed C_p in (c), one sees that the filtering is accompanied by optimal wind power acquisition.

5.5 Conclusion

The research of this chapter has shown that the large moments of inertia of large wind turbines together with decoupled P-Q control of the DFIGs, which they are now equipped with, can play a very useful role in filtering out the power fluctuations which come from wind turbulence. Decoupled P-Q control allows a variety of strategies to be implemented from the real power reference setting. The setting in general is a polynomial of the speed ω_m such as $P_{ref}(\omega_m)= p_0+p_1\omega_m+p_2\omega_m^2+p_3\omega_m^3+p_4\omega_m^4+\ldots$ The two promising ones are: Linear Slope Strategy and Optimal Wind Power Acquisition Strategy.

(1) The Linear Slope Strategy is based on $P_{ref}(\omega_m)=p_0+p_1\omega_m$. It has the best filtering.

(2) The Optimal Wind Power Acquisition Strategy is based on $P_{ref}(\omega_m)= p_3\omega_m^3$. The high frequency power fluctuations are removed when the wind turbines have large inertias. The computed C_p shows that this strategy acquires more of the power from the wind than other strategies.

The case of the Constant-Speed Squirrel Cage Induction Generator has been studied as the base to highlight the improvement which comes in using DFIGs.

The simulation studies have been accompanied by system analyses which identify the factors contributing to filtering.

CHAPTER 6

FLUCTUATING WIND POWER PENETRATION LIMIT

6.1 Introduction

The primary objective of the thesis is to estimate the fluctuating wind power penetration limit, which is an estimate of the power fluctuations due to wind turbulence, which can be tolerated, without causing the frequency of the utility grid to deviate by 1% from the 60 Hz standard. In chapter 4, it has been estimated that, with filtering by the governor system of thermal power plants, the sinusoidal power fluctuation concentrated in a single frequency is around 5% of the power capacity of the power plants. Chapter 4 is based on a deterministic approach using the transfer functions of the sub-systems of the power plants.

Chapter 5 has shown that the kinetic energy in the inertia of the wind turbine, characterized by H, can play its part in filtering at the wind farm end. Departing from the deterministic approach in chapter 4, chapter 5 introduces an 18-second sample of wind velocity as the reference to evaluate different kinds of wind generators: the constant speed squirrel-cage induction generator and doubly-fed induction generators (DFIG). From comparing the simulated outputs, the conclusion is that the DFIG with Optimal Wind Power Acquisition strategy is the most promising.

This chapter combines the methods of the 2 previous chapters to make a rough but conservative estimate of the wind power fluctuation which can be tolerated when the filtering comes from the turbine inertia at the wind-farm end and from the governor system at the power plant end. The estimate is conservative because the same 18-second sample of wind velocity is used in representing the wind turbulence experienced by all the wind turbines in a wind farm. The benefit of spatial filtering is not factored in, in the estimate.

As the 18-second sample of wind velocity is used in the tests, statistical measures are introduced in this chapter. The limit of frequency deviation from the 60 Hz is now expressed as the Standard Deviation (STD) of $\omega_r \leq 0.01$ pu. The measure of wind power fluctuation is the STD of the wind power P_W. This chapter introduces the definition

$$fluctuation - penetration = \frac{(STD\ of\ P_W)_{\max}}{\text{Capacity of Power System}} \times 100\% \qquad (6\text{-}1)$$

$$\text{when } (\text{STD of } \Delta\omega_r) \leq 0.01 \text{ per unit}$$

It is important to note that *fluctuation penetration* is related to wind turbulence. Fluctuating power rides on the statistical expected value which is subtracted from the wind velocity. The wind power associated with the statistical expected value is the firm power traded in the energy market. As the statistical expected wind power is usually larger than the standard deviation of the wind power, what is normally called *wind penetration* is usually higher that *fluctuation penetration.*

6.2 Method of Estimation

Fig. 6-1 recapitulates the relationships of V_W the wind velocity, P_W the turbine power, P_e the induction generator power and ω_r, the frequency of the power plant. In the wind turbine generator (WTG) stage (chapter 5), ΔV_W as input results in fluctuating wind turbine power ΔP_W. After filtering by the turbine blade inertia the output is the induction generator power ΔP_e. The transmission line connects the wind turbine generator to the power plant. In the power plant stage (chapter 4), the input ΔP_e is the cause of frequency deviation $\Delta\omega_r$.

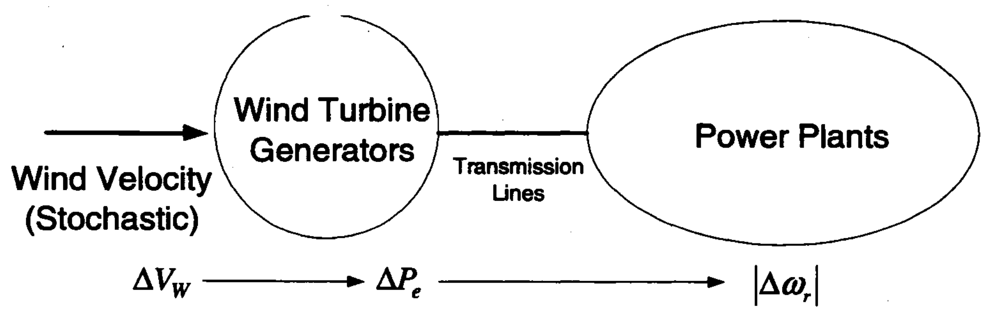

Fig. 6.1. Relationship between stochastic wind velocity and frequency deviation

The single wind farm/single power plant model as shown in Fig. 6.2 is used to make the rough estimate. This approach is reasonable because per unitization is used in the computation. In modeling the wind turbulence in all the wind farms, it is assumed that the same wind velocity from the 18-second wind data file passes simultaneously through all the wind turbine generators in the many wind farms. As already mentioned, this assumption neglects spatial filtering but the estimate errs on the conservative side. It is assumed that there are K units of the wind turbine generators of chapter 5, K being the algebraic unknown which increases the frequency deviation $\Delta\omega_r$ to 1%.

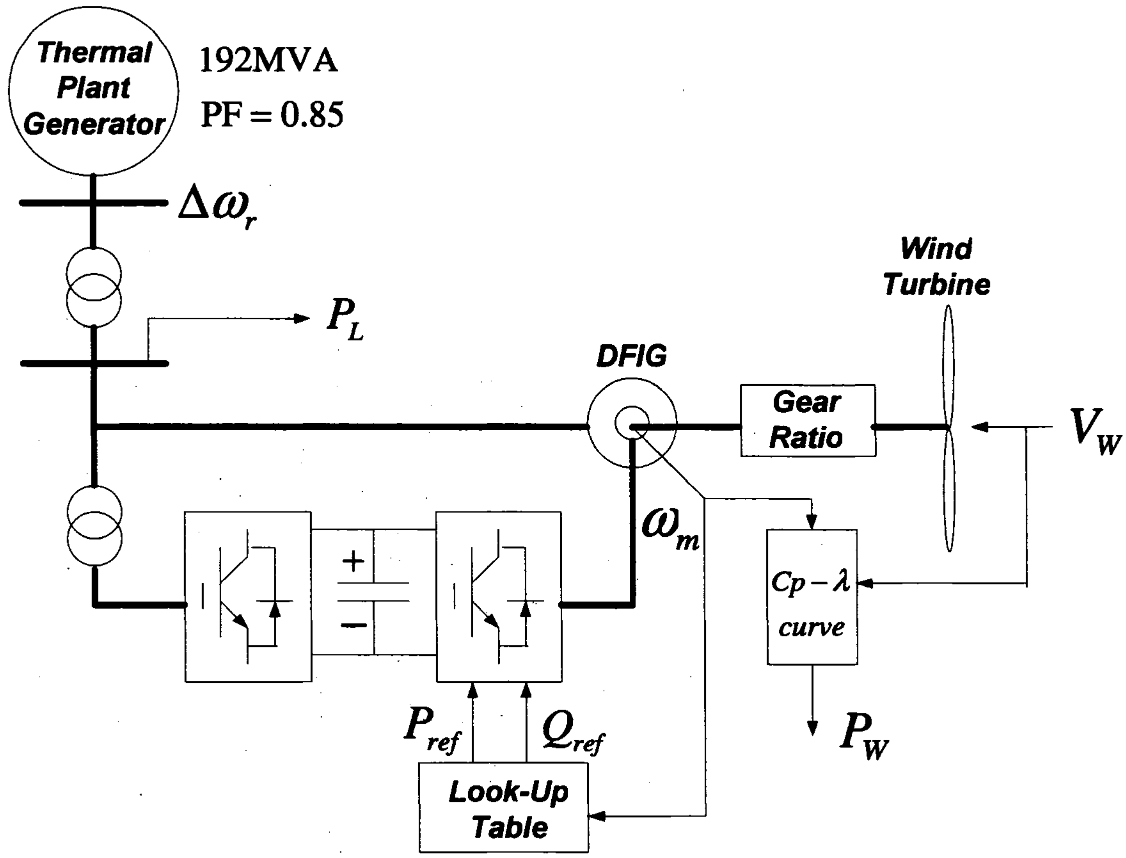

Fig. 6.2. Single WTG/single thermal power plant model used in estimation.

6.3 Estimation Procedures

The procedures consist of two parts:

(i) Based on the results from Off-line simulation on HYPERSIM in Chapter 4, transfer function of the Thermal Power Plant using $G_3(s)$ in the state equation formulation (see Appendix B and C) is realized in Laplace domain. The droop has been set as r=0.05 pu.

(ii) Off-line simulation of a WTG using the DFIG model of Mr. Baike Shen in conjunction with the computation of wind power P_W from the C_p-vs-λ curve of Fig. 5.1 in chapter 5 in EMTP-RV

All the estimations are based on the same 18-second wind velocity data file which is run repeatedly in simulations. The results of 2 estimates are given for:

(1) Wind generators which are squirrel cage induction generators (or Constant-Speed WTG).

(2) Wind generators which are doubly-fed induction generators (DFIGs) operating under Optimal Wind Power Acquisition Strategy ($P_{ref} = p_3 \omega_m^3$).

Data Collection

From V_W of the 18-second wind velocity data file, simulations runs are made to obtain the files of $\Delta\omega_r(t)$, $\Delta P_e(t)$ and $P_W(t)$. The standard deviation quantities, $\mathrm{STD}_{\mathrm{measured}}(\Delta\omega_r)$, $\mathrm{STD}_{\mathrm{measured}}(\Delta P_e)$ and $\mathrm{STD}_{\mathrm{measured}}(P_W)$ are computed from the files.

Treatment of Standard Deviation Measurements

For a single power plant rated at 163.2 MW, the impact the fluctuating power of a single WTG is small and $\mathrm{STD}_{\mathrm{measured}}(\Delta\omega_r)$ is very much less than 1%. Therefore the allowable Standard Deviation of fluctuating wind power or $\mathrm{STD}(P_W)$ is higher by a multiplication constant K given by

$$K = \frac{0.01}{STD_{measured}(\Delta\omega_r)} \qquad (6\text{-}2)$$

The fluctuation penetration is computed as:

$$fluctuation - penetration = \frac{K \cdot STD_{measured}(P_W)}{P_{\max}} \times 100\% \qquad (6\text{-}3)$$

where P_{max} is the real power capacity of the power plant.

<u>Attenuation Factor F_a</u>

Based on standard deviation measurements, it is possible to define an attenuation factor, F_a an indicator of the power filtering by different types of wind turbine generators:

$$F_a = \frac{STD_{measured}(\Delta P_e)}{STD_{measured}(P_W)} \tag{6-4}$$

The Constant Speed WTG is chosen to emphasize that it offers virtually no filtering when the wind turbine blades have small H. The Optimal Wind Power Acquisition Strategy offers the least filtering of the 3 options discussed in Chapter 5. It is chosen because it offers good filtering when H=5 s and good wind power acquisition.

6.3.1 Power System with Constant-Speed WTG (Squirrel-cage Induction Generator)

Fig. 6.3, 6.4 and 6.5 display $\omega_f(t)$ for H=0.6 s, 5 s and 12 s respectively. The computed values of K and the attenuation factor F_a are presented below the curves. The zero of the y-axis represents 60 Hz. The vertical scale of the STD($\Delta\omega_f$) curves shows that the frequency deviation due to a single WTG is small and the wind farm can accommodate K number of WTGs. K is determined by (6-1). These curves show that the high frequency fluctuations have been filtered. Because the attenuation factor F_a is large, the filtering comes mainly from the power plant. The fluctuating power penetration is around 8%.

(1) H=0.6 s

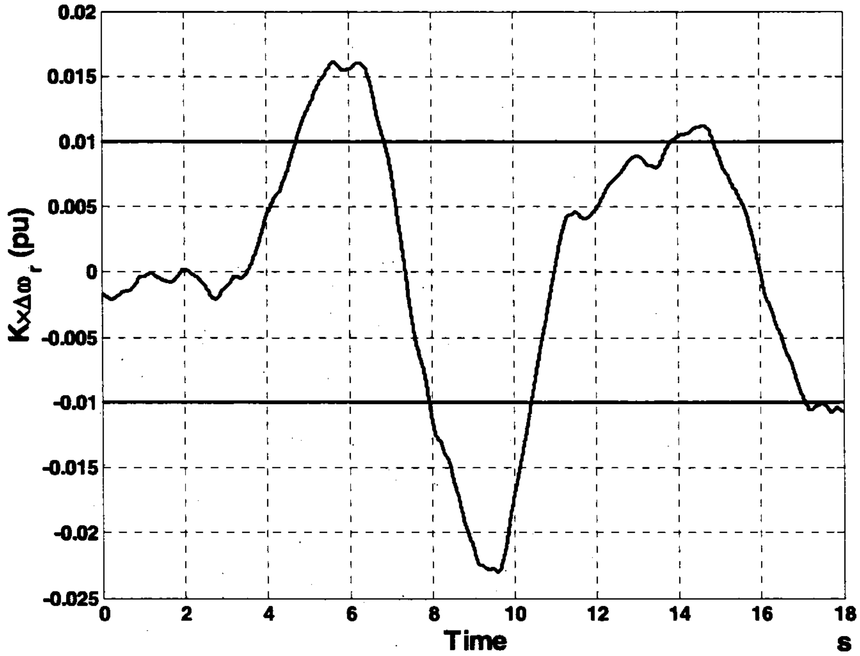

Fig. 6.3. $\Delta\omega_r$-vs-t, Squirrel-cage induction generator $H=0.6$ s

$P_{max} = 163.2\,\text{MW or } 1\,\text{pu}$

$STD_{measured}(\Delta\omega_r) = 1.3728\times10^{-4}$ in pu

$STD_{measured}(P_W) = 1.1454\times10^{-3}, STD_{measured}(\Delta P_e) = 1.0266\times10^{-3}$ in pu

$$F_a = \frac{STD_{measured}(\Delta P_e)}{STD_{measured}(P_W)} = \frac{1.0266}{1.1454} = 0.896$$

$$K = \frac{0.01}{STD_{measured}(\Delta\omega_r)} = 72.844$$

$$Fluctuation - Penetration = \frac{K \cdot STD_{measured}(P_W)}{P_{max}} \times 100\% = 8.344\%$$

(2) H=5 s

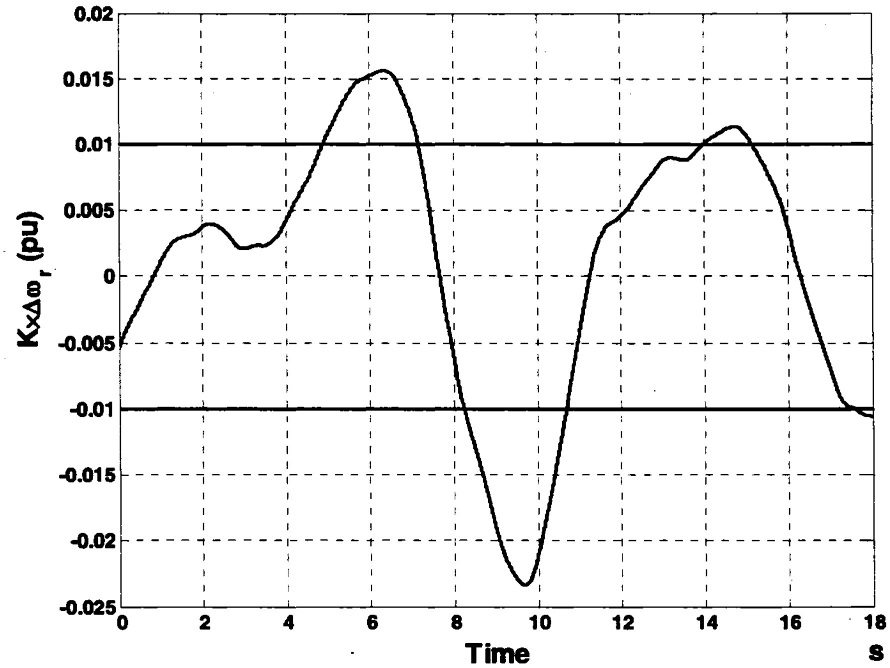

Fig. 6.4. $\Delta\omega_r$-vs-t, Squirrel-cage induction generator H=5 s

$P_{max} = 163.2\,\text{MW or } 1\,\text{pu}$

$STD_{measured}(\Delta\omega_r) = 1.3057\times10^{-4}$ in pu

$STD_{measured}(P_W) = 1.1446\times10^{-3}, STD_{measured}(\Delta P_e) = 8.9582\times10^{-4}$ in pu

$$F_a = \frac{STD_{measured}(\Delta P_e)}{STD_{measured}(P_W)} = \frac{0.89582}{1.1446} = 0.783$$

$$K = \frac{0.01}{STD_{measured}(\Delta\omega_r)} = 76.587$$

$$Fluctuation - Penetration = \frac{K \cdot STD_{measured}(P_W)}{P_{max}} \times 100\% = 8.766\%$$

(3) H=12 s

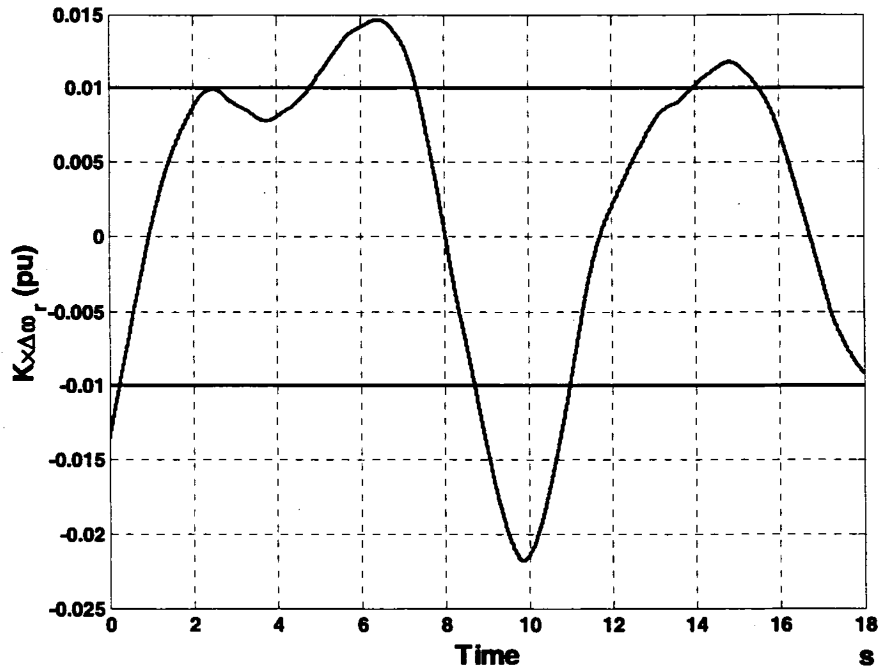

Fig. 6.5. $\Delta\omega_r$-vs-t, Squirrel-cage induction generator $H=12\ s$

$$P_{\max} = 163.2\,\text{MW or } 1\,\text{pu}$$

$$STD_{measured}(\Delta\omega_r) = 1.1964\times10^{-4} \text{ in pu}$$

$$STD_{measured}(P_W) = 1.1445\times10^{-3}, STD_{measured}(\Delta P_e) = 7.3984\times10^{-4} \text{ in pu}$$

$$F_a = \frac{STD_{measured}(\Delta P_e)}{STD_{measured}(P_W)} = \frac{0.73984}{1.1445} = 0.646$$

$$K = \frac{0.01}{STD_{measured}(\Delta\omega_r)} = 83.584$$

$$Fluctuation - Penetration = \frac{K\cdot STD_{measured}(P_W)}{P_{\max}}\times100\% = 9.566\%$$

6.3.2 Power System with Variable-Speed WTG

The fluctuation penetration is considered for DFIGs operating under real power reference ($P_{ref}=p_3\omega_m^3$) of Optimal Wind Power Acquisition Strategy. Fig. 6.6, 6.7 and 6.8 display $\Delta\omega_r(t)$ for H=0.6 , 5 and 12 s respectively.

(1) H=0.6 s

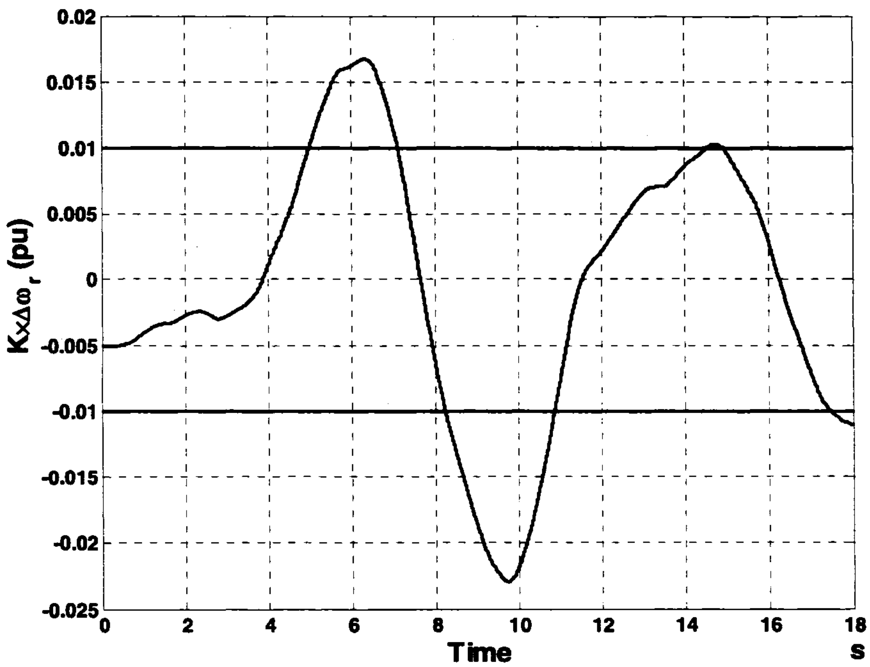

Fig. 6.6. $\Delta\omega_r$-vs-t, DFIG Optimal Power Strategy $H=0.6$ s

$P_{\max} = 163.2$ MW or 1 pu

$STD_{measured}(\Delta\omega_r) = 1.3612\times10^{-4}$ in pu

$STD_{measured}(P_W) = 1.1016\times10^{-3}, STD_{measured}(\Delta P_e) = 9.2174\times10^{-4}$ in pu

$$F_a = \frac{STD_{measured}(\Delta P_e)}{STD_{measured}(P_W)} = \frac{0.92174}{1.1016} = 0.837$$

$$K = \frac{0.01}{STD_{measured}(\Delta\omega_r)} = 73.465$$

$$Fluctuation - Penetration = \frac{K \cdot STD_{measured}(P_W)}{P_{\max}} \times 100\% = 8.093\%$$

(2) H=5 s

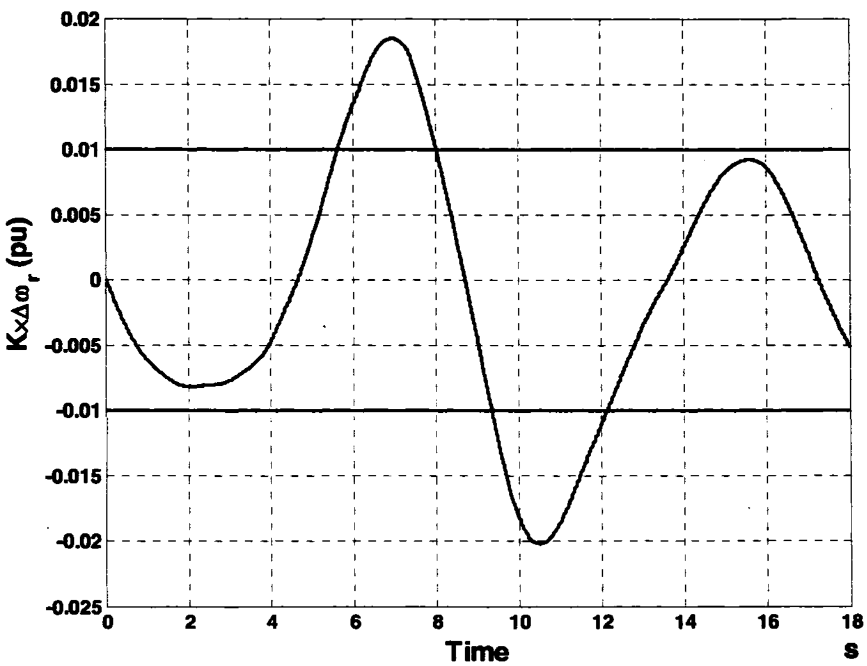

Fig. 6.7. $\Delta\omega_r$-*vs-t*, DFIG Optimal Power Strategy *H=5 s*

$P_{\max} = 163.2\,\text{MW or 1 pu}$

$STD_{measured}(\Delta\omega_r) = 5.8856 \times 10^{-5}$ in pu

$STD_{measured}(P_W) = 1.0728 \times 10^{-3}, STD_{measured}(\Delta P_e) = 3.657 \times 10^{-4}$ in pu

$$F_a = \frac{STD_{measured}(\Delta P_e)}{STD_{measured}(P_W)} = \frac{3.657 \times 10^{-4}}{1.0728 \times 10^{-3}} = 0.3409$$

$$K = \frac{0.01}{STD_{measured}(\Delta\omega_r)} = 169.91$$

$$Fluctuation - Penetration = \frac{K \cdot STD_{measured}(P_W)}{P_{max}} \times 100\% = 18.275\%$$

(3) H=12 s

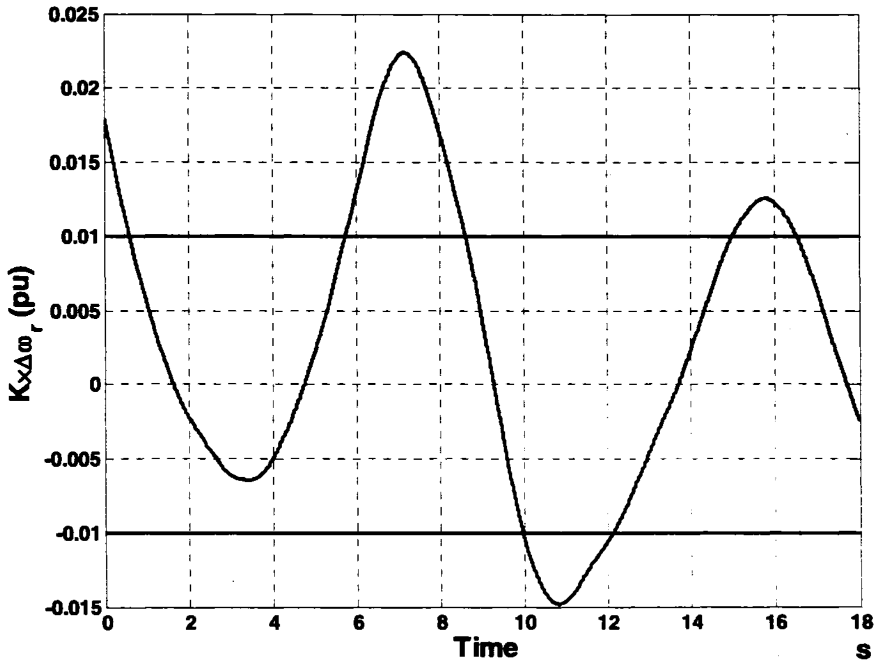

Fig. 6.8. $\Delta\omega_r$-*vs-t*, DFIG Optimal Power Strategy $H=12\ s$

$P_{max} = 163.2$ MW or 1 pu

$STD_{measured}(\Delta\omega_r) = 2.772 \times 10^{-5}$ in pu

$STD_{measured}(P_W) = 1.068 \times 10^{-3}, STD_{measured}(\Delta P_e) = 1.9235 \times 10^{-4}$ in pu

$$F_a = \frac{STD_{measured}(\Delta P_e)}{STD_{measured}(P_W)} = \frac{1.9235 \times 10^{-4}}{1.068 \times 10^{-3}} = 0.1801$$

$$K = \frac{0.01}{STD_{measured}(\Delta\omega_r)} = 360.75$$

$$Fluctuation - Penetration = \frac{K \cdot STD_{measured}(P_W)}{P_{max}} \times 100\% = 38.528\%$$

6.3.3 Comparison of Constant-Speed and Variable-Speed WTG

WTG Inertia (s)	Constant-Speed WTG		DFIG with optimal control	
	Fluctuation-Penetration	Attenuation Factor F_a	Fluctuation-Penetration	Attenuation Factor F_a
H=0.6	8.344%	0.896	8.093%	0.837
H=5.0	8.766%	0.783	18.275%	0.3409
H=12	9.566%	0.646	38.528%	0.1801

Table. 6.1. Comparison of wind power penetration and attenuation factor between Constant-Speed and Variable-Speed WTG

Table 6.1 gives a comparison between the constant-speed WTG and the variable speed DFIG-wind turbine. Of the 3-strategies of DFIG control in chapter 5, the Optimal Wind Power Acquisition Strategy is chosen because it offers the lowest attenuation factor and therefore the conclusion, drawn here, is the most conservative.

Because the size of WTG inertia is not disclosed by manufacturers, H=0.6, 5.0 and 12.0 s have been used to indicate the possible range. From the attenuation factor F_a, it is clear that filtering improves with increase in H. Constant speed squirrel cage induction generators belong to the early generation of wind turbines which, because of their small size, have small H. On the other hand the 1.5, 3.0 MW size wind turbines driving DFIGs are variable speed turbines with large H.

6.4 Conclusion

This chapter introduces the concept of Standard Deviation of grid frequency and Standard Deviation of wind power to quantify the impact of wind power fluctuations on the utility grid frequency. By combining the filtering in the thermal power plants and the filtering in the wind farms, the fluctuation penetration of wind power into the utility grid has been conservatively estimated. Using wind turbine inertia in the range around H=5 s, the Fluctuation-Penetration of DFIG with Optimal Wind Power Acquisition is approximately 18%.

As the 18% represents the wind power fluctuations which ride on the statistical mean power which is used by customers, the wind power penetration is a higher percentage by a factor of (Mean/Standard Deviation) of wind power.

If a high level of wind penetration is the objective, then squirrel cage induction generators should be discouraged.

Variable-Speed WTG with high inertias should be welcome. Constant real power control ($P_{ref}= p_0$) can run into instability regions. The Constant Slope Strategy ($P_{ref}= p_0 + p_1\omega_m$) can avoid running into instability regions while achieving the best filtering. The Strategy ($P_{ref}= p_3\omega_m^3$) combines good filtering with optimal wind power acquisition.

It should be remembered that spatial filtering (cancellation among random signals) has not been included in the estimates. It should also be remembered that the wind turbine characteristic is based on the C_p-vs-λ as shown in Fig. 5.1. As variable pitch control should improve performance, the estimate errs on the conservative side.

CHAPTER 7

CONCLUSIONS

7.1 Introduction

The objective of this thesis is to estimate the level wind power penetration in thermal power systems vis-à-vis respecting frequency standards. The margin of frequency deviation from 60 Hz is set at 1% or ±0.6Hz. In general, wind power can be decomposed into:

(1) The firm component of wind power which is traded in the hourly market.

(2) The fluctuating component associated with wind turbulence. The penetration limit of this thesis is in regard to the fluctuating component only.

As wind turbulence is more orderly [7-1] when viewed in the frequency spectrum, the methodology is based on the transfer function approach considering wind power at each frequency f_W in the spectrum of wind turbulence.

7.2 Conclusions of Thesis

The research in chapter 4 has found that the penetration limit set by turbulent wind power is around 5% of the total power rating of the thermal plants. The "virtual storage" in the speed governor system and the kinetic energy storage in the inertias of the HP, IP, LP turbines and the synchronous generator provide filtering of the fluctuating power.

The research in chapter 5 has found that there is additional filtering in the wind farm.

This is by taking advantage of the kinetic energy associated with the large moments of inertia of the large diameter wind turbine blades. There is excellent filtering when the Constant Power Output Strategy is adopted but its operation can run into instability problems. The Optimal Wind Power Acquisition Strategy is preferred although the filtering is poorer.

Chapter 6 shows that a combination of filtering in the wind farms and in the thermal power plants raises the limit to a conservative 8%. The number is conservative because the filtering in the wind farm is based on DFIG with Optimal Wind Power Acquisition for low turbine inertia. The limit can be raised very much higher when very large turbine inertia is the case.

It needs to be emphasized that the 8% consists of the fluctuating power associated with wind turbulence. The turbulent wind power is some fraction of the firm component of wind power which is traded in the energy market. Therefore, the level of penetration of commercial grade wind power should be much higher than 8%.

(1) Implication to Electricity Market

The filtering by the speed governors increases the wear and tear of hardware. The filtering should be recognized as an ancillary service and charges should be levied to defray the cost of replacement and repair of equipment.

(2) Implication to Regulatory Bodies

Wind farms should be obliged to filter the turbulent wind power before admission into the utility grid. If the regulation is simply to comply with the frequency deviation margin, this regulation is insufficient to promote a very high level of wind penetration. This is because the research in chapter 4 shows that the entire grid enjoys the same frequency, for the short transmission lines of this study. The unfiltered power fluctuations from any wind farm affect the frequency deviation of the entire grid and it is not possible to convict the culprits. There is the need of a regulation similar to Total Harmonic Distortion Standards in allowing power electronic equipment to be connected. Instead of voltage or current waveforms, the relevant quantity is power waveform. Another difference is that the frequencies are sub-harmonics of 60 Hz. Such regulation will need instrumentation customized to assess fitness for admission.

7.3 Conclusions from Individual Chapters

Chapter 2 has presented a Complex Power or S-Modulator which can be used in conjunction with power system simulation software such as HYPERSIM, EMTP-RV or EMTDC PSCAD. In the research of the thesis, the S-Modulator represents the complex power output of a wind farm at the point of connection. In the deterministic study of this thesis, the real power control of the S-Modulator has been used to inject sinusoidal power fluctuations representing of wind farm power output at a fixed frequency f_W. When data files of wind farm power output become available, it is a matter of feeding the time series data to the real power control of the S-Modulator.

To ensure that the simulation experiments are "scientific" to establish input to output relationship in transfer function analysis, control has been exercised so that there is only one input (wind farm power fluctuation) and one output (frequency deviation). In order the keep the ac voltage regulated at the point of connection of the wind farm, the reactive power control of the S-Modulator forms part of the negative feedback loop to null the error between the voltage reference and the measured voltage. In essence, the S-Modulator makes the point of connection a P-V bus.

The S-Modulator is an important contribution of this thesis, and because of its generality, it has more applications than the wind power research of this thesis.

Chapter 3 lays the groundwork for chapter 4.

Chapter 4 shows that that frequency deviation from 60 Hz can be predicted accurately by the transfer function of the power plants. The transfer functions are derived by small perturbation linearizing of the sub-systems of power plants. The good agreement between simulations of the originally nonlinear power plants and predictions from transfer functions validates the transfer function approach.

From the interaction of a single wind farm with a single thermal power plant, an original prediction method has been developed for any number of thermal plants and any number of wind farms. The method is again validated by simulation by HYPERSIM in a 9-bus system with 3 thermal plants. Although this thesis is concerned with thermal power plants only, the method has generality so that it applies to hydro-plants and mixed hydro/thermal plants. This is because the only change is in the transfer function representing the hydro-plant.

The key to this method is the fact that the entire electric utility grid has the same instantaneous frequency deviation from 60 Hz.

The research shows that the filtering of power fluctuation at high frequency is by kinetic storage in the rotating inertias and at low frequency is by "virtual storage" by the speed governor system.

Chapter 5 shows that there is further filtering at the wind farm end when variable speed wind turbine generators are used in wind farms. As a reference for comparison, constant speed wind turbines (based on cheap squirrel cage induction generators which are used in the early generation of small wind turbines) are shown to provide very little filtering. The variable speed wind turbine generator under study is the doubly-fed induction generator (DFIG) under decoupled P-Q control. The DFIG is presently widely used in conjunction with MW-size wind turbines with long turbine blade radius (large moment of inertia). Three strategies of control have been evaluated:

(1) $P_{ref}(=p_0)$-vs-ω_m. This Constant Power Strategy offers the best filtering but when there is prolonged deviation of wind velocity from the predicted mean, the operating point is blown beyond the stability limits.

(2) $P_{ref}(=p_0+p_1\omega_m)$-vs-$\omega_m$. The Linear Slope Strategy provides the generating counter-torque to prevent the operating point from leaving the stable operating region. There is deterioration in the filtering capability.

(3) $P_{ref}(=p_3\omega_m^3)$-vs-ω_m. When k_3 is correctly chosen, this strategy provides automatic Optimal Wind Power Acquisition. There is good filtering but it is the worst of the 3 strategies.

In all, the Constant Power Strategy should never be used. When filtering is the priority, the Linear Slope Strategy is the best, with p_1 to be kept as small as possible. The Optimal Wind Power Acquisition maximizes wind power revenue and is an acceptable strategy as long as the residual power fluctuation is tolerable.

The chapter has developed analytical formulas which evaluate the filtering capabilities of wind turbine generator systems.

<u>Chapter 6</u> combines the filtering available in a single thermal power plant and the filtering available in a single variable speed wind turbine generators to make an assessment. For an allowable 1% standard deviation of the frequency from the 60 Hz standard, the allowable standard deviation of wind power fluctuation is estimated as 8%. This estimate is on the conservative side because it does not take into account of the spatial filtering of the many wind turbine generators in a wind farm and the many wind farms in a utility grid.

As the 8% is for fluctuating power component from wind turbulence, the commercial component, which is the firm wind power predicted from the statistical mean wind velocity, is a higher percentage. This augurs well for the wind power industry.

7.4 Suggestions of Future Work

This thesis has limited its scope to thermal power plants which are equipped with speed governors only. There are opportunities for future work because of the variety of plants.

There are two other categories of power plants: plants with speed governors and automatic governor control (AGC); plants with neither speed governors nor automatic governor control (AGC). There are utility grids with hydro-plants and mixes of hydro and thermal plants. Nuclear plants are excluded because they have no flexibility.

Power fluctuations, besides affecting the frequency, affect the ac voltages. In this study, voltage fluctuations have been eliminated by using the Q control of the S-Modulator to regulate the voltages at all the buses. Although wind farms are obliged to keep their voltages at the points of connection regulated, the power pulsations can cause voltage fluctuations further inside the utility network. This has not been studied.

Appendix A

States: $x = [\omega_r \quad gov_1 \quad x \quad mhuh \quad T_h \quad tur_2 \quad T_i \quad tur_3 \quad T_l]^T$

Inputs: $u = [\Delta P_e \quad P_{w-ave} \quad \omega_{ref}]^T$

The state space matrix is: $E\dot{x} = Fx + Gu$

$$E = \begin{bmatrix} 2H\omega_0 & 0 & 0 & 0 & 0 & 0 & 0 & 0 & 0 \\ 0 & tsr & 0 & 0 & 0 & 0 & 0 & 0 & 0 \\ 0 & 0 & tcv & 0 & 0 & 0 & 0 & 0 & 0 \\ 0 & 0 & 0 & 1 & 0 & 0 & 0 & 0 & 0 \\ 0 & 0 & 0 & -F_h t_4 & t_5 & 0 & 0 & 0 & 0 \\ 0 & 0 & 0 & 0 & 0 & tr_1 & 0 & 0 & 0 \\ 0 & 0 & 0 & 0 & 0 & -F_i t_6 & t_7 & 0 & 0 \\ 0 & 0 & 0 & 0 & 0 & 0 & 0 & tr_2 & 0 \\ 0 & 0 & 0 & 0 & 0 & 0 & 0 & -F_l t_{11} & t_{12} \end{bmatrix}$$

$$F = \begin{bmatrix} 0 & 0 & 0 & 0 & \omega_0 & 0 & \omega_0 & 0 & \omega_0 \\ -\frac{K_l}{r} & -1 & 0 & -(K_l - 1) & 0 & 0 & 0 & 0 & 0 \\ 0 & 1 & -1 & 0 & 0 & 0 & 0 & 0 & 0 \\ 0 & 0 & \frac{1}{t_3} & -\frac{1}{t_3} & 0 & 0 & 0 & 0 & 0 \\ 0 & 0 & 0 & F_h & -1 & 0 & 0 & 0 & 0 \\ 0 & 0 & 0 & ai & 0 & -ai & 0 & 0 & 0 \\ 0 & 0 & 0 & 0 & 0 & F_i & -1 & 0 & 0 \\ 0 & 0 & 0 & 0 & 0 & al & 0 & -al & 0 \\ 0 & 0 & 0 & 0 & 0 & 0 & 0 & F_l & -1 \end{bmatrix}$$

$$G = \begin{bmatrix} -1 & -1 & 0 \\ 0 & K_I & \frac{K_I}{r} \\ 0 & 0 & 0 \\ 0 & 0 & 0 \\ 0 & 0 & 0 \\ 0 & 0 & 0 \\ 0 & 0 & 0 \\ 0 & 0 & 0 \\ 0 & 0 & 0 \end{bmatrix}$$

From (4), $G_3(s)$ is a transfer function to show the relation of $\Delta\omega_r(s)$ and $\Delta P_e(s)$. In the other form,

$$G_3(t) = \frac{\Delta\omega_r}{\Delta P_e} = \frac{\omega_r - \omega_{ref}}{\Delta P_e} \tag{8}$$

In order to get $G_3(s)$, it is necessary to convert the state space above to the nominal form:

$$\dot{x} = Ax + Bu$$
$$y = Cx + Du$$

$$A = E^{-1}F$$

$$B = E^{-1}G$$

$$C = [1 \quad 0 \quad 0 \quad 0 \quad 0 \quad 0 \quad 0 \quad 0 \quad 0]^T$$

$$D = [0 \quad 0 \quad 0]^T$$

In order to determine the phasor diagrams in Fig. 3.14, it is likely to measure transfer functions of ΔP_{accel} and ΔP_m over ΔP_e.

$$\frac{\Delta P_{accel}}{\Delta P_e} = \frac{\omega_0 (T_h + T_i + T_l) - \Delta P_e - P_{w-ave}}{\Delta P_e} \tag{9}$$

$$\frac{\Delta P_m}{\Delta P_e} = \frac{\omega_0 (T_h + T_i + T_l) - P_{w-ave}}{\Delta P_e} \tag{10}$$

For (9), $C = [0 \quad 0 \quad 0 \quad 0 \quad \omega_0 \quad 0 \quad \omega_0 \quad 0 \quad \omega_0]^T$

$D = [-1 \quad -1 \quad 0]^T$

For (10), $C = [0 \quad 0 \quad 0 \quad 0 \quad \omega_0 \quad 0 \quad \omega_0 \quad 0 \quad \omega_0]^T$

$D = [0 \quad -1 \quad 0]^T$

Appendix B

$t_3 = 0.3$	Time constant of steam tank
$t_4 = 0.5, t_5 = 1$	HP turbine constant
$t_6 = 1, t_7 = 1$	IP turbine constant
$t_{11} = 1, t_{12} = 1$	LP turbine constant
$ai = 1, al = 1$	IP and LP valve opening
$r = 0.05$	Permanent droop
$K_l = 6$	Speed regulator gain
$tsr = 5$	Time constant of speed valve relay
$tcv = 0.3$	Inverse of valve speed
$psih = 1$	Steam pressure at high-pressure stage
$K_S = 0$	Gain of power system stabilizer
$F_h = 0.28, F_i = 036, F_l = 0.36$	Mechanical power provide by HP, IP and LP turbine respectively
$H_1 = 0.946, H_2 = 3.68, H_3 = 0.337, H_4 = 0.099$	Inertia of masses on the generator

Appendix C

By using MATLAB, the transfer function of single thermal plant with parameters as in Appendix B can be reconstructed according the parameters below in Table A.

Numerator		Denominator	
Order	Parameter	Order	Parameter
9	0	9	1
8	-0.098775	8	113.2
7	-11.181	7	1388.9
6	-137.19	6	12630
5	-1247.5	5	56525
4	-5401.2	4	1.1976e+005
3	-10363	3	1.4016e+005
2	-9333.1	2	1.0033e+005
1	-3688.3	1	43533
0	-439	0	8780

Table A. Parameters of the single thermal plant with droop=0.05

The IEEE 9-bus system also can be reconstructed in MATLAB. Three thermal units are with same parameters except the droop. They have 0.05, 0.08 and 0.02 respectively.

Numerator		Denominator	
Order	Parameter	Order	Parameter
25	0	25	0.02927
24	-0.0009637	24	9.94
23	-0.32727	23	1247.2
22	-41.063	22	71179
21	-2343.6	21	1.9882e+006
20	-65459	20	3.7582e+007
19	-1.2368e+006	19	5.1943e+008
18	-1.706e+007	18	5.5367e+009
17	-1.8115e+008	17	4.6566e+010
16	-1.5136e+009	16	3.1228e+011
15	-1.0047e+010	15	1.6739e+012

14	-5.303e+010	14	7.1329e+012
13	-2.2081e+011	13	2.3989e+013
12	-7.1755e+011	12	6.3448e+013
11	-1.8056e+012	11	1.3213e+014
10	-3.5041e+012	10	2.1748e+014
9	-5.233e+012	9	2.8404e+014
8	-5.9965e+012	8	2.9486e+014
7	-5.2425e+012	7	2.4265e+014
6	-3.4603e+012	6	1.5692e+014
5	-1.6947e+012	5	7.839e+013
4	-5.9942e+011	4	2.9409e+013
3	-1.4684e+011	3	7.9236e+012
2	-2.3312e+010	2	1.4265e+012
1	-2.1325e+009	1	1.5093e+011
0	-8.4605e+007	0	6.9799e+009

Table B. Parameters of the 9-bus system

Appendix D

Type	MVA Rating	Source (KV)	Source (Hz)
Squirrel Cage Rotor	1.0	3.3	60

R_S [p.u.]	R_R [p.u.]	L_m [p.u.]	L_S [p.u.]	L_R [p.u.]
0.00662	0.01	3.1	0.085	0.11

Table C. Parameters of Squirrel Cage Induction Generator

Type	MVA Rating	Source (KV)	Source (Hz)
Wound Rotor	1.0	3.3	60

R_S [p.u.]	R_R [p.u.]	L_m [p.u.]	L_S [p.u.]	L_R [p.u.]
0.00662	0.01	3.1	3.185	3.21

Table D. Parameters of Wound Induction Generator

References

[1-1] American Wind Energy Association, "Global Wind Energy Market Report," 2004, pp. 1

[1-2] American Wind Energy Association, Europe Wind Energy Association, "Global Wind Power Installations," AWEA-EWEA News Release, March 2004, pp. 3

[1-3] B.K. Parsons, Y.Wan and B.Kirby, "Wind Farm Power Fluctuations, Ancillary Services, and System Operating Impact Analysis Activities in United States," European Wind Energy Conference, Denmark July 2-6, 2001, IEEE Committee Report, "Recommended Phasor Diagram for Synchronous Machines", *IEEE Trans.* Vol. PAS-88, pp. 1593-1610, 1969.

[1-4] IEEE Committee Report, "Proposed Excitation System Definitions for Synchronous Machines," *IEEE Trans.* Vol. PAS-88, pp. 1248-1258, 1969.

[1-5] P. Kundur, M. Klein, G.J. Rogers, and M.S. Zywno, "Application of Power System Stabilizer for Enhancement of Overall System Stability," *IEEE Trans.* Vol. PWRS-4, pp. 614-626, May 1989.

[1-6] IEEE working Group Report, "Dynamic Models for Fossil Fueled Steam Units in Power System Studies," *IEEE Trans.* Vol. PAS-94, pp. 1275-1287, July/August 1975.

[1-7] IEEE Committee Report, "Dynamic Models for Steam and Hydro Turbines in Power System Studies," *IEEE Trans. Power Apparatus and Systems*, Vol. PAS-92, n 6, pp. 1904-1915, Nov/Dec 1973.

[1-8] TransEnergie, Hydro-Quebec group, "HYPERSIM 8.9 reference guide manual," Jun 2002, pp. 208

[1-9] UNFCCCCOP-4, "The Fourth Meeting of the Conference of the Parties to the UN Framework Convention on Climate Change Buenos Aires, Argentina," November, 1998.

[1-10] Gary L. Johnson, "Wind Energy Systems," Prentice-Hall, Inc, 1985, pp. 50-78

[1-11] TransEnergie, Hydro-Quebec group, "HYPERSIM 8.9 reference guide manual," Jun 2002, pp. 181-230

[1-12] Hydro-Quebec's Research Institute, "Technical Facts Sheet of HYPERSIM Simulator," http://www.hydroquebec.com/technology/ireq/fiches/pdf/transhypersim .pdf

[3-1] TransEnergie, Hydro-Quebec group, "HYPERSIM 8.9 reference guide manual," Jun 2002, pp. 181-230

[3-2] P. Kundur, "Power System Stability and Control," McGraw-Hill, Inc, 1994, pp. 770.

[4-1] Paul M. Anderson, A.A. Fouad, "Power System Control and Stability," New York: IEEE Press, 1994, pp. 38.

[4-2] Norbert Wiener, "Cybernetics," 2nd, Boston: MIT Press, pp. 201.

[4-3] F.D. Galiana, Francois Bouffard, Jose M. Arroyo, Jose F. Restrepo, "Scheduling and Pricing of Coupled Energy and Primary, Secondary and Tertiary Reserves," IEEE Proc., invited paper and to be published.

[4-4] A.A. Samad, "Application of Kinetic Energy Storage Systems to Power systems operation," Master dissertation, Dept. Elec. Eng. Univ. McGill, Montreal, 2004.

[5-1] Lianwei Jiao, Boon-Teck Ooi, Géza Joós, Fengquan Zhou, "Doubly-Fed Induction Generator (DFIG) as a Hybrid of Asynchronous and Synchronous Machines", to be published in Electric Power Systems Research, 2005.

[5-2] Baike Shen, "Slip Frequency Phase Lock Loop for Decoupled P-Q Control for Doubly-fed Induction Machine (DFIG)", Master dissertation, Dept. Elec. Eng, McGill University, Montreal, 2004.

[5-3] Baike Shen, Victor Low and Boon-Teck Ooi, "Slip Frequency Phase Lock Loop for Decoupled P-Q Control for Doubly-fed Induction Machine (DFIG)", The 30th Annual Conference of the IEEE Industrial Electronics Society, November 2-6, 2004, Busan, Korea, WC3-3 "Induction Motor Drive 1"

[7-1] H. A. Panofsky, J.A. Duttoon, "Atmospheric Turbulence--Models and Methods for Engineering Applications," John Wiley & Sons, Inc, 1984